

University of Nottingham
UK | CHINA | MALAYSIA

SIGNATURES OF ASSOCIATIVE MEMORY BEHAVIOR IN OPEN QUANTUM SYSTEMS

by Eliana Fiorelli, MSc

A thesis submitted to the University of Nottingham for the degree of Doctor of Philosophy

September 2020

Abstract

Nowadays, the research field of Machine Learning (ML) is undergoing a rapid expansion. In addition, in the last decades, within the research area of quantum computation, several quantum protocols and algorithms have shown the ability to outperform their classical counterparts. In the light of these twofold advances, a frontier field investigating the potentiality of quantum implementations of ML architectures arose. Among the latter, many efforts are concentrated on Artificial Neural Networks (ANNs), which represent a highly successful ML architecture.

This thesis focuses on characterizing and understanding the role of quantum effects on the behavior of an instance of ANN, the so-called Hopfield Neural Network (HNN). The HNN is an example of an associative memory model and it permits the recognition, or retrieval, of patterns, such as letters of an alphabet. Formally, it can be described in terms of a classical spin network with an all-to-all interaction, ruled by a stochastic dynamics. Its relatively intuitive behavior, and its physical description make the HNN being a good candidate for a theoretical investigation of its possible quantum generalizations.

In the first part of our work we deal with the implementation of fully connected Ising models, such as the HNN one, in terms of quantum systems. To this end, we refer to the cases where the theory of Open Quantum System (OQS) is exploited for engineering steady states of out-of-equilibrium dynamics. This paradigm allows us to build a dissipative - yet quantum - dynamics which encodes in its stationary state the thermal state of the original (classical) problem. Such a construction gives us the chance to address the question as to whether the quantum description could lead to a speed-up in reaching the shared stationary state with respect to the classical counterpart. We show that a suitable choice of the parameters allows the system to switch between a classical regime and a quantum one, the latter being characterized by an accelerated approach towards the long-time limit state.

In the second part of our work we focus on practically relevant implementations of quantum systems that can show analogies with the HNN model. To this end, we consider spin-boson models as described by the Dicke Hamil-

tonian. Indeed, at strong spin-boson interaction couplings, and when the latter are additionally characterized by disorder, the equilibrium Dicke model is able to reproduce the retrieval mechanism typical of HNNs. When dissipation is included, the theoretical description becomes more challenging. We analyze the open, disordered Dicke model by employing some perturbative techniques in order to deal with the out-of-equilibrium dynamics at strong coupling. As a result, we are able to highlight similarities and differences between the quantum model and HNNs.

Acknowledgements

The work presented in this thesis is the result of three intense years, during which many people contributed to the outcome of the scientific part and, not less important, to the ongoing human growth.

I would like to thank my supervisor Igor Lesanovsky for the constant support and all the advices and feedback; my second advisor Matteo Marcuzzi, who spent many hours listening and sharing his brilliant knowledge with me. These projects wouldn't have been possible without the continuous consultations with Pietro Rotondo. I would like to thank him for his scientific passion that, no matter of the obstacles, stands like a lighthouse. I would also like to thank Federico Carollo for his patience and perseverance during the time spent with me, working on the projects. The last three years would have been much harder without all the coffee breaks: a special thanks to Stefano, Filippo and Gary.

The energy used to put these projects together comes also from having found some friends. A huge thanks goes to all the "65 Derby Street" folks, who undoubtedly contributed to make me feel home. Fabio, Mariele and Carmine, your lives are windows to look through this bizarre universe. I have been lucky enough to be part of the PostGraduate New Theater group, which has awakened my creativity. A special thanks to Pietro, Pete, Maria and Gordon. They taught me the art of holding together all the emotions and the self-control necessary to express them at the right time. All of my performances had, and still have, the best audience, Loredana and Elisabetta. Beyond all the past memories, I would like to thank them for having been able to hold one other, especially when the world was asked to execute the famous "social" distancing.

If I landed in Nottingham, it was also because of some people that trusted me, even before I did. Thanks to Valentina, Pierluigi and all my undergraduate colleagues, and thanks to my friend Erica. I am grateful for the encouragement and the scientific inspiration given by Paola Verrucchi and Alessandro Cuccoli. Finally, I would like to thank my parents, as they have learned to be (quite) ready to watch me jumping on the next flight or train or car, looking for my next adventure.

Contents

Abstract ii

Acknowledgements iv

List of Figures viii

Introduction 1

I Theoretical background 6

1 Associative memories 7
- 1.1 Artificial neural networks . . . 7
- 1.2 Hopfield neural networks . . . 9
  - 1.2.1 Deterministic Dynamics . . . 10
  - 1.2.2 From the Lyapunov function to the all-to-all Ising model 14
  - 1.2.3 Stochastic dynamics . . . 16
  - 1.2.4 Storage Capacity . . . 22
- 1.3 Towards a generalization of Hopfield neural networks via quantum systems . . . 22

2 Open Quantum Systems 24
- 2.1 Composite quantum system . . . 25
- 2.2 Dynamics of open quantum systems . . . 26
  - 2.2.1 Dynamical maps for isolated quantum systems . . . 26
  - 2.2.2 Dynamical maps for open quantum systems . . . 27
  - 2.2.3 Temporal continuity . . . 29
- 2.3 Markovian approximation for open quantum system dynamics 30
  - 2.3.1 GKSL master equation . . . 31
  - 2.3.2 Microscopic derivation . . . 32

3 A spin-boson Hamiltonian: The Dicke model 38
- 3.1 Equilibrium Dicke model . . . 38
  - 3.1.1 Superradiant phase transition . . . 39

3.2 Out-of-equilibrium phase transition 42
3.3 Disordered Dicke model 43
3.3.1 From the equilibrium disordered Dicke model to the Hopfield neural network 44

II An open quantum generalization of classical spin models 46

4 Quantum accelerated approach to the thermal state of classical spin systems with applications to pattern-retrieval in the Hopfield neural network 47
4.1 Quantum generalization of classical stochastic processes . . . 48
4.2 Fully connected quadratic models 51
4.2.1 Fully connected Ising model 52
4.2.2 Application to the Hopfield neural network 54
4.3 Summary and outlook 57

III Out of equilibrium dynamics of disordered, dissipative spin-boson models 58

5 Dynamics of strongly coupled disordered dissipative single-mode spin-boson systems 59
5.1 Non-equilibrium spin-boson model 61
5.1.1 Spin dynamics at strong coupling 62
5.2 Large η: infinite temperature dynamics 65
5.3 Small η: approximate low-temperature dynamics 66
5.4 Thermal versus non-thermal rates 67
5.5 Breakdown of detailed balance 71
5.6 Summary and outlook 72

6 Signatures of associative memory behavior in a multi-mode spin-boson model 73
6.1 Non-equilibrium multi-mode spin-boson model 74
6.1.1 Energy function, overlaps and coupling distribution . . 75
6.2 Non-equilibrium dynamics 76
6.3 Stationary properties 78
6.4 Influence of pattern noise 79
6.5 Summary and outlook 80

Conclusions 81

Appendices **84**

A Technical details for Part II **84**
A.1 Construction of the jump operators 84
A.2 Derivation of the equations of motion 85
A.2.1 Unitary transformation of the jump operators 87
A.3 Stability analysis of the fully connected Ising model 88
A.4 Dynamical equations for the p memory case 89
A.4.1 Stability analysis 90
A.4.2 Symmetries within the θ-ϕ plane 91

B Technical details for Part III **93**
B.1 Rate equation for a strongly coupled spin-boson model 93
B.2 Approximate expression of the rate for η small 96
B.3 Impact of pattern noise in the Hopfield Neural Network 98
B.4 Considerations on the reliability of the rate equation at long times 100

Bibliography **103**

List of Figures

1.1 From biological to logical neuron. 9
1.2 Pattern retrieval. 11
1.3 Energy landscape. 15
1.4 Phase diagram of the Hopfield neural network. 21

3.1 Superradiant phase transition. 41

4.1 Quantum accelerated approach towards stationarity. 49
4.2 Comparison between the "classical" and "quantum" dynamics of a fully connected Ising model. 54
4.3 Comparison between the "classical" and "quantum" dynamics of a HNN. 56

5.1 Dissipative spin-boson system. 60
5.2 Regimes of effectively thermal spin dynamics. 64
5.3 Ground state population for two different distributions of the spin-boson couplings. 68
5.4 Asymmetry of the rates. 69
5.5 Non-equilibrium regime. 71

6.1 Disordered, dissipative spin-boson system. 74
6.2 Stochastic dynamics and stationary properties. 77

B.1 Impact of pattern noise on the phase transition in the HNN. . 99
B.2 Quantum-jump Monte Carlo simulation of the simplified model. 102

Introduction

In the last decades several scientific research areas, ranging from computer science to neurobiology, contributed to improve the development of theoretical and practical aspects of Machine Learning (ML). Moreover, recent remarkable advances in data storage and processing have given rise to a significant boost to the field. The interest towards building systems that, without being explicitly programmed, can learn how to accomplish a task and improve from experience is indeed increasing. At the heart of such a growing, beyond the purely scientific curiosity, it certainly lies the potentiality of ML for many practical applications. Indeed, multiple sectors, such as medical diagnosis, image processing and autonomous driving industry, among the others, are exploiting the progress in such a field.

One of the most successful architectures in machine learning is represented by Artificial Neural Networks (ANNs). These are able to mimic, to an extent, what we know about the inner workings of the brain. Amongst the many instances of ANNs, in this thesis we consider the Hopfield Neural Network (HNN), which is an associative memory model. The reason why we focused on HNN is dual. First, it provides an intuitive and relatively simple description of an ANN example; second, it can be represented in terms of a classical spin system subject to thermal fluctuations, and thus explained by adopting concepts that are commonly used in the context of Statistical Mechanics.

An instance of Artificial Neural Network: Hopfield Neural Network
HNNs are among the simplest models of ANN, which are interconnected group of units based on biological neurons' models [1]. They have been used to solve computational complex tasks such as speech recognition and pattern recognition. A HNN displays the feature of associative memory, which is the ability to retrieve from a set of stored network states the one which is closest to the input pattern, allowing to compute incomplete input information. To give an example, let the stored states coincide with the letters of an alphabet. If the input state of the network is closest to the first letter, say "A", the associative memory is able to recover it completely.

Formally, ANNs such as the HNN can be modelled in terms of classical

spin systems whose time evolution is ruled by a certain dynamical prescription. The latter leads the network state into fixed points of the dynamics, that represent the "target" states. Such a mechanism allows to make ANNs accomplishing a specific task. Equivalently, one can associate an "energy landscape" to the classical spin network: once the dynamics brings the initial state of the network into one of the valleys, the task of the NN is accomplished. In other words, these types of NN have a distinctive connection to a thermodynamic potential. Here, when noise is taken into account, in the form of a "temperature parameter", the dynamics is described in terms of a stochastic process [1]. A key example is given by the HNN, whose behavior can be described by an Ising model with all-to-all interactions: At finite temperature, such a model undergoes a second order phase transition from a high temperature phase, called "paramagnetic", to a low temperature phase, called "ferromagnetic" [1,2]. The retrieval of information of the HNN takes place within the latter phase, that is indeed also referred to as the "retrieval" phase.

The physical description that can be employed for dealing with HNN makes the latter being an ideal testing ground for starting our investigation: in this thesis we are interested in characterizing and understanding the role of quantum effects on an ANN as given in terms of the HNN. In other words, we are interested in finding meaningful ways and models for analyzing how quantum implementations may affect the behavior of HNNs.

Hopfield Neural Networks and and (Open) Quantum Systems In the last decades, the research area related to quantum simulation and computation has received a significant boost. It has been proven that genuine quantum features such as superposition of states and entanglement provide remarkable advantages for solving many computational problems [3,4]. Additional paradigms such as quantum annealing have shown that quantum fluctuations can also be exploited for improving the effectiveness of classical optimization algorithms [5–9].

In the light of these advances, many models have been proposed in order to combine the striking properties of ANNs with quantum mechanics, aiming at understanding if ANNs' computing can take advantage of quantum effects [10,11]. This field of investigation aims at building a satisfactory framework that fully exploits both the advantages of quantum physics and computing in ANNs. The essential challenge is understanding how to combine the dissipative dynamics of classical ANNs and the linear, unitary dynamics which characterizes quantum systems. In this thesis, the paradigm that allows us to deal with this issue is to take into account a framework based on Open Quantum Systems (OQSs) [11–14].

In the following we better illustrate the kind of quantum description that we adopt for building HNNs with the tools that are provided by OQSs.

An open quantum proposal of Hopfield Neural Network Addressing the question of whether quantum effects can yield some advantages to the HNN problem of pattern retrieval can be split into two conceptual steps: providing a quantum description of the HNN, and eventually finding a meaningful way of comparison with its classical counterpart.

We consider a quantum generalization of the classical HNN that exploits a relatively recent paradigm, based upon the idea that the theory of OQSs may provide useful tools for engineering the long-time limit state of a given out-of-equilibrium dynamics [15]. In this scenario, not only quantum coherences, but also quantum dissipation is exploited to harness the OQS dynamics towards a "desired" state, that may be for instance the result of a quantum computation [16, 17].

In our case, we aim at engineering an OQS dynamics whose long-time limit state resembles the properties of the pattern retrieval typical of HNNs. Bearing in mind that a HNN can be described in terms of the evolution of a classical spin system, we formulate the NN dynamics in terms of a network of interacting spins. Here each spin - which encodes the state of the neuron - changes its state dynamically, depending on the configuration of the spins in its neighborhood. Following the above described paradigm, this dynamics can be modeled in terms of a master equation that takes in consideration the presence of an environment.

As a first attempt, we describe such dynamical evolution by means of a GKSL (Gorini-Kossakowsky-Susarshan-Lindblad), commonly referred to as Lindblad, master equation [12, 13]. As a result, we deal with a well defined way to include the presence of an environment, by adopting a time-local master equation. We define the model so that the dynamical evolution leads the OQS to a pure stationary state. In particular, the dissipation is engineered so that the long-time limit state of the quantum spin system embodies the classical configurations of the HNN. Yet, we deal with a quantum dynamics, as it involves the generation of coherences.

This setting provides us with a meaningful way for highlighting similarities and differences between the classical and the quantum model. In particular, we analyze the dynamical properties of fully connected Ising models, and HNN models, showing that, under some specific choice of parameters, the quantum model is characterized by an accelerated approach to the stationary state with respect to the classical one.

Spin-boson models for realizing Hopfield Neural Networks Our initial theoretical investigation gives us some insights to progress onto considering a physical characterization of the quantum systems that can possibly reproduce the behavior of HNN models. To this end, we consider once again that HNNs can be described in terms of all-to-all interacting classical spins. For mimicking this kind of systems, we take in consideration spin-boson models, i.e. ensembles of spin-$1/2$ particles interacting with a multi-mode bosonic field. Indeed, as bosons mediate long-range interaction among the spins, we can implement a dynamics that is HNN-like. In addition to this, spin-boson models are relevant because they actually underlie possible experimental realizations of a (quantum) HNN dynamics [18,19]. To take in consideration this scenario, i.e. to reproduce a realistic system, the model we focus on is an OQS, in contact with additional surroundings.

A fundamental model describing the interactions between an ensemble of two-level systems (spins) with a bosonic mode (e.g. photons of a given frequency) is the Dicke model [20]. It undergoes a second order phase transition when varying the spin-boson interaction coupling. Indeed, in the weak coupling regime the system is in a so-called normal phase, where the average number of bosons is sub-extensive (it grows slower than the number of spins). Instead, at strong coupling the system is in a so-called superradiant phase, where the average number of bosons is extensive, i.e. proportional to the number of spins [21–23]. The Dicke model can be adapted for modelling a variety of physical situations, such as circuit, cavity or waveguide QED, and trapped ions systems [24–26]. However, the description of these realistic scenarios commonly requires to take in consideration the effects of their environments. These surroundings, often taken into account in the form of quantum dissipation, give rise to phenomena such as, for instance, cavity loss and atomic decay. Remarkably, also the open Dicke model undergoes the superradiant phase transition upon varying of the spin-boson interaction coupling [27,28].

Furthermore, recent results show that, when considering interaction couplings that are both spin and boson dependent, or "disordered", the superradiant phase transition shares fundamental features with the phase transition characteristic of the HNN [18,19,29–31]. In other words, at equilibrium there is an analogy between the disordered Dicke model at strong coupling and the retrieval phase of the HNN. The question that we approach in our work is whether a similar analogy holds when considering the out-of-equilibrium dynamics that characterizes the open Dicke model.

Analyzing how a HNN-like dynamics may emerge in the open, disordered Dicke model at strong coupling is technically challenging. In this thesis, we tackle this problem by employing a perturbative technique that is

valid at strong coupling. We concentrate upon the spin system by tracing over the bosons, deriving an effective spin dynamics. The latter is governed by a classical master equation describing an out-of-equilibrium dynamics. We show that there exists a parameter regime where such an effective model is reminiscent of typical properties characterizing the HNN.

Thesis structure The structure of the thesis is as follows. Part I summarizes the theoretical aspects that constitute the background of this work. In Chapter 1 we give a brief introduction of the classical theory describing associative memories, with a particular focus on the HNN. In Chapter 2 we move to the quantum theory, introducing the description of open quantum systems. Finally, Chapter 3 analyzes some main results concerning the equilibrium properties of spin-boson models described by the Dicke Hamiltonian.

The remaining Chapters are dedicated to present the original work that has been carried out. Part II deals with the analysis of the quantum generalization of HNN. Here we explore the question as whether quantum effect may yield a speed-up in reaching a stationary state constructed having in mind the classical counterpart of the model. Part III takes into account the out of equilibrium dynamics of a spin-boson system, when disorder and dissipation are present. In particular, in Chapter 5 and 6 we analyze the single-mode Dicke model and the multi-mode one, respectively, highlighting similarities and differences with the behavior of the HNN.

Part I

Theoretical background

Chapter 1

Associative memories

1.1 Artificial neural networks

Artificial neural networks (ANNs) are, at the most basic level, systems that process information. They do so, as their name suggests, by analogy with the microscopic structure of the brain, which can be regarded as a huge network of interconnected neurons. Similarly, ANNs consist of a large number of interconnected units (digital bits, circuit elements, spins, ...) [1, 32]. In general, ANNs have the ability to learn how to fulfill some tasks, by analyzing examples, and without being programmed with rules that refer to the specific task, i.e. without the need for a task-solving algorithm to be spelled out by the programmer as in standard computation. For example, a typical problem where ANNs are employed is "image recognition". In this case, an ANN can be trained for distinguishing images that contain specific subjects, e.g. cats, by first analyzing sample images that are labeled as "cat" or "non-cat", and eventually exploiting such examples to identify cats in different images. Here, no prior knowledge about the details of a cat, like fur, tails, whiskers etc, is necessary for the ANN.

The elementary units of an ANN, referred to as artificial neurons, represent a logical description of the biological neurons that constitute the brain. In general, the human nervous system is made of many types of neurons, which play different roles, and additionally display slightly different structures. However, when neglecting these differences, a schematic representation of a biological neuron as a device divided in input signal, central processing, and output signal, is adopted [1, 32, 33]. This coarse division is illustrated in Fig. [1.1a] and it is as follows: A neuron receives signals from other neurons through synapse connections. The combination of these multiple signals determines the new state of the neuron on the receiving end. This is calculated by taking a weighted sum of the individual signals, with the weights, also called synaptic efficacies, measuring how effective an emit-

ting neuron is at affecting a receiving one. If the weighted summation of the input signals exceeds a certain threshold, which represents the value of the membrane potential, the neuron sends out a signal through its own axon. In this case the neuron is said to be "firing", otherwise is said to be "resting".

The interest for ANNs arises in various research fields, each one modeling ANNs depending on their specific focuses. For instance, neuroscientists aim to increase the knowledge on how the human brain works, i.e. to provide new insights on the connection between the microscopic processes that occur in the brain and the higher levels of information processing we experience. For this reason, they need to model neural networks including several biological details. At variance with this, both computational scientists and physicists loosely model the way in which the brain is believed to work. The first ones focus on implementing machines that feature high performances in computational tasks such as pattern and speech recognition, attempting to exploit human brain features as tolerance to faults, robustness to external noise, capacity to deal with noisy and inconsistent information. The second ones are mainly interested in analyzing the dynamics that occurs in the highly interconnected number of units represented by ANNs; they focus on the fact that the connections determine, for each unit, which ones can influence its value in the course of the computation, thus leading to interesting effects in the time evolution of ANNs. In this thesis, ANNs are presented following the latter point of view.

The simplest logical description of a neuron is given in terms of a binary unit, say σ, that can take two values, e.g. $\sigma = \pm 1$, corresponding to the states firing and resting, respectively [34]. An ANN made of N neurons is described in terms of binary variables configurations, $\vec{\sigma} = (\sigma_1, ..., \sigma_N)^T$, with $\sigma_i = \pm 1 \; \forall i$. The synapse strength, or connection, of an input coming to the i-th neuron from the j-th one is a real number identified by J_{ij}. The activation mechanism of the i-th unit can be formulated as follows: the configuration σ_i at the time $t + \Delta t$, due to the input of the others $N - 1$ neurons in the state σ_j, $\forall j \neq i$, at the time t, is

$$\sigma_i(t + \Delta t) = \mathrm{sgn}\left(\sum_{j=1, j\neq i}^{N} J_{ij}\sigma_j(t) - \mu_i \right), \tag{1.1}$$

where $\mathrm{sgn}(x)$ is the sign function, such that $\mathrm{sgn}(x) = +1(-1)$ if $x \geq (<)0$. The parameter μ_i is the threshold value that the weighted sum of inputs has to exceed in order for the i-th neuron to fire. The process is schematically reproduced in Fig. [1.1b] for the $i = 1$ neuron.

The choice of the connections J_{ij} determines what task the ANN is actually solving. In the following, we will show a choice of synaptic strengths which produces associative memory behavior.

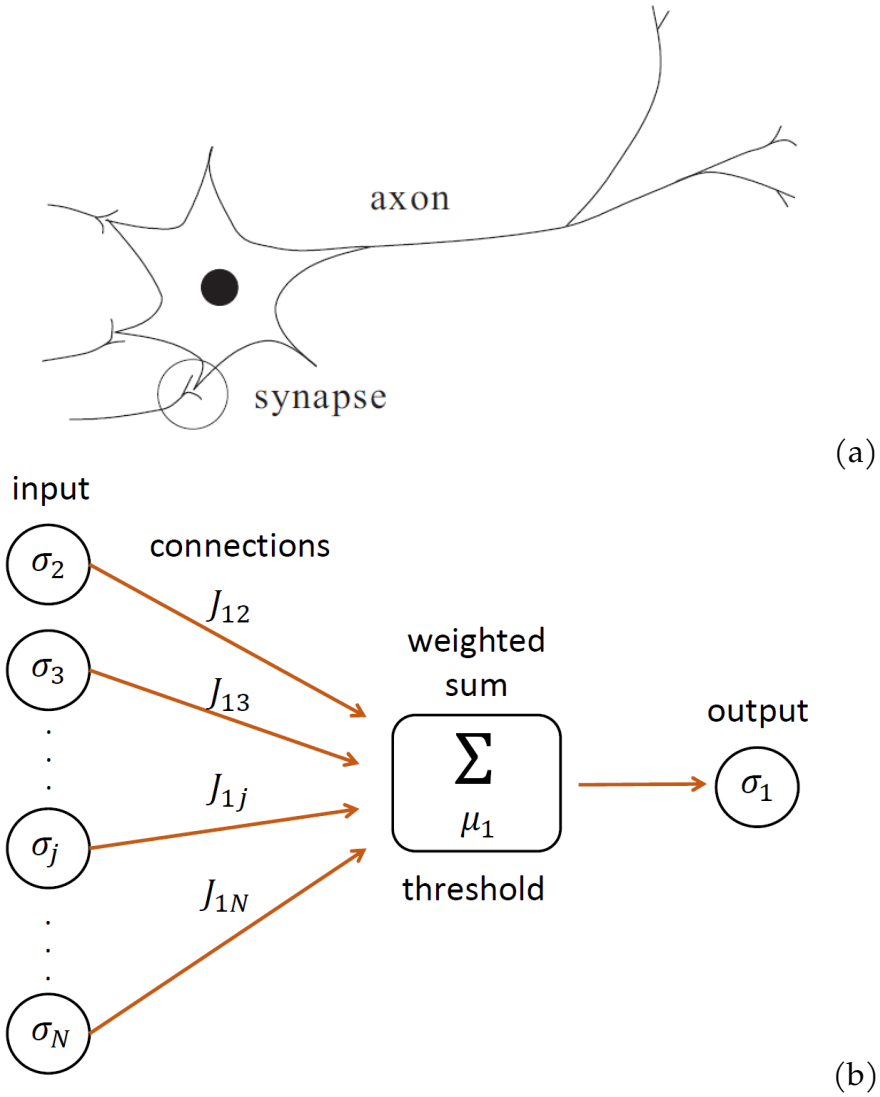


Figure 1.1: **From biological to logical neuron.** (a) Coarse division of a neuron in input signal, central processing, output signal. The input signal is received by means of synapses, elaborated in the central body and a possible output signal is sent through the axon. Reproduced from [33]. (b) Activation mechanism of the first neuron in an ANN. The first neuron receives inputs from the others $N-1$ neurons. The sum of the input signals is weighted with the connection J_{1j} and compared to the threshold value μ_1. Accordingly, an output signal can be sent.

1.2 Hopfield neural networks

The Hopfield neural network (HNN) [35] is the simplest model showing the features of an associative memory. That is, the ability to store information in the form of special configurations, or *patterns*, and to reconstruct them dynamically when provided with a portion. To cite an example, the retrieval

process characterizes our brain when it reconstructs an entire word from its first half.

In a neural network made of N neurons, patterns are defined as set of p network states, $\{\vec{\xi}^{\mu} = (\xi_1^{\mu}, ..., \xi_N^{\mu})^T\}_{\mu=1,...,p}$, where the elements $\xi_i^{\mu} = \pm 1$ encode the information stored into the system. For instance, patterns can be employed to encode images, by relating the value of each pattern element, ξ_i^{μ}, to a given outcome (black or white) of a pixel. In this way, the dynamical retrieval of information can be easily represented as an image reconstruction, as sketched in Fig. [1.2a]. Here, letters of an alphabet are converted into pattern configurations, and the retrieval of the letter "A", when given with a portion of it, is outlined.

From the physical viewpoint, when studying the dynamical retrieval of information, it would be desirable that the latter was described be *uncorrelated* patterns, so as to have maximally *distinguishable* patterns. In order to fulfill such requirement, it is a common choice to treat the pattern components as independent, identically distributed random variables, with probability distribution

$$G(\xi_i^{\mu}) = \frac{1}{2}\left[\delta(\xi_i^{\mu} - 1) + \delta(\xi_i^{\mu} + 1)\right], \tag{1.2}$$

being $\delta(x) = 1$ if $x = 0$ and $\delta(x) = 0$ if $x \neq 0$. Indeed, in the thermodynamic limit, $N \to +\infty$, and $p/N \to 0$, patterns with probability distribution (1.2) are characterized by the following properties:

- $\langle \xi_i^{\mu} \rangle = \sum_i \xi_i^{\mu}/N = 0$, i.e. patterns are unbiased;
- $\langle \xi_i^{\mu} \xi_i^{\nu} \rangle = \vec{\xi}^{\mu} \cdot \vec{\xi}^{\nu}/N = 0$, $\forall \mu \neq \nu$, i.e. patterns are uncorrelated.

1.2.1 Deterministic Dynamics

The Hopfield model dynamics is constructed by considering that one wants to dynamically retrieve the stored patterns in the long-time limit. For this reason, the idea is to implement a dynamics where patterns behave as *stable fixed points* or *fixed point attractors*, which are defined as follows:

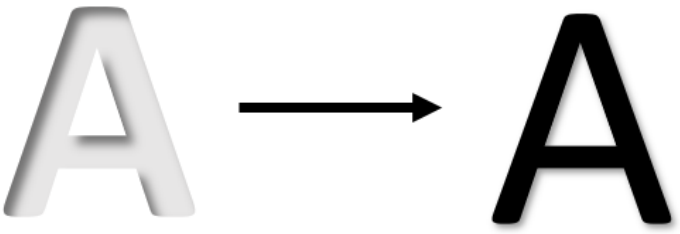
Definition 1.2.1. Let $f(t, \cdot)$ be a function from the set of possible states to itself. It specifies the dynamics of the system, with x_i the initial state, such that $f(0, x_i) = x_i$. An *attractor* is a close set S of the phase space with the following properties:

- S is an invariant set under f: $\forall x_s \in S$, $f(t, x_S) \in S$, $\forall t > 0$;
- there exists an open set of the phase space containing S, called *basin of attraction* for S and denoted $B(S)$, made of all points x_b that enter S under the dynamics in the limit $t \to +\infty$;

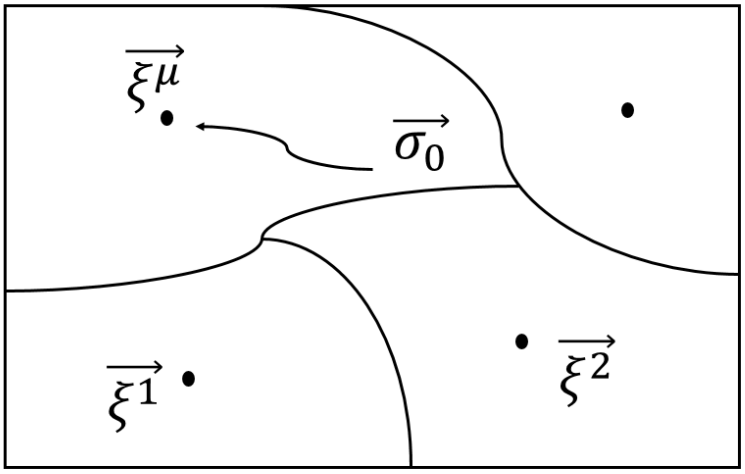
- S is a minimal set: there is no proper subset of S that satisfies the first two conditions.

Stable fixed points are attractor points that are mapped onto themselves by the transformation f.

That is, as illustrated in Fig. [1.2b], constructing the HNN dynamics with the patterns being the stable point attractors means that, given an input network state, $\vec{\sigma}_0 = (\sigma_{01}, ..., \sigma_{0N})$, this is evolved into one of the pattern states, say $\vec{\xi}^{\mu}$. Once the pattern is reached the network state does not evolve further, as patterns are mapped onto themselves by the HNN dynamics.



(a)



(b)

Figure 1.2: **Pattern retrieval.** (a) Letters of an alphabet as patterns to be stored in a neural network and retrieval of the letter A. (b) Qualitative sketch of the phase space structure. Patterns as stable fixed points. Lines delimiting each pattern represents the boundary of their basin of attraction. If the inital state of the network, $\vec{\sigma}_0$, is inside the basin of attraction of one of the pattern, $\vec{\xi}^{\mu}$ in figure, then it will evolve dynamically towards that pattern.

Formally, the Hopfield dynamics is defined by considering the update rule defined in Eq. (1.1), and simplifying it to the special case of vanishing

threshold, $\mu_i = 0, \forall i = 1, ..., N$, so that it reads

$$\sigma_i(t + \Delta t) = \text{sgn}\left(\sum_{j=1}^{N} J_{ij}\sigma_j(t)\right). \tag{1.3}$$

Moreover, the connections J_{ij} are chosen as follows

$$J_{ij} = \frac{1}{N}\sum_{\mu=1}^{p} \xi_i^\mu \xi_j^\mu, \quad J_{ii} = 0. \tag{1.4}$$

The choice (1.4) is usually dubbed *Hebb's rule*, because of the similiarity with the Hebbian hypothesis about the learning mechanism in neural networks [36]. Indeed, Hebb formulated the learning process as a dynamical adjustment of the synapse strength J_{ij} due to the past neuron activity. To better clarify this point, a formal description of Hebbian learning is the following: the past neuron activity modifies the synapse strength J_{ij} as $\Delta J_{ij} \approx \langle \sigma_i \sigma_j \rangle_t$, with $\langle \cdot \rangle_t$ representing a time average over a time interval occurring before t. It is worth noticing that this prescription gives the same result whether both neurons are firing or non-firing: the connection J_{ij} is in any case enhanced. Instead, J_{ij} is reduced only when any of the neurons is firing, and the other one non-firing. Following the Hebb's learning hypothesis, it has been eventually proposed as a *storage prescription* [37] such that, when a new pattern $\vec{\xi}^\mu$ is added to the memory of a neural network, the synapse strengths are modified by adding the term $\Delta J_{ij} = \frac{1}{N}\xi_i^\mu \xi_j^\mu$ to the pre-existing connections. In this framework, the Hebb's rule defined by Eq. (1.4) can be understood as a generalization of the storage prescription, for a N-network with p stored patterns.

The connections J_{ij} defined by the Hebb's rule (1.4) show the following properties:

- *additivity*, that originates from the Hebb's learning hypothesis;
- *locality*, i.e. the fact that only the product of the components ξ_i and ξ_j contributes to the connection J_{ij};
- *patterns symmetry*, i.e. all the patterns are imprinted with the same amplitude.

A remarkable feature that characterizes the dynamical rule (1.3) is the fact that it can be fulfilled either asynchronously, updating one σ_i at a time, or synchronously, updating all the σ_i simultaneously. In the first case, either the updated unit is picked at random, or an updating order is defined at the very beginning. In the second case, a central clock to the system that keeps the units synchronized is needed. It is worth noticing that, in order

to compare the result of these two types of dynamics, an updating time step Δt characterizing a synchronous process corresponds to a time $N \times \delta t$ for the asynchronous dynamics, where δt identifies the updating time step of the single unit. However, in a synchronized dynamics oscillation phenomena can occur, and a stable network state may never be reached. In order to avoid these possible outcomes, we will consider as a HNN model the one defined by the Hebb's rule (1.4) with discrete two-state units which are *asynchronously* updated through Eq. (1.3).

Pattern stability considerations

The dynamical rule (1.3), together with the prescription (1.4), is formulated with the stated intent that patterns behave as stable fixed point attractors. In this Section, we analyze to what extent the patterns satisfy Def. (1.2.1), with respect to the HNN dynamics.

From the definition (1.2.1) follows that a generic network state $\vec{\sigma}$ is a fixed point attractor with respect to the update rule (1.3) if the latter maps the state into itself, i.e. if it is $\sigma_i = \mathrm{sgn}\left(\sum_j J_{ij}\sigma_j\right)$. This relation is satisfied if the local field acting on the i-th neuron, defined as

$$h_i \equiv \sum_j J_{ij}\sigma_j, \tag{1.5}$$

is of the same sign as the i-th neuron configuration, i.e.

$$\sigma_i h_i > 0. \tag{1.6}$$

Considering the network state as one of the pattern, say $\vec{\xi}^{\nu}$, the condition (1.6) reads

$$0 < \xi_i^{\nu} h_i = \xi_i^{\nu} \frac{1}{N} \sum_{j \neq i} \sum_{\mu} \xi_i^{\mu} \xi_j^{\mu} \xi_j^{\nu} = \frac{N-1}{N} + \frac{1}{N} \sum_{j \neq i} \sum_{\mu \neq \nu} \xi_i^{\nu} \xi_i^{\mu} \xi_j^{\mu} \xi_j^{\nu}. \tag{1.7}$$

The second term of the last step is usually referred to as the crosstalk term. Under the assumption that both N and p are much larger than one, it is the sum of about $p \times N$ independent random variables, each of them with possible values ± 1. Thus, its mean value fluctuates about zero and its mean square displacement from the origin is proportional to $p \times N$. Taking into account the factor $1/N$, in the limit $N \to \infty$ it is

$$\xi_i^{\nu} h_i \approx 1 \pm \sqrt{\frac{p}{N}}. \tag{1.8}$$

Therefore, if p is set smaller than N, such that $\sqrt{(p/N)} \ll 1$, patterns are, statistically speaking, fixed point attractors of the dynamics.

In addition, patterns are *stable* attractors with respect to small perturbations. Indeed, as it shown in Ref. [1], if a small fraction of the network state is flipped with respect to one of the patterns, the network is still capable of aligning with the pattern itself.

It is worth noticing that if the condition (1.6) holds for the pattern $\vec{\xi}^{\nu}$, it is valid also for the opposite pattern, $-\vec{\xi}^{\nu}$. Hence, given a set of p patterns $\{\vec{\xi}^{\mu}\}_{\mu=1,\dots,p}$, the collection of opposite network states, $\{-\vec{\xi}^{\mu}\}_{\mu=1,\dots,p}$, represents an ensemble of stable fixed point attractors with respect to the dynamics defined by Eqs. (1.3) and (1.4). This is a straightforward consequence of the fact that the HNN dynamics is characterized by a Z_2 symmetry, i.e. it is invariant under flipping all the binary variables, $\sigma_i \leftrightarrow -\sigma_i,\ \forall i$.

Until now we have shown that patterns are stable fixed points of the dynamics, but not that they are unique. Indeed, the non-linear dynamics defined by Eqs. (1.3) and (1.4) generates additional attractors, that are referred to as *spurious states*. For instance, certain combinations of an odd number of patterns, called *mixture states*, turn out to be stable attractors [2, 33]. The network state

$$\sigma_i^{\text{mix}} = \text{sgn}(\pm\xi_i^{\mu_1} \pm \xi_i^{\mu_2} \pm \xi_i^{\mu_3}) \tag{1.9}$$

represents one of the simplest examples of a mixture state.

A reasonable question that may arise at this stage is if it possible to avoid that the network configuration remains trapped in a solution that corresponds to a spurious fixed point attractor. In order to fully answer this question, it is useful to introduce the deterministic dynamics of a HNN as described in Eq. (1.3) from the viewpoint of the Lyapunov function.

1.2.2 From the Lyapunov function to the all-to-all Ising model

Starting from the deterministic update rule (1.3), it is possible to construct a function of the network configurations, whose value decreases along any chosen dynamical trajectory. From the theory of dynamical systems, these are effective potentials, referred to as *Lyapunov functions*, and their formal definition can be formulated as follows:

Definition 1.2.2. Consider a dynamical system specified by the function $f : \mathbb{R}^n \to \mathbb{R}^n$, such that $f : x \to f(x)$, with a fixed point at x_0. A continuously differentiable, real-valued function $V : \mathbb{R}^n \to \mathbb{R}$ is called a Lyapunov function if it satisfies the properties:

- $V(x) > V(x_0), \forall x \neq x_0$,;
- $V(f(x)) - V(x) < 0, \forall x \neq x_0$.

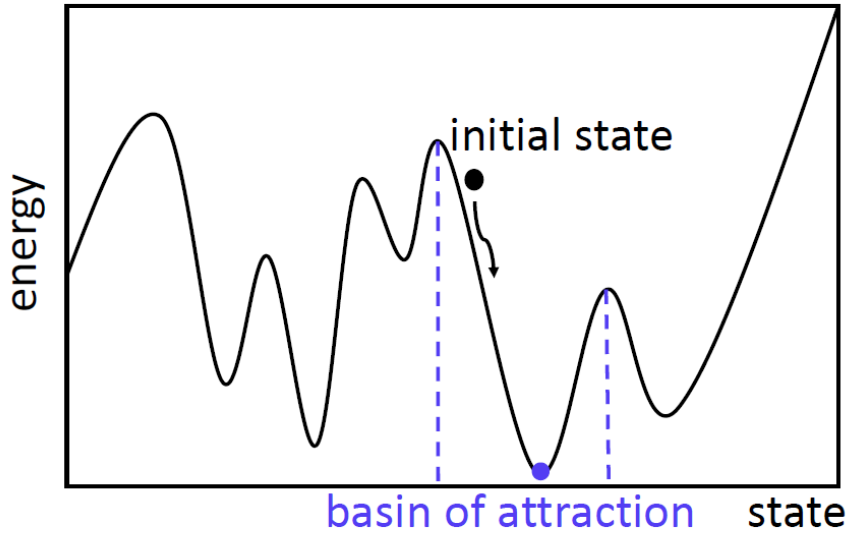


Figure 1.3: **Energy landscape.** The minima represent stable fixed points of a gradient descent dynamics. One of the basins of attraction has been delimited by vertical dashed lines. All initial states within them will fall towards the minimum in between in the course of the dynamics.

The asynchronous HNN dynamical process, specified by Eqs. (1.3) and (1.4), can be described in terms of the Lyapunov function

$$E(\vec{\sigma}) = -\frac{1}{2}\sum_{i,j,i\neq j} J_{ij}\sigma_i\sigma_j, \tag{1.10}$$

whose value monotonically decreases as the neural network evolves dynamically from a given initial network configuration to a final fixed point. Indeed, we can express $E(\vec{\sigma})$ in terms of the local field h_i, defined by Eq. (1.5), as $E(\vec{\sigma}) = -1/2\sum_i \sigma_i h_i$. At each time step, a neuron σ_i gets aligned with the direction of the local field h_i, leading to a monotonic decrease of the function $E(\vec{\sigma})$. When the network state reaches one of the fixed point attractors, the function (1.10) reaches one of many possible local minima. Hence, the stable fixed points described in the previous Section, i.e. the p patterns, with $p \ll N$ and $N \to +\infty$, as well as the spurious states, are all local minima of the Lyapunov function (1.10). A sketch of the landscape of an energy function is displayed Fig. [1.3], with the local minima representing the stable fixed points and the slopes surrounding them delimiting their the basins of attraction.

Remarkably, it is straightforward to see that the landscape function (1.10) is the energy of a classical spin model characterized by fully connected interactions [33]. In other words, the HNN can be equivalently described in terms of a system made of N classical spins that interact according to the

all-to-all connected Ising model (1.10), with interaction couplings given by the Hebb's rule (1.4). In what follows, we will thus indistinctly refer to the elementary units of a HNN as either "neurons" or "spins". Moreover, some of the features of the HNN can be reformulated in terms of properties of the energy function. First of all, the all-to-all Ising model displays a Z_2 symmetry, i.e. it is invariant upon inversion of the spin configuration ($\sigma_i \leftrightarrow -\sigma_i \, \forall i$). Due to this symmetry, any reversed pattern configuration, $-\vec{\xi}^{\mu}$, is virtually indistinguishable from the original and must therefore behave as a memory too, i.e. it corresponds to a local minimum of E. Secondly, the quantity h_i, that has been referred to as a local field, is the energy difference ΔE_i due to the flipping down of the i-th spin, i.e. it is

$$\Delta E_i = E(\sigma_i = -1) - E(\sigma_i = 1) = \sum_{j \neq i} J_{ij}\sigma_j = h_i. \tag{1.11}$$

We point out that the sought stationary states of the HNN dynamics, i.e. the pattern states, are global minima of the energy function. However, due to the presence of spurious states, the dynamics may remain trapped in these type of minima (if started in one of the corresponding basins of attraction). As we will see in the next Section, this problem may be tackled via the introduction of a certain amount of noise in the system, which adds energy-increasing dynamical processes, thus allowing the network state to reach one of the deepest minima, despite the presence of energy barriers. In order to fully characterize this situation, in the next Section we will describe the HNN stochastic dynamics, analyzing the properties of the system at different levels of noise. To this end, the description of the HNN as an all-to-all Ising model will play a crucial rule, as it allows us to exploit typical methods widely used in the analysis of the statistical mechanics of classical spin models.

1.2.3 Stochastic dynamics

We have described the dynamical evolution of a HNN, via the Eq. (1.3), in terms of a deterministic dynamics. However, and for the reasons explained at the end of the previous Section, HNN dynamics can be generalized to the case of stochastic processes. To this end, we introduce an inverse "temperature" parameter, $\beta = 1/(K_B T)$, which represents the inverse strength of the source of noise in the system. Without loss of generality, we further set $K_B = 1$.

A finite temperature induces spin flips which can increase the energy, differently from the dynamical rule (1.3) that leads the i-th spin to align with the local field h_i. In this case, the deterministic time evolution (1.3) is replaced by a *Glauber dynamics* [38], a stochastic process that describes the

single spin flip dynamics of an Ising model interacting with a heat bath at temperature β^{-1} as follows. Whenever the i-th spin is updated, say after a time step Δt, the probability that it takes one of the two possible value ± 1, given all the $N-1$ spins in a configuration $\{\sigma_j\}_{j=1,\dots,N, j\neq i}$, is

$$P\left[\sigma_i(t+\Delta t)=\pm 1\right]=\frac{1}{1+e^{\mp 2\beta\Delta E_i(t)}}, \tag{1.12}$$

where ΔE_i has been defined by Eq. (1.11) and depends on the $\{\sigma_j\}_{j=1,\dots,N,j\neq i}$ configuration. It is worth noticing that the probabilistic update rule (1.12) reduces to the deterministic one (1.3) in the limit of zero temperature, $\beta\to\infty$, as $\sigma_i=1(-1)$ if $\Delta E_i>0(<0)$. Conversely, at infinite temperature $\beta=0$, the network becomes perfectly random. Thus, the temperature β^{-1} controls the level of stochastic noise in the dynamics.

Similarly to the zero-temperature case, we want to understand if and to what extent the retrieval of patterns occurs, given the probabilistic update rule (1.12). Here, the concept of stable fixed points, that has been considered for the deterministic dynamics, will be replaced by the one of the stationary distributions peaked around one of the zero-temperature attractor states. In the stochastic dynamics, this manifests in the state of the system fluctuating around one of the zero-temperature fixed points.

Before going ahead, it is useful to point out some properties of the Glauber dynamics. This describes an ergodic single-spin-flipping process that is a *Markov process*: the probability distribution of each one of the spins after one time step depends only on the configuration of all the other spins at the current time. A Markov process can be fully characterized by the definition of the transition probability $\pi_{\vec{\sigma}\to\vec{\sigma}'}$ of switching from a configuration $\vec{\sigma}$ to a configuration $\vec{\sigma}'$. In the case of the Glauber dynamics (1.12), $\vec{\sigma}$ and $\vec{\sigma}'$ differ by a single spin flip only and the transition probability reads

$$\pi_{\vec{\sigma}\to\vec{\sigma}'}=\frac{1}{1+e^{2\beta\Delta E_i\sigma_i}}, \tag{1.13}$$

where the index i denotes which one of the spins is being flipped. In general, it is then possible to write a *master equation* describing the time evolution of the probability for the HNN to be in a configuration $\vec{\sigma}$ as

$$p_{\vec{\sigma}}(t+\Delta t)=p_{\vec{\sigma}}(t)+\sum_{\vec{\sigma}'\neq\vec{\sigma}}\left[\pi_{\vec{\sigma}'\to\vec{\sigma}}p_{\vec{\sigma}'}(t)-\pi_{\vec{\sigma}\to\vec{\sigma}'}p_{\vec{\sigma}}(t)\right]. \tag{1.14}$$

One could also derive a differential equation for the probability distribution of the states, $p_{\vec{\sigma}}(t)$, from Eq. (1.14). However, for our purposes, it is sufficient to say that it is possible to verify that the stochastic process (1.12) admits an equilibrium probability distribution. That is, there exists a probability distribution such that $p_{\vec{\sigma}}(t+\Delta t)=p_{\vec{\sigma}}(t)$, $\forall\vec{\sigma}$, that we will denote by $P_{\rm eq}(\vec{\sigma})$,

and call stationary distribution. A sufficient condition for the existence of the latter is

$$P_{\text{eq}}(\vec{\sigma})\pi_{\vec{\sigma}\to\vec{\sigma_i}'} = P_{\text{eq}}(\vec{\sigma}')\pi_{\vec{\sigma}'\to\vec{\sigma_i}}, \tag{1.15}$$

which is referred to as *detailed balance*. By inserting the expression of the transition probability (1.13) into (1.15), it follows that the long-time limit distribution of the network states approaches the equilibrium Gibbs-Boltzmann distribution

$$P_{\text{eq}}(\vec{\sigma}) = \frac{e^{-\beta E(\vec{\sigma})}}{Z(\beta)}, \tag{1.16}$$

where $Z(\beta) = \sum_{\{\vec{\sigma}\}} e^{-\beta E(\vec{\sigma})}$ is the partition function.

The existence of the stationary distribution (1.16) implies that the pattern retrieval problem of a stochastic HNN reduces to the equilibrium statistical mechanics of a fully connected Ising model with energy (1.10). In order to better clarify this, it is useful to notice that the energy (1.10) can be seen as a generalization of an Ising model with constant couplings J, $E_I(\vec{\sigma}) = -\frac{1}{2}J\sum_{i,j}\sigma_i\sigma_j$. At equilibrium, the properties of this system are described by the behavior of macroscopic variables such as the magnetization $M = \frac{1}{N}\sum_i \sigma_i$. Indeed, this parameter signals the occurrence of a second order phase transition between a high temperature disordered phase, called paramagnetic phase, where the average magnetization is 0, and a low temperature, ordered phase, called ferromagnetic phase, where the magnetization takes a finite value.

In a similar way, an understanding of the extent to which the retrieval of patterns occurs in the stationary distribution of a HNN can be derived by analyzing macroscopic quantities, called *overlaps*, between the spin configurations and the p patterns, which read

$$m^\mu = \frac{1}{N}\sum_{i=1}^{N}\xi_i^\mu\sigma_i, \tag{1.17}$$

$\forall\mu = 1, ..., p$. From this definition, we see that a vanishing value for all the overlaps implies that none of the patterns is retrieved, as the network configuration is not aligned with any of the p patterns. On the contrary, if one of the p patterns, say the μ-th, takes a finite value, the spin configuration is aligned with the pattern $\vec{\xi^\mu}$, with the value $|m^\mu| = 1$ signaling a perfect retrieval of the memory. The analysis of the behavior of the overlaps at stationarity, upon varying of the noise parameter β, is performed in the next Section.

Mean field theory

The equilibrium statistical properties of the model can be derived by applying the mean field (MF) approximation. A description of how the MF

approximation is applied to HNNs is explained in the following.

From the stochastic dynamical rule (1.12), the steady state probability for the i-th spin to take the values ± 1 is $P(\sigma_i = \pm 1) = 1/(1 + e^{\mp 2\beta h_i})$, so that the average value reads

$$\langle \sigma_i \rangle = (+1) \times P(\sigma_i = 1) + (-1) \times P(\sigma_i = -1) \approx \tanh(\beta \langle h_i \rangle). \tag{1.18}$$

In the last step of Eq. (1.18) we exploited the MF approximation by considering $\langle \tanh(\beta h_i) \rangle \approx \tanh(\beta \langle h_i \rangle)$. Indeed, the local field h_i would in principle fluctuate, due to the dependence on all the other the spin variables $\sigma_j, \forall j \neq i$. The MF approximation consists in replacing the fluctuating local field with the average value of all the spins connected to the site i, $h_i \approx \langle h_i \rangle$. Thus, the average field $\langle h_i \rangle$ reads

$$\langle h_i \rangle = \frac{1}{N} \sum_{j, j \neq i}^{N} J_{ij} \langle \sigma_j \rangle = \sum_{\mu=1}^{p} \xi_i^\mu \frac{1}{N} \sum_{j \neq i} \xi_j^\mu \langle \sigma_j \rangle . \tag{1.19}$$

where the couplings J_{ij} have been written according to the Hebb's rule. By exploiting the expression of the overlaps (1.17), Eq. (1.19) reads

$$\langle h_i \rangle = \sum_{\mu=1}^{p} \langle m_\mu \rangle \xi_i^\mu - \frac{p}{N} \langle \sigma_i \rangle . \tag{1.20}$$

In the thermodynamic limit, $N \to +\infty$, and for a finite number of patterns, by plugging Eq. (1.18) and (1.20) in the mean value of the overlaps (1.17), we get

$$\langle m^\mu \rangle = \frac{1}{N} \sum_{i=1}^{N} \xi_i^\mu \tanh \left(\beta \sum_{\mu=1}^{p} \xi_i^\mu \langle m^\mu \rangle \right) , \tag{1.21}$$

In addition, as $N \to +\infty$ and $p/N \to 0$, the sum over i of a function of the p values the various patterns take at site i, say $f(\{\xi_i^\mu\}_{\mu=1,\dots,p})$, is equivalent to the average over the pattern distribution $G(\{\xi^\mu\})$, i.e.

$$\frac{1}{N} \sum_i f(\{\xi_i^\mu\}) \to \sum_{\{\xi^\mu = \pm 1\}} G(\{\xi^\mu\}) f(\{\xi^\mu\}) = 2^{-p} \sum_{\{\xi^\mu = \pm 1\}} f(\{\xi^\mu\}) \equiv \langle\langle f(\xi) \rangle\rangle , \tag{1.22}$$

which is referred to as self-averaging property [1, 2], and can be also seen as an instance of the law of large numbers. In Eq. (1.22), we introduced the notation $\langle\langle \cdot \rangle\rangle$, which identifies the average over the pattern distribution. For the sake of simplicity, we omit the spin average bracket, $\langle \cdot \rangle$, and simply replace $\langle m \rangle$ with m. Thus, the mean value of the overlaps reads

$$m^\mu = \langle\langle \xi^\mu \tanh \left(\beta \vec{\xi} \cdot \vec{m} \right) \rangle\rangle , \tag{1.23}$$

for $\mu = 1, ..., p$, where we have defined $\vec{\xi} = (\xi^1, ..., \xi^p)^T$ and $\vec{m} = (m^1, ..., m^p)^T$.

More formal derivations of Eq. (1.23) can be found in Refs. [1, 2, 32]. Moreover, as shown in Ref. [33], in the thermodynamic limit, and as long as p/N is kept small, the MF approximation captures the exact results when applied to the all-to-all Ising model. As the number of patterns p increases, the model may develop a glassy phase and more complex techniques have to be employed. Furthermore, it can be shown that the various solutions of the Eq. (1.23) correspond to the extrema of the free energy density $FN^{-1} = -(\beta N)^{-1} \log Z(\beta)$ [2, 39], and they can be classified depending on the type of extrema, i.e. minima or maxima, they are related to, as described in the following paragraphs.

Paramagnetic solution

Above the temperature $T_c = 1$, the MF Eq. (1.23) admits a unique solution, corresponding to a unique minimum of the free energy. This solution shows vanishing overlaps, i.e. it reads

$$\vec{m} = (0, 0, ..., 0). \tag{1.24}$$

As a result, a high level of thermal noise implies that at equilibrium the network state is not aligned with any of the p patterns, and no retrieval of information is possible. This state is referred to as a *paramagnetic solution*. Here, the average overlaps between the state of the network and the memories vanish as the dynamical behavior of the network is ergodic.

Retrieval solutions

Below the temperature $T_c = 1$, the paramagnetic solution becomes unstable, while solutions with non-vanishing overlaps appear. In this regime, global minima of the free energy are solutions with only a single non-zero overlap [1]. Considering the number p of overlap variables, and that each one of them can assume both positive and negative values, there are in total $2p$ solutions of this kind. Without loss of generality, we can choose the first overlap to be the finite one, and a generic solution can be written as

$$\vec{m} = (\pm m, 0, ..., 0) \tag{1.25}$$

with m some finite, positive value. Moreover, for vanishing temperature, the attractor state (1.25) is characterized by $m = 1$, this corresponding to a network state that is perfectly aligned (+) or anti-aligned (-) with the pattern. Because of the described phenomenology, the solutions defined by Eq. (1.25) are referred to as *ferromagnetic* or *retrieval solutions*.

At the critical point $\beta_c = 1$, the network undergoes a second order phase transition [33]. The order parameter, i.e. the distinguishing variable between different phases, is the overlap variable m^μ. As displayed in Fig. [1.4],

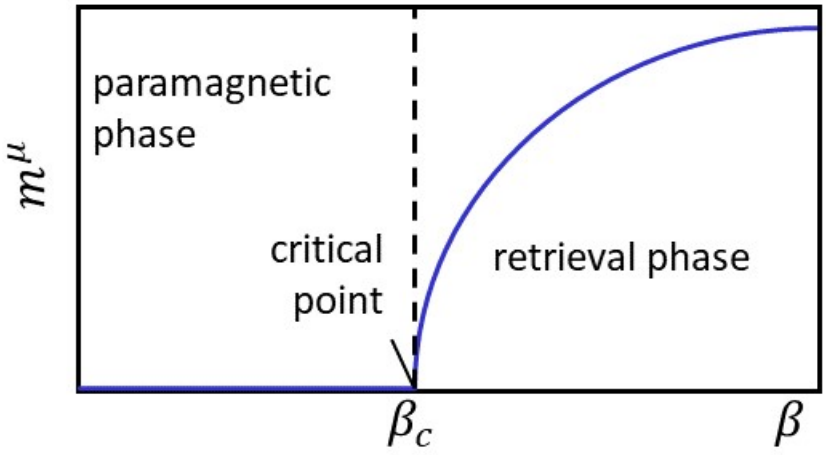


Figure 1.4: **Phase diagram of the Hopfield neural network.** Overlap variables as a function of the inverse temperature. At the critical point, $\beta_c = 1$, a second order phase transition occurs. For $\beta < \beta_c$ the network is in a paramagnetic phase, where all overlaps vainish. For $\beta > \beta_c$ the network is in a retrieval phase, where one of the overlaps (the μ-th in the figure) aquires a finite value, meaning that the corresponding pattern is retrieved.

all overlaps vanish at high temperature ($\beta < \beta_c$), identifying a so-called paramagnetic phase, and only one of the overlaps assumes a finite value below the critical temperature ($\beta > \beta_c$), identifying a so-called retrieval phase. When the system is in the latter phase, a spontaneous symmetry breaking occurs, with the broken symmetries being the Z_2 one and the permutation of different patterns. As a result, ergodicity breaking takes place: the network configurations are dynamically led into restricted subspaces of states, which are characterized by a macroscopic, or finite, overlap with one of the memories.

Spurious solutions

In addition to the retrieval state, for $\beta > \beta_c$, more complicated solutions of the Eq. (1.23) appear. These do not correspond to pure retrieval of memories, and are referred to as spurious solutions.

First of all, there are *symmetric mixture states*, which read

$$\vec{m} = (\underbrace{m, m, ..., m}_{n}, \underbrace{0, 0, ..., 0}_{p-n}), \tag{1.26}$$

and they are a generalization of the mixture states introduced by Eq. (1.9). It can be shown that the even mixture states, i.e. mixture states with an even

n, correspond to unstable solutions. Conversely, odd mixture states are extrema of the free energy landscape, corresponding to local minima for temperatures lower than $T_3 = 0.46$. More specifically, lower n mixture states become stable at higher temperature, e.g. the $n = 3$ odd states at $T < T_3$, the $n = 5$ odd states at $T < T_5 = 0.385$, etc.

Additionally, other spurious states, referred to as *non-symmetric* spurious states, can be identified. The first one ever detected reads

$$\vec{m} = (\frac{1}{2}, \frac{1}{2}, \frac{1}{4}, \frac{1}{4}, \frac{1}{4}, 0, 0, 0, ...). \tag{1.27}$$

At variance with the symmetric states, the non-symmetric ones have not been fully classified nor counted. Nonetheless, none of them is stable above the temperature T_3. Therefore, when the noise level is raised just above the latter temperature, but kept much lower than the critical one, the retrieval quality, i.e. the absolute value of the overlap variable, is about $m = 0.97$.

1.2.4 Storage Capacity

In the previous Section, we treated the problem of pattern retrieval in the limit $p \ll N$. Generalization of the MF analysis to the case in which p is of the order of N can be found in Ref. [1,39,40]. This regime has not been considered in any of the research works described further below in this thesis, so we shall only provide here a basic account.

When p is extensive, it is useful to define the load parameter $\alpha = p/N$, the ratio between the number of patterns to be stored and the number of network components. It can be shown that, upon varying the parameter α, the phase diagram of the Hopfield model becomes richer. In particular, at $T = 0$ there exists a critical value,

$$\alpha_c \approx 0.138, \tag{1.28}$$

above which all the non-trivial solutions $m \neq 0$ disappear. At finite temperature, the critical load parameter depends on the temperature itself, and around the critical value $T_c = 1$ it scales as $\alpha_c(T) \to (1-T)^2$. At any temperature $T < 1$, varying α across the threshold α_c causes a first-order phase transition from a region with $m \neq 0$ towards one characterized by $m = 0$. Such a transition becomes instead continuous at the critical temperature $T_c = 1$ [40].

1.3 Towards a generalization of Hopfield neural networks via quantum systems

In this Chapter we have introduced HNNs as classical spin systems that are able to retrieve stored information, or patterns, in the long-time limit of a

Glauber dynamics. HNNs are among the simplest models of ANNs and lack many of the most advanced features which make ANNs capable of solving complex tasks. However, their intrinsic simplicity makes them the ideal starting point to analyze how NNs may be affected by the introduction of non-standard terms, such as quantum fluctuations.

In the last decades, an increasing theoretical and experimental control on quantum systems and devices gave rise to thriving research on quantum computation. In particular, it has been shown that genuine features of quantum mechanics, such us superposition of states and entanglement, can result in quantum protocols and algorithms that outperform their classical counterpart [3, 4], e.g. the prime number factorization algorithm. In this framework, a relatively recent question, that is triggering interest in the scientific community, is understanding whether quantum effects may be an advantage for neural network computing [10, 14].

With the aim of considering a quantum generalization of HNN, a natural starting point is replacing the ensemble of classical spins that represent neurons, with quantum spin-$1/2$ systems. The second, and less straightforward aspect is translating the non-linear, stochastic dynamics typical of neural networks in the formalism typical of quantum mechanics. Indeed, the latter describes the dynamical evolution by means of unitary operators. In fact, a proposal for overcoming this conceptual problem consists in generalizing HNN by means of Open Quantum Systems (OQS) [11, 14], whose evolution is in general non-unitary, due to their interaction with an environment. The works that are presented in this thesis start from this strategy and develop an analysis of proposals of HNN-like models realized via open quantum system. First, we formulate the HNN dynamics in terms of a quantum master equation that involves coherences, with the aim of comparing the quantum model with the classical counterpart. Eventually, we consider a dynamics realized via an open quantum system of strongly coupled spins and bosons, analyzing similarities and differences with respect to a HNN model. Before describing further such works, in the next Chapter we present the necessary tools for the analysis of the OQS dynamics.

Chapter 2

Open Quantum Systems

In this Chapter we want to introduce the necessary tools for dealing with quantum systems that interact with their quantum surroundings. We will do so, in the spirit that any quantum system is never completely isolated, as it always interacts with a physical environment. Of course, there exist some physical settings where the phenomenology of the system is not severely altered by this interaction: in these cases, the latter can thus be ignored. However, we will neglect such scenarios. Indeed, we will focus on the more general situation where a formalism for dealing with non-isolated quantum systems has proved necessary, such as when considering macroscopic properties of many body systems.

A first approach for treating non-isolated quantum systems consists in the introduction of time-dependent parameters of the Hamiltonian of the system, e.g. oscillating external fields, or randomly fluctuating couplings. Such kind of description is adopted when dealing with an environment that can be regarded as classical, as the operators acting on the Hilbert space of the latter are replaced by c-number parameters, reducing the interaction Hamiltonian to an effectively local one for the sole non-isolated quantum system. However, this case prevents one from taking into account genuine quantum effects that may arise from the generation of entanglement with the environment itself. Indeed, by definition, there cannot be entanglement between a quantum system and a classical one. Here, the quantum system is said to be *closed*, to signify that it is neither isolated, nor open, as further described below.

A more general way to tackle non-isolated quantum systems is considering their interactions with equally quantum surrounding. Thus, we call *open quantum system* (OQS) a non-isolated quantum system that interacts with a quantum environment. The former is further dubbed *principal system* and will be denoted by A in this Chapter, with B its environment. In the next Sections, we will derive an effective evolution restricted to the princi-

pal quantum system A from the higher one governing the evolution of the whole composite one $A \cup B$, and we will focus on the particular dynamics that arises in some relevant physical scenarios, e.g. a large environment that weakly interacts with the principal system.

2.1 Composite quantum system

The states of any isolated, composite quantum system $S = A \cup B$ belong to the tensor product of the Hilbert spaces of its subsystems. If we denote by $\mathcal{H}_S$ the Hilbert space of S, any normalized vector $|\Psi\rangle \in \mathcal{H}_S = \mathcal{H}_A \otimes \mathcal{H}_B$ represents a state of the system S, and vice versa. A generic state $|\Psi\rangle \in \mathcal{H}_S$ can be generally written in terms of two orthonormal bases $\{|\alpha\rangle\}_{\mathcal{H}_A}$ and $\{|\beta\rangle\}_{\mathcal{H}_B}$ on the Hilbert spaces $\mathcal{H}_A$ and $\mathcal{H}_B$, respectively, as

$$|\Psi\rangle = \sum_{\alpha,\beta} c_{\alpha,\beta} |\alpha\rangle \otimes |\beta\rangle , \tag{2.1}$$

where the coefficients $c_{\alpha,\beta}$ have to satisfy $\sum_{\alpha,\beta} |c_{\alpha,\beta}|^2 = 1$. Any state describing an isolated quantum system is dubbed *pure*. From the tensor product structure that is present in Eq. (2.1), we can see that there are some states for which it is not possible to write $|\Psi\rangle$ as a *factorized* state, i.e. as a tensor product of two pure states of the two subsystems, a vector in $\mathcal{H}_A$ and a vector in $\mathcal{H}_B$. In this case, $|\Psi\rangle$ is an *entangled* state.

When dealing with entangled states of S, the notion of physical state for each of the two subsystems is provided in terms of the density operator formalism [41]. States of quantum systems can be in general described in terms of positive, hermitian operators, ρ, acting on their Hilbert spaces, with $\mathrm{Tr}(\rho) = 1$. In the case of an isolated system S in the state $|\Psi\rangle$, the density operator is a projector, i.e. $\rho = |\Psi\rangle \langle\Psi|$. Physical states of either subsystems of $S = A \cup B$ are described in terms of the *reduced density operator*, that for A reads

$$\rho_A = \mathrm{Tr}_B(\rho), \tag{2.2}$$

where Tr_B is the partial trace over the degrees of freedom of the system B. For instance, by choosing the basis $\{|\beta\rangle\}_{\mathcal{H}_B}$, it is $\mathrm{Tr}_B(\cdot) = \sum_\beta \langle\beta| \cdot |\beta\rangle$. The definition (2.2) assures that ρ_A is a hermitian positive operator, with $\mathrm{Tr}_A(\rho_A) = 1$, and thus it defines a density operator. When the state ρ_A cannot be written as a projector onto a single vector, it is said to be *mixed*. It is worth noticing that one can equivalently define the reduced density operator of the subsystem B, and carry out a similar derivation with respect to the two subsystems A and B. However, from now on we will consider A being the principal system and B its quantum environment and we thus shall focus on characterizing the former.

From the properties of a density operator, and the spectral theorem, it follows that there exist an orthonormal basis $\{|\alpha\rangle\}_{\mathcal{H}_A}$ and a set of real, non negative numbers $\{p_\alpha\}$, such that ρ_A can be written as

$$\rho_A = \sum_\alpha p_\alpha |\alpha\rangle \langle\alpha| , \tag{2.3}$$

where $\sum_\alpha p_\alpha = 1$. The number p_α can be interpreted as the probabilities for the principal system A to be in the state $|\alpha\rangle$. It is worth mentioning that this can be recognized as the density matrix often encountered in Statistical Mechanics. The latter deals usually with situations where a detailed description of the environment cannot be known, as for instance it often occurs when $\dim\mathcal{H}_B \gg \dim\mathcal{H}_A$. As a result, the quantum principal system A is usually described in terms of a statistical ensemble $\{|\alpha\rangle , p_\alpha\}$ which gives rise to a density operator that has the form of Eq. (2.3). This kind of density operator, at variance with the reduced one, is not formally derived by tracing away the degrees of freedom of the environment as in Eq. (2.2), being the global state unknown. As a result, in this context may happen that the terms "open system" and "environment" are understood.

When the principal system A is in turn a composite system, e.g. a bipartite one $A = A_1 \cup A_2$, its mixed state ρ_A is dubbed *separable* [42] if it can be written as a convex combination

$$\rho_A = \sum_i p_i \rho^{(i)}_{A_1} \otimes \rho^{(i)}_{A_2} \tag{2.4}$$

where $\rho^{(i)}_{A_{1(2)}}$ is a density operator for $A_{1(2)}$ and $p_i > 0\ \forall i$, and $\sum_i p_i = 1$. If the mixed state ρ_A cannot be written as in Eq. (2.4), ρ_A is dubbed *inseparable*. Despite not being factorized, a separable state is not entangled and yet, it can display quantum correlations [43, 44].

2.2 Dynamics of open quantum systems

Before introducing a description for the dynamics of OQSs, it is useful to recall some basic aspects of the unitary evolution characterizing isolated systems' dynamics. Without loss of generality, we will set $\hbar = 1$.

2.2.1 Dynamical maps for isolated quantum systems

The evolution of an isolated system is given in terms of a unitary evolution. Let us consider the isolated system S with Hamiltonian H in the state $\rho(t_0) = |\Psi(t_0)\rangle \langle\Psi(t_0)|$ at the time t_0. It evolves according to the Liouville-von Neumann equation, which reads

$$\dot{\rho} = -i[H, \rho]. \tag{2.5}$$

A formal solution of this equation reads

$$\rho(t) = U_{(t,t_0)}\rho(t_0)U^{\dagger}_{(t,t_0)} \tag{2.6}$$

where $U_{(t,t_0)}$ is the time-dependent, unitary evolution operator, with $U_{(t_0,t_0)} = 1$. The Eq. (2.6) can be also written as

$$\rho(t) = \mathcal{U}_{(t,t_0)}[\rho(t_0)], \tag{2.7}$$

where we have defined $\mathcal{U}_{(t,t_0)}[\cdot] = U_{(t,t_0)}[\cdot]U^{\dagger}_{(t,t_0)}$. In order to be more precise, given a Hilbert space $\mathcal{H}$, we can identify the set of trace-class operators $\{O\}$, i.e. the set of operators such that $\mathrm{Tr}(OO^{\dagger})$ is finite. This set is usually referred to as the *Liouville space*, and it is indicated by $L(\mathcal{H})$. The operator $\mathcal{U}_{(t,t_0)}$ is a linear map that acts on the Liouville space of the density operators, $\mathcal{U}_{(t,t_0)} : L(\mathcal{H}_S) \to L(\mathcal{H}_S)$, and it is said to be a *dynamical map* [12]. Let us consider the following definition

Definition 2.2.1. A dynamical map is said to be a *universal* dynamical map (**UDM**) if it is independent of the state it acts upon.

According to this definition, the dynamical map $\mathcal{U}_{(t,t_0)}$ is a UDM. In general, operators acting on a space of operators, like the dynamical map $\mathcal{U}_{(t,t_0)}$ does, are dubbed *superoperators*.

2.2.2 Dynamical maps for open quantum systems

As we mentioned above, an OQS is a quantum system interacting with an equally quantum environment. The starting point of our discussion will be that the environment is as large as required to include everything which significantly interacts with it, so that we can consider the larger system $S = A \cup B$ isolated.

Let us consider the system S, in the initial state $\rho(t_0) = |\Psi(t_0)\rangle \langle\Psi(t_0)|$. From Eq. (2.6), the reduced density matrix of the principal system A has evolved at the time t to

$$\rho_A(t) = \mathrm{Tr}_B[U_{(t,t_0)}\rho(t_0)U^{\dagger}_{(t,t_0)}], \tag{2.8}$$

which defines a dynamical map, acting on $L(\mathcal{H}_{\mathcal{A}})$, that connects the states of the subsystem A at times t_0 and t. We shall denote this map as

$$\rho_A(t) = \mathcal{M}_{(t,t_0)}[\rho_A(t_0)], \tag{2.9}$$

where $\rho_A(t_0) = \mathrm{Tr}_B[\rho(t_0)]$. The main difference between the dynamical map for an isolated system's dynamics, as defined by Eq. (2.7), and the dynamical map $\mathcal{M}_{(t,t_0)}$ is that, in general, the latter depends also on the initial global

state upon which it acts [12], i.e. it is not universal. In order to clarify better this point, let us consider the initial state of the isolated system S as

$$\rho(t_0) = \rho_A(t_0) \otimes \rho_B(t_0) + \rho_{corr}(t_0), \tag{2.10}$$

where $\rho_{corr}(t_0)$ contains all the correlations between the two subsystems A and B and satisfies $\mathrm{Tr}_A[\rho_{corr}(t_0)] = \mathrm{Tr}_B[\rho_{corr}(t_0)] = 0$ [45]. By applying Eq. (2.8), the reduced density operator $\rho_A(t)$ reads

$$\rho_A(t) = \sum_b K_b(t,t_0)\rho_A(t_0)K_b(t,t_0)^\dagger + \delta\rho(t,t_0), \tag{2.11}$$

with $b = \{\beta, \beta^{'}\}$, $K_{\{\beta,\beta'\}}(t,t_0) = \sqrt{p_\beta}\,\langle\phi_\beta|U_{(t,t_0)}|\phi_{\beta'}\rangle$, and we have used the spectral decomposition (2.3) for the state $\rho_B(t_0)$. From Eq. (2.11), we can see that $\rho_A(t)$ is the sum of two terms. The first one, originating from the separable part of the global initial state $\rho(t)$, represents an action on $\rho_A(t_0)$ independent of $\rho_A(t_0)$ itself. However, the second term, that reads $\delta\rho(t,t_0) = \mathrm{Tr}_B[U_{(t,t_0)}\rho_{corr}(t_0)U^\dagger_{(t,t_0)}]$, cannot be represented as an action of a UDM on $\rho_A(t_0)$. This means that a dynamical map $\mathcal{M}_{(t,t_0)}$, with some values of $K_b(t,t_0)$ and $\delta\rho(t,t_0)$, may describe a physical evolution for some states $\rho_A(t_0)$ and a non-physical one for others, as different initial states will evolve under different maps.

In general, it is possible to show that if and only if the initial global state $\rho(t_0)$ is factorized, [$\rho_{corr}(t_0) = 0$ in Eq. (2.10)], then the time evolution of A from t_0 to t is given in terms of a UDM, $\mathcal{E}_{(t,t_0)} : \rho_A(t_0) \to \rho_A(t) \equiv \mathcal{E}_{(t,t_0)}[\rho_A(t_0)]$, such that

$$\rho_A(t) = \sum_b K_b(t,t_0)\rho_A(t_0)K_b(t,t_0)^\dagger, \tag{2.12}$$

with the equality

$$\sum_b K_b^\dagger(t,t_0)K_b(t,t_0) = \mathbb{I}, \tag{2.13}$$

that has to be fulfilled to ensure that that $\mathrm{Tr}[\rho_A(t)] = 1$ [12]. The set of operators $\{K_b\}$ are called *Kraus operators* [12,41], and the expression of the UDM map in terms of the Kraus operators (2.12) is dubbed Kraus decomposition.

The importance for a dynamical map of being universal is that UDMs evolve unambiguously any principal system physical state into another physical state; the latter statement is mathematically expressed as follows. For each (t,t_0), a UDM $\mathcal{E}$ such that $\mathcal{E}_{(t,t_0)} : \rho_A(t_0) \to \rho_A(t) \equiv \mathcal{E}_{(t,t_0)}[\rho_A(t_0)]$ satisfies [12,13,41]:

Property 1. $\mathrm{Tr}[\mathcal{E}(\rho)] = 1$, i.e. it is *trace preserving*;

Property 2. $\mathcal{E}$ is a *convex linear map*, so that $\mathcal{E}\left(\sum_i p_i \rho_A^{(i)}\right) = \sum_i p_i \mathcal{E}\left(\rho_A^{(i)}\right)$, with $p_i \geq 0$ and $\sum_i p_i = 1$;

Property 3. $\mathcal{E}$ is a *completely positive* (**CP**) map, i.e. the map $(\mathcal{E} \otimes \mathbb{I}_n)$, is a positive map $\forall n \geq 1$, where $\mathbb{I}_n$ is the identity map on $\mathbb{C}^n$.

In defining the last property one considers that the global isolated system is made of a principal one, A, and an inert n-dimensional ancilla. As the map $\mathcal{E}$ rules the dynamics of the system A, the time-evolution of the compound system is given by $\mathcal{E} \otimes \mathbb{I}_n$. The Property 3 prevents the possibility that the latter map becomes non-positive, i.e. it prevents the non-physical situation such that, if another system not interacting with A is brought into the picture, the dynamics becomes non-physical.

If a linear map is a UDM, it is also completely positive and trace preserving (**CPT**). It has been proved that also the converse statement, i.e. that any linear, completely positive and trace-preserving map is a UDM [12, 46]. Indeed, some textbooks define UDMs as trace preserving linear maps which are completely positive (see for instance [13]).

To summarize, we have seen that, for a generic composite system evolution, the reduced density operator evolves in terms of a UDM if and only if the initial global state is in a tensor product form, or, equivalently, if the dynamical map can be written in terms of the Kraus decomposition (2.12).

2.2.3 Temporal continuity

An important problem of the reduced density operator evolution arises when considering compositions of the reduced evolutions. This can be formulated as follows: let us consider the initial global state of the composite system $S = A \cup B$ at the time t_0 as a factorized state. Thus, the principal system A will evolve to a time t_1 by means of a UDM, $\mathcal{E}_{(t_1,t_0)}$. Equivalently, the evolution from t_0 to a time $t_2 > t_1$ is ruled by a UDM, $\mathcal{E}_{(t_2,t_0)}$. One may expect that the evolution from the time t_0 to the time t_2 would be given in terms of the composition of the map $\mathcal{E}_{(t_1,t_0)}$ with a second, UDM map between the times t_1 and t_2, i.e. that $\mathcal{E}_{(t_2,t_0)} = \mathcal{E}_{(t_2,t_1)} \circ \mathcal{E}_{(t_1,t_0)}$. However, it is worth noticing that even if the initial global state is factorized, due to the dynamical generation of entanglement, the final state at t_1 will in general contain quantum correlations. This situation prevents one to derive a UDM describing the reduced evolution for some intermediate time, i.e. it is

$$\mathcal{E}_{(t_2,t_0)} \neq \mathcal{E}_{(t_2,t_1)} \circ \mathcal{E}_{(t_1,t_0)}, \tag{2.14}$$

with the reduced dynamics at the intermediate time t_1 given in terms of a non-universal map, $\mathcal{M}_{(t_2,t_1)}$ [12]. The condition (2.14) defines a *non-markovian*

evolution, as it implies that the state of an OQS at a certain time t depends on the whole history of its past evolution and not just on the previous configuration at $t - \delta t$. As entanglement can be considered a key feature of states characterizing OQSs, non-markovianity, which originates from the dynamical generation of entanglement itself, is the key feature of OQSs dynamics.

As a consequence, in general it is not possible to define a differential equation for $\rho_A(t)$ that is local in time, namely a Master Equation for the evolution of the principal system. In fact, there are some physical situations in which one can introduce approximations such that markovianity is restored, as we will see in the next Sections.

2.3 Markovian approximation for open quantum system dynamics

Some remarkable approximations that are employed for describing the OQS dynamics allows one to restore the property of *markovianity*, or *divisibility condition*. A quantum system undergoes a *markovian* evolution if the composition law for UDMs is recovered,

$$\mathcal{E}_{(t,t_0)} = \mathcal{E}_{(t,s)} \circ \mathcal{E}_{(s,t_0)}, \tag{2.15}$$

i.e. if the set of maps $\{\mathcal{E}_{(t,s)}\}$, with $t > s$, is provided with a semigroup structure, being $\mathcal{E}_{s,s} = \mathbb{I}$ the identity element.

We stress that, as the dynamics of an OQS is in general non-markovian, the condition (2.15) can result only from an approximation performed on the original dynamics. However, the advantage is the derivation of a differential equation for the dynamical evolution of the reduced density operator. Indeed, let us assume that Eq. (2.15) holds, and consider, for $\epsilon > 0$, the following difference

$$\rho_A(t+\epsilon) - \rho_A(t) = [\mathcal{E}_{(t+\epsilon,0)} - \mathcal{E}_{(t,0)}]\rho_A(0) = [\mathcal{E}_{(t+\epsilon,t)} - \mathbb{I}]\mathcal{E}_{(t,0)}\rho_A(0) = [\mathcal{E}_{(t+\epsilon,t)} - \mathbb{I}]\rho_A(t). \tag{2.16}$$

Provided that the limit $\epsilon \to 0$ is well defined, we can now derive a differential equation for the reduced density operator, i.e. a master equation, as

$$\dot{\rho}_A(t) = \lim_{\epsilon \to 0} \frac{\rho_A(t+\epsilon) - \rho_A(t)}{\epsilon} = \lim_{\epsilon \to 0} \frac{[\mathcal{E}_{(t+\epsilon,t)} - \mathbb{I}]}{\epsilon} \rho_A(t) \equiv \mathcal{L}_t[\rho_A(t)], \tag{2.17}$$

where $\mathcal{L}_t = \lim_{\epsilon \to 0} [\mathcal{E}_{(t+\epsilon,t)} - \mathbb{I}]/\epsilon$ is dubbed *generator* of the evolution [12,13].

2.3.1 GKSL master equation

The the most general form of a markovian master equation that follows the assumption (2.15) on a UDM (i.e. CPT map) can be written as [12, 13]

$$\dot{\rho}_A(t) = -i[H(t), \rho_A(t)] + \sum_k \gamma_k(t) \left[V_k(t)\rho_A(t)V_k^\dagger(t) - \frac{1}{2}\{V_k^\dagger(t)V_k(t), \rho_A(t)\} \right], \tag{2.18}$$

where $H(t)$ and $V(t)$ are time-dependent operators, with $H(t) = H(t)^\dagger$ and $\gamma_k(t) \geq 0$ for every k and t. This result is a generalization of the famous Gorini, Kossakowski, Sudarshan and Lindblad (GKSL) master equation [47, 48], that has been derived in the case of time-homogeneity. That is, when the family of UDMs $\mathcal{E}_{(t,t_0)}$ satisfying the property (2.15) depends only on the difference $\tau = t - t_0$. In this case, it represents a one-parameter family of dynamical maps that defines a semigroup, dubbed *quantum dynamical semigroup* [1], where the identity element is $\mathcal{E}_{(t_0,t_0)} = \mathbb{I}$. Under the continuity assumption, the markovian UDM can be defined as $\mathcal{E}_\tau[\cdot] = e^{\mathcal{L}\tau}[\cdot]$, where the generator $\mathcal{L}$ is time independent, and Eq. (2.18) reads

$$\dot{\rho}_A(t) = \mathcal{L}[\rho_A(t)] = -i[H, \rho_A(t)] + \mathcal{D}[\rho_A(t)], \tag{2.19}$$

where we have defined

$$\mathcal{D}[\rho_A(t)] = \sum_k \gamma_k \left[V_k \rho_A(t) V_k^\dagger - \frac{1}{2}\left\{ V_k^\dagger V_k, \rho_A(t) \right\} \right] \tag{2.20}$$

that is usually referred to as *dissipator*. The operators V_k are also called *Lindblad* or *jump operators*.

The form of the generator $\mathcal{L}$ does not uniquely fix the form of the operators H and V_k. Indeed, it is invariant under the following transformations:

- unitary transformations on the Lindblad operators:

$$\sqrt{\gamma_k} V_k \to \sqrt{\gamma'_k} V'_k = \sum_j u_{kj} \sqrt{\gamma_j} V_j, \tag{2.21}$$

  where $(u^{-1})_{kj} = u^*_{jk}$;

- inhomogeneous transformations:

$$\begin{aligned} V_k &\to V'_k = V_k + c_k, \\ H &\to H' = H + \frac{1}{2i} \sum_k \gamma_k \left(c_k^* V_k - c_k V_k^\dagger \right) + d, \end{aligned} \tag{2.22}$$

  where c_k are complex numbers, and d is real.

[1] The quantum dynamical semigroup cannot be a group because in general the inverse of a UDM is not a UDM.

Steady state of GKSL equation

Let us now see what the long-time properties are of a homogeneous markovian process defined by an equation in GKSL form.

In general, a completely positive semigroup $\mathcal{E}_\tau = e^{\mathcal{L}\tau}$ is said to relax to a steady state if there exists a unique state $\rho_{\rm ss}$ such that

$$\mathcal{E}_\tau(\rho_{\rm ss}) = \rho_{\rm ss}\ \forall\tau \tag{2.23}$$

$$\lim_{\tau\to+\infty} \mathcal{E}_\tau(\rho) = \rho_{\rm ss},\ \forall\rho. \tag{2.24}$$

From Eq. (2.24), it follows that a steady state $\rho_{\rm ss}$ is an eigenoperator of the UDM $\mathcal{E}_\tau$ with eigenvalue one, and thus it is an eigenoperator of the generator $\mathcal{L}$ with zero eigenvalue,

$$\mathcal{L}(\rho_{\rm ss}) = 0. \tag{2.25}$$

It is worth noticing that if this equation admits more than one solution, the semigroup $\mathcal{E}_t$ is not relaxing. To this regard, it is possible to show that necessary and sufficient condition for a completely positive semigroup to relax is that the generator has a non-degenerate zero eigenvalue, and the rest of the eigenvalues has negative real part.

An important theorem that assures that the semigroup is relaxing, given some conditions on the structure of the generator is the following [49]:

Theorem 2.3.1. *Consider a completely positive semigroup $\mathcal{E}_\tau = e^{\mathcal{L}\tau}$ with generator*

$$\mathcal{L}[\cdot] = -i[H,\cdot] + \sum_{k\in I}\gamma_k\left[V_k(\cdot)V_k^\dagger - \frac{1}{2}\{V_k^\dagger V_k,\cdot\}\right]. \tag{2.26}$$

A sufficient condition for the map $\mathcal{E}_\tau$ to relax is that the set $\{V_k, k\in I\}$ is self-adjoint, (the adjoint of every element of the set is inside of the set), and the only operators commuting with all of them are proportional to the identity.

2.3.2 Microscopic derivation

Until now we have seen that if the initial state of a compound system is factorized, its evolution is ruled by a UDM. Moreover, when a homogeneous Markov process approximates such evolution, the most general form of the dynamical map is given by the GKSL equation. However, it would be useful to know, when the microscopic details of a quantum system are considered, if it is possible to derive a master equation of the type (2.19). To clarify this point, in this Section we review the conditions for which a UDM can be approximated by a quantum Markov process, when starting from a microscopic description of a composite system.

Nakajima-Zwanzig projection technique

Let us consider the compound system $S = A \cup B$, with A the principal system and B playing the role of the environment, with the total Hamiltonian being

$$H = H_A + H_B + V, \tag{2.27}$$

where H_A (H_B) is the Hamiltonians of the subsystem A (B), and V encodes their interaction.

In the following, we retrace the approach of Nakajima and Zwanzig [50, 51], that is explained in more detail in Refs. [12,13] among others. We introduce the projection operators $\mathcal{P}$, $\mathcal{Q}$, with $\mathcal{P}^2 = \mathcal{P}$, $\mathcal{Q}^2 = \mathcal{Q}$, and $\mathcal{P}\mathcal{Q} = \mathcal{Q}\mathcal{P} = 0$ as

$$\mathcal{P}[\rho] = \mathrm{Tr}_B(\rho) \otimes \rho_B, \tag{2.28}$$

$$\mathcal{Q}[\rho] = (\mathbb{I} - \mathcal{P})[\rho], \tag{2.29}$$

where ρ is the state of the total system, and ρ_B, the environmental state, is chosen to be, without loss of generality, the physical initial state of the environment. This is further assumed to be a thermal state, $\rho_B = \rho_{\mathrm{th}} = e^{-\beta H_B}/[\mathrm{Tr}(e^{-\beta H_B})]$. Furthermore, we consider the interaction picture, that will be identified by the notation $\tilde{(\cdot)}$, e.g. $\tilde{\rho}(t) = e^{i(H_A+H_B)t}\rho(t)e^{-i(H_A+H_B)t}$ for the density operator. In the interaction picture, projecting the von Neumann Eq. (2.5) by means of $\mathcal{P}$ and $\mathcal{Q}$, it is

$$\frac{d}{dt}\mathcal{P}[\tilde{\rho}(t)] = -i\mathcal{P}\left[[\tilde{V}(t), \tilde{\rho}(t)]\right], \tag{2.30}$$

$$\frac{d}{dt}\mathcal{Q}[\tilde{\rho}(t)] = -i\mathcal{Q}\left[[\tilde{V}(t), \tilde{\rho}(t)]\right]. \tag{2.31}$$

By using the notation $\mathcal{V}(t)[\cdot] = -i[\tilde{V}(t), \cdot]$ and exploiting that $\mathcal{P} + \mathcal{Q} = \mathbb{I}$, the above equations can be written as

$$\frac{d}{dt}\mathcal{P}[\tilde{\rho}(t)] = \mathcal{P} \circ \mathcal{V}(t) \circ \mathcal{P}[\tilde{\rho}(t)] + \mathcal{P} \circ \mathcal{V}(t) \circ \mathcal{Q}[\tilde{\rho}(t)], \tag{2.32}$$

$$\frac{d}{dt}\mathcal{Q}[\tilde{\rho}(t)] = \mathcal{Q} \circ \mathcal{V}(t) \circ \mathcal{P}[\tilde{\rho}(t)] + \mathcal{Q} \circ \mathcal{V}(t) \circ \mathcal{Q}[\tilde{\rho}(t)]. \tag{2.33}$$

The solution of the second equation can be written formally as

$$\mathcal{Q}[\tilde{\rho}(t)] = \mathcal{G}(t,0) \circ \mathcal{Q}[\tilde{\rho}(0)] + \int_0^t ds \mathcal{G}(t,s) \circ \mathcal{Q} \circ \mathcal{V}(s) \circ \mathcal{P}[\tilde{\rho}(s)], \tag{2.34}$$

where $\mathcal{G}(t,s) = \mathcal{T}e^{\int_s^t dt' \mathcal{Q} \circ \mathcal{V}(t')}$ is the propagator associated to the homogeneous equation $\frac{d}{dt}\mathcal{Q}[\tilde{\rho}(t)] = \mathcal{Q} \circ \mathcal{V}(t) \circ \mathcal{Q}[\tilde{\rho}(t)]$. Inserting the expression (2.34) into (2.32), one gets the generalized Nakajima-Zwanzig equation, which reads

$$\begin{aligned}\frac{d}{dt}\mathcal{P}[\tilde{\rho}(t)] = \mathcal{P} \circ \mathcal{V}(t) \circ \mathcal{P}[\tilde{\rho}(t)] + \mathcal{P} \circ \mathcal{V}(t) \circ \mathcal{G}(t,0) \circ \mathcal{Q}[\tilde{\rho}(0)] \\ + \int_0^t du \mathcal{P} \circ \mathcal{V}(t) \circ \mathcal{G}(t,u) \circ \mathcal{Q} \circ \mathcal{V}(u) \circ \mathcal{P}[\tilde{\rho}(u)].\end{aligned} \tag{2.35}$$

Under the assumptions that the initial state is factorized, $\rho(0) = \rho_A(0) \otimes \rho_B(0)$, so that $\mathcal{Q}[\rho(0)] = 0$, and assuming also $\mathcal{P} \circ \mathcal{V}(t) \circ \mathcal{P} = 0$, one gets the following integro-differential equation

$$\frac{d}{dt}\mathcal{P}[\tilde{\rho}(t)] = \int_0^t du \mathcal{K}(t,u) \circ \mathcal{P}[\tilde{\rho}(u)], \tag{2.36}$$

where

$$\mathcal{K}(t,u) = \mathcal{P} \circ \mathcal{V}(t) \circ \mathcal{G}(t,u) \circ \mathcal{Q} \circ \mathcal{V}(u). \tag{2.37}$$

In order to transform the integro-differential equation (2.36) in a markovian master equation, one may intuitively ask that the kernel $\mathcal{K}$ behaves as a delta function for the state $\tilde{\rho}(u)$. That implies that the typical variation time τ_A of the projection of $\tilde{\rho}(u)$ has to be much larger than the time, say τ_B, characterizing the speed at which the kernel is vanishing in the regime $|t-u| \gg 1$. For this approximation to hold, some assumptions are made that involve the size of the environment and the couplings of the Hamiltonian. In the next Section we will give a brief account on one of the possible limiting procedures that studies the case $\tau_A/\tau_B \to +\infty$ under some further conditions, and which is referred to as the *weak coupling limit* [52, 53].

Weak coupling limit

Let us consider the interaction term V of the Hamiltonian, and let us rewrite it as

$$V \to \alpha V, \tag{2.38}$$

where α accounts for the strength of the interaction, or interaction coupling. The weak coupling limit relies on the fact that, for small values of the interaction coupling α, the variation of $\tilde{\rho}(u)$ is going to be slow, and in the limit $\alpha \to 0$ one would get $\tau_A \to +\infty$, and thus $\tau_A/\tau_B \to +\infty$, for every fixed τ_B. As in the case $\alpha = 0$ there is no interaction, the time parameter has to be rescaled appropriately before taking the limit. In the following, we review the procedure that allows one to derive the GKSL Eq. (2.19), starting from the integro-differential Eq. (2.36). A more detailed discussion can be found in Refs. [12, 13].

Firstly, we exploit the von Neumann equation for the whole state $\tilde{\rho}(t)$ in the interaction picture. This implies that a unitary solution connects the whole state at the time t and u as $\tilde{\rho}(u) = \tilde{\mathcal{U}}(u,t)[\tilde{\rho}(t)]$. Secondly, in Eq. (2.36) a perturbative expansion of the superoperators $\mathcal{G}(t,u)$ and $\mathcal{U}(u,t)$ with respect to the coupling α is performed. By substituting $u \to t-u$, at the order $O(\alpha^2)$, Eq. (2.36) becomes

$$\dot{\tilde{\rho}}_A(t) \approx -\alpha^2 \int_0^t du \mathrm{Tr}_B \left[\tilde{V}(t), \left[\tilde{V}(t-u), \tilde{\rho}_A(t) \otimes \rho_B\right]\right]. \tag{2.39}$$

The dynamical map resulting from this equation, dubbed *Redfield equation*, does not meet the requirement of a completely positive map. We thus proceed further in performing the limiting procedure. Let us first reformulate the above expression: The interaction Hamiltonian can be written as $V = \sum_k A_k \otimes B_k$, with $A_k = A_k^\dagger$ and $B_k = B_k^\dagger$. We also consider a discrete spectrum for the Hamiltonian H_A, whose eigenstates and eigenenergies are $\{|\psi_\varepsilon\rangle\}$, $\{\varepsilon\}$, respectively. Thus, the eigenoperators of H_A read $A_k(\omega) = \sum_{\varepsilon'-\varepsilon=\omega} |\psi_\varepsilon\rangle\langle\psi_\varepsilon| A_k |\psi_{\varepsilon'}\rangle\langle\psi_{\varepsilon'}|$, where the sum runs over all the possible energy differences $\varepsilon' - \varepsilon = \omega$ of the system A. The interaction Hamiltonian in the interaction picture can be written as $\tilde{V}(t) = \sum_{k,\omega} e^{-i\omega t} A_k(\omega) \otimes B_k(t)$. Thus, Eq. (2.39) can be reformulated as

$$\dot{\tilde{\rho}}_A(t) \approx \alpha^2 \sum_{\omega,\omega'} \sum_{k,l} e^{i(\omega-\omega')t} \Gamma_{kl}^t(\omega) [A_l(\omega)\tilde{\rho}_A(t), A_l^\dagger(\omega')] + \text{h.c.}, \tag{2.40}$$

where, exploiting the fact that ρ_B commutes with $e^{iH_B t}$, it is

$$\Gamma_{kl}^t(\omega) = \int_0^t du\, e^{i\omega u} \text{Tr}_B \left[\tilde{B}_k(u) B_l \rho_B\right]. \tag{2.41}$$

In order to obtain a markovian evolution, let us consider a rescaled time $\tau = \alpha^2 t$, and take the limit $\alpha \to 0$. In this way, it is possible to let the upper limit of the integral (2.41) go to infinity. However, as it is shown in Ref. [12], a necessary condition for making the resulting integral convergent, is that the system B has to have infinite degrees of freedom, in such a way that H_B has a continuous spectrum. The expression resulting from Eq. (2.40) is sometimes obtained by applying a series of approximations named *Born-Markov* approximation, that can be found in Ref. [13].

In order to obtain the form of the generator as in Eq. (2.19), a *secular approximation* is further applied, which consists in taking the oscillatory factors in Eq. (2.40) to be vanishing. The underlying physical condition is that the inverse frequency differences involved, $|\omega - \omega'|^{-1}$, are much smaller than the typical relaxation time of the system. If this is the case, the final equation reads

$$\dot{\tilde{\rho}}_A(\tau) \approx \sum_{\omega} \sum_{k,l} \Gamma_{kl}^\infty(\omega) [A_l(\omega)\tilde{\rho}_A(\tau), A_k^\dagger(\omega)] + \text{h.c.} = \tilde{\mathcal{L}}[\tilde{\rho}_A(\tau)]. \tag{2.42}$$

To see that the generator $\tilde{\mathcal{L}}$ has the correct form of a markovian master equation (2.19), the terms $\Gamma_{kl}^\infty(\omega)$ are decomposed in the sum of an Hermitian and anti-Hermitian part,

$$\begin{aligned} \gamma_{kl}(\omega) &= \Gamma_{kl}^\infty(\omega) + \Gamma_{lk}^{\infty *}(\omega), \\ S_{kl}(\omega) &= \frac{1}{2i}[\Gamma_{kl}^\infty(\omega) - \Gamma_{lk}^{\infty *}(\omega)], \end{aligned} \tag{2.43}$$

as $\Gamma^{\infty}_{k,l}(\omega) = \frac{1}{2}\gamma_{kl}(\omega) + iS_{kl}(\omega)$. With these definitions, and going back to the Schrodinger picture, the master equation reads

$$\dot{\rho}_A(t) = -i[H_A + \alpha^2 H_{LS}, \rho_A(t)] + \mathcal{D}[\rho_A(t)], \tag{2.44}$$

where H_{LS} is defined as $H_{LS} = \sum_{\omega}\sum_{k,l} S_{kl}(\omega)A^{\dagger}_k(\omega)A^{\dagger}_l(\omega)$. As it commutes with H_A, it just produces a shift in the energy levels of A. For this reason, it is usually dubbed Lamb shift Hamiltonian. However, it is worth pointing out that the produced shift may not be the same for all levels, meaning that in general this is not a constant term. The dissipator term reads

$$\mathcal{D}[\rho_A(t)] = \alpha^2 \sum_{\omega}\sum_{k,l} \gamma_{kl}(\omega)\left[A_l(\omega)\rho_A(t)A^{\dagger}_l(\omega) - \frac{1}{2}\left\{A^{\dagger}_k(\omega)A_l(\omega), \rho_A(t)\right\}\right], \tag{2.45}$$

and can be easily expressed in the form (2.20) by diagonalizing the matrices $\gamma_{kl}(\omega)$. For the sake of clarity, we point out that, in order to prove that the generator in Eq. (2.45) has the form of a markovian homogeneous evolution, it is necessary that $\gamma_{kl}(\omega)$ are positive semidefinite matrices, $\forall\omega$. As explained in detail in Ref. [12], this can be shown by means of the Bochner theorem.

To conclude this Chapter, we name here two of the most common cases where the weak coupling limit procedure allows one to derive a GKSL equation. Let us consider a two-level system, playing the role of the principal system A, damped by a bath of harmonic oscillators B, that represents the quantum environment. The Hamiltonian of the system reads

$$\begin{aligned} H =& H_A + H_B + V \\ =& \frac{\omega_0}{2}\sigma^z + \int_0^{\omega_{\max}} d\omega a^{\dagger}_{\omega}a_{\omega} + \int_0^{\omega_{\max}} d\omega h(\omega)(\sigma^{+}a_{\omega} + \sigma^{-}a^{\dagger}_{\omega}), \end{aligned} \tag{2.46}$$

where σ^{α}, for $\alpha = x, y, z$, are the Pauli operators, with $\sigma^{\pm} = (\sigma^x \pm i\sigma^y)/2$, and a_{ω}, $a^{\dagger}_{\omega}$ are the annihilation and creation bosonic operators, with $[a_{\omega}, a^{\dagger}_{\omega'}] = \delta(\omega - \omega')$. The frequency ω_0 is the splitting of the two level system, ω is the frequency of each bosonic mode, with $\omega_{\max}$ being the maximum frequency present in the bath. By following the weak coupling limiting procedure, the time evolution of the system A is described by the master equation of the type (2.19). By neglecting the Lamb shift Hamiltonian term H_{LS}, it is

$$\begin{aligned} \dot{\rho}_A(t) = -i\left[\frac{\omega_0}{2}\sigma^z, \rho_A(t)\right] &+\Gamma[\bar{n}(\omega_0) + 1]\left(\sigma^{-}\rho_A(t)\sigma^{+} - \frac{1}{2}\left\{\sigma^{+}\sigma^{-}, \rho_A(t)\right\}\right) \\ &+\Gamma\bar{n}(\omega_0)\left(\sigma^{+}\rho_A(t)\sigma^{-} - \frac{1}{2}\left\{\sigma^{-}\sigma^{+}, \rho_A(t)\right\}\right), \end{aligned} \tag{2.47}$$

where $\Gamma = 2\pi J(\omega_0)$, being $J(\omega_0) = h^2(\omega_0)$ the spectral density of the bath at frequency ω_0, and $\bar{n}(\omega_0)$ is the mean number of bosons in thermal state ρ_B of the bath with frequency ω_0, i.e. $\bar{n}(\omega_0) = (e^{\omega_0\beta} - 1)^{-1}$.

A similar case is the one of a principal system A made of an harmonic oscillator at frequency ω_0, which is damped by a bath of harmonic oscillators, with Hamiltonian

$$\begin{aligned} H =& H_A + H_B + V \\ =& \omega_0 a^\dagger a + \int_0^{\omega_{\max}} d\omega a_\omega^\dagger a_\omega + \int_0^{\omega_{\max}} d\omega h(\omega)(a^\dagger a_\omega + a a_\omega^\dagger). \end{aligned} \tag{2.48}$$

Here, by following the procedure of the weak coupling case, the master equation reads

$$\begin{aligned} \dot{\rho}_A(t) = -i\left[\omega_0 a^\dagger a, \rho_A(t)\right] &+ \Gamma[\bar{n}(\omega_0)+1]\left(a\rho_A(t)a^\dagger - \frac{1}{2}\left\{a^\dagger a, \rho_A(t)\right\}\right) \\ &+ \Gamma\bar{n}(\omega_0)\left(a^\dagger \rho_A(t) a - \frac{1}{2}\left\{a a^\dagger, \rho_A(t)\right\}\right), \end{aligned} \tag{2.49}$$

where, as in the previous case, we have neglected the Lamb shift Hamiltonian.

Chapter 3

A spin-boson Hamiltonian: The Dicke model

This Chapter introduces a physical model made of ensembles of two-level systems interacting with bosonic degrees of freedom, described by a spin-boson Hamiltonian widely known as the Dicke model.

In general, in the last few decades, the study of the spin-boson Hamiltonians received a significant boost, in relation to the study of quantum matter in and out of equilibrium. Indeed, spin-boson Hamiltonians represent an effective description for numerous quantum many-body systems, such as atoms interacting with photons, or phonon modes in ion crystals. As a result, they are of particular relevance in modeling systems and phenomena such as cavity, waveguide electrodynamics and trapped ion systems, which are prominent platforms for implementing quantum simulations.

The end of this Chapter describes an important result which connects the equilibrium properties of the Dicke model with those of an associative memory as described by the Hopfield model. This result can be considered as the starting point of our work and has indeed inspired its development.

3.1 Equilibrium Dicke model

One of the most fundamental spin-boson Hamiltonians is the so-called Dicke model, that describes N spin-$1/2$ particles interacting with a multi-mode bosonic field. The Hamiltonian of this model reads

$$H_{\text{Dicke}} = \sum_{\mu=1}^{p} \omega_\mu a_\mu^\dagger a_\mu + \Omega \sum_{i=1}^{N} s_i^z + \tilde{g} \sum_{\mu=1}^{p} \sum_{i=1}^{N} (a_\mu^\dagger + a_\mu)(s_i^+ + s_i^-), \tag{3.1}$$

where s_i^α, with $\alpha = x, y, z$, are spin-$1/2$ operators referring to the i-th spin, their commutation relations being $[s_i^\alpha, s_j^\beta] = i\epsilon_{\alpha\beta\gamma} s_i^\gamma \delta_{ij}$, and $\epsilon_{\alpha\beta\gamma}$ is the Levi-Civita symbol; $a_\mu^\dagger$, a_μ are the annihilation and creation operator for the μ-th

bosonic mode, with $[a_\mu, a^\dagger_{\mu'}] = \delta_{\mu\mu'}$. The parameter ω_μ is the frequency of the μ-th bosonic mode, Ω is the frequency of the splitting of the spin $1/2$ levels, and $\tilde{g}$ represents the interaction coupling. It is worth mentioning that this Hamiltonian is invariant under the Z_2 transformation $a_\mu \to -a_\mu$ and $s_i^{x,y} \to -s_i^{x,y}$.

The model was first introduced by Dicke [20] for describing the emission of light by a collection of N atoms that individually interact with a common light field. Dicke showed that, if the separation of the atoms is kept much smaller than the wavelength of the light, the individual emission process interferes constructively, giving rise to an electromagnetic field with an amplitude proportional to N and an energy density proportional to N^2. This result was surprising, given its significant difference with respect to the decay process of an ensemble of N independent atoms, where light is emitted incoherently and with an energy density proportional to N. The original work of Dicke was followed by the two generalizations of Refs. [21,22], that analyzed the macroscopic behavior of the system when the light field is treated as a quantum system, i.e. described in terms of a bosonic field, as in Eq. (3.1). In the next Section, we review the behavior of the Dicke model, following the more recent presentation by Emary and Brandes [23]. A general review of the Dicke model, that goes beyond the goals of this Chapter, can be found in Refs. [54,55].

3.1.1 Superradiant phase transition

In this Section we will see that the Dicke model undergoes a zero-temperature phase transition upon varying the interaction coupling. In general, a zero-temperature phase transition is characterized by a qualitative change in the properties of the ground state(s) of the system, as a result of the variation of a non-thermal control parameter. In analogy with the phase transition at finite temperature, one can identify an operator whose expectation value on the ground state is the order parameter, as its value varies when moving between different phases: it is typically zero in the disordered phase and finite in the ordered one. Since at zero temperature there are no thermal fluctuations, the order can be destroyed solely by quantum fluctuations, arising from the Heisenberg uncertainty principle. For this reason, this kind of phase transition is referred to as quantum phase transition (QPT).

Without loss of generality, we restrict the following analysis to the single mode case, $p = 1$, of the spin-boson Hamiltonian (3.1). However, the results presented in this Section can be generalized to the multi-mode case. Let us then consider the single-mode Dicke Hamiltonian, which reads

$$H = \omega a^\dagger a + \Omega S^z + \tilde{g}(a^\dagger + a)(S^+ + S^-), \tag{3.2}$$

where we have further introduced the total spin operators $S^z = \sum_i s_i^z$ and $S^\pm = \sum_i s_i^\pm$, which satisfy the commutation relations $[S^z, S^\pm] = \pm S^\pm$, and $[S^+, S^-] = 2S^z$. The 2^N-dimensional Hilbert space spanned by the algebra of the total spin operator can be decomposed into sectors spanned by the eigenstates of the commuting operators S^2 and S^z, $\{|S, M\rangle ; M = -S, -S + 1, ..., S - 1, S\}$, which are known as the Dicke states and satisfy $S^z |S, M\rangle = M |S, M\rangle$ and $S^2 |S, M\rangle = S(S + 1) |S, M\rangle$. As the Hamiltonian (3.2) commutes with the total spin operator S^2, one can, without loss of generality, keep its eigenvalue to a fixed value. Let us denote, in the following, such an eigenvalue as $\bar{S}(\bar{S} + 1)$. In terms of these quantities, we can define an operator representing a conserved parity, i.e. an operator that commutes with the Hamiltonian (3.2). This reads

$$\Pi = \exp(i\pi N), \tag{3.3}$$

where $N = a^\dagger a + S^z + \bar{S}$ is the operator counting the total number of excitations in the spin-boson system.

In the thermodynamic limit $N \to +\infty$, the single mode Dicke model (3.1) undergoes a second order phase transition at the critical value

$$g_c = \frac{1}{2}\sqrt{\omega\Omega}, \tag{3.4}$$

where $g = \sqrt{N}\tilde{g}$. The ratio $\langle a^\dagger a\rangle_{\mathrm{GS}} / N$, can be taken as an order parameter for distinguishing between different phases, $\langle a^\dagger a\rangle_{\mathrm{GS}}$ being the expectation value the bosonic occupation number on the ground state. The behavior of the latter quantity as a function of g is represented in Fig. [3.1]. Here we can see that below the critical point, i.e. in the weak coupling regime $g < g_c$, the average number of bosons does not grow with N, meaning that the bosonic degrees of freedom are not extensively excited. This is referred to as normal phase. Instead, above the critical point, i.e. in the strong coupling regime $g > g_c$, the bosonic occupation number grows with N, and the system is macroscopically excited. This phase is referred to as superradiant phase. The normal phase corresponds to a disordered phase, while the superradiant one is an ordered, symmetry-broken phase, where the broken symmetry is the one associated with the conserved parity (3.3). This is highlighted by the behavior of the total magnetization $\langle S^x\rangle_{\mathrm{GS}} / N$ which is zero in the normal phase, and finite in the superradiant phase, i.e. not invariant upon inversion.

The model (3.2) undergoes a second order phase transition also at a finite temperature β, where the critical point reads

$$g_c = \frac{1}{2}\sqrt{\omega\Omega \coth\left(\frac{\beta\Omega}{2}\right)}. \tag{3.5}$$

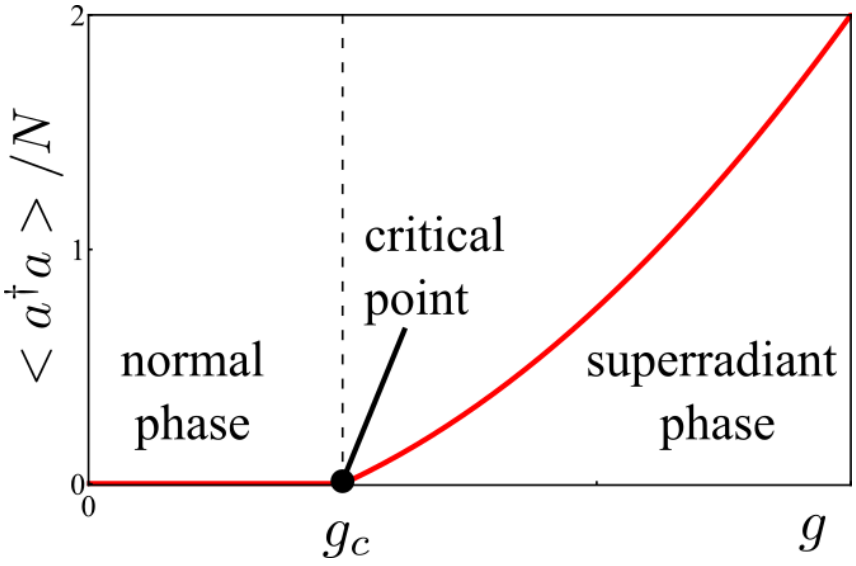


Figure 3.1: **Superradiant phase transition.** Average bosonic number as a function of the coupling strength. At the critical value g_c a second order phase transition occurs. At weak coupling the system is in a normal phase, where the average number of boson is a sub-extensive quantity with respect to the number of spins, N. At strong coupling the average number of boson grows with N.

The order parameter, $\langle a^\dagger a \rangle /N$, which is now an average on the thermal state, shows the same phenomenology described for the QPT. For this reason, the phase transition at finite temperature is still referred to as superradiant phase transition. However, there are some differences between the two regimes, $\beta \to +\infty$ and a finite β.

Firstly, it is possible to show that near the critical temperature quantum effects can be neglected. In this regime, thermal fluctuations, quantified by β^{-1}, are larger than the typical energy of the relevant order parameter fluctuations, say ε, being the latter a vanishing quantity as $g \to g_c$. In other words, the gap closes at the critical point and any finite temperature will be sufficient to populate states beyond the ground level. As a consequence, a classical description can be adopted in the neighborhood of the critical point g_c at finite temperature. For this reason, we will refer to this kind of superradiant phase transition as a classical phase transition (CPT).

Secondly, from the general theory of phase transitions, it is known that as g approaches the critical point g_c, all the relevant macroscopic observables depend on the external parameter difference $|g - g_c|$ via power laws, whose corresponding exponents are the so-called critical ones. Because of the scaling hypothesis, i.e. that systems at a critical point display scale-invariant properties, universality holds, meaning that critical exponents are independent of microscopic details, and many different systems share the same ones.

Such systems show the same critical behavior and are said to belong to the same universality class. It turns out that the critical exponents of the superradiant QPT and the ones of the superradiant CPT take different values [21, 23, 54]. As a consequence, the finite-temperature system and the zero-temperature one belong to different universality classes.

The theoretical investigation of the superradiant phase transition has been followed only in relatively recent times by experimental realizations. The major difficulty encountered by the latter has been the fact that a strong interaction coupling between spin and boson is required for the phase transition to occur. Among the experimental proposals, we name here a few, such as optical cavity QED schemes [24, 56], gases of thermal atoms inside cavities [57, 58], which was later extend to the case of a Bose-Einstein condensate [25], and trapped ion scenarios [26]. In many of the cited proposals, however, the system that has been taken into account cannot be regarded as an isolated quantum system. Indeed, processes such as spontaneous emission or photon losses often cannot be neglected, and imply an additional role played by dissipation in the system. In the next Section, we give a brief account for these scenarios.

3.2 Out-of-equilibrium phase transition

Initially motivated by the dissipation arising from the experimental settings for realizing the Dicke model, non-isolated generalizations of the latter have been taken into account. In what follows we consider the more common dissipative processes affecting the above mentioned physical scenarios, focusing, for the sake of simplicity, on the single mode Hamiltonian (3.2). Moreover, with such kind of dissipative processes, a phenomenological equation that effectively describes the evolution of the state ρ of the spin-boson Dicke model is a GKSL equation of the type (2.19). It reads

$$\dot{\rho} = -i[H, \rho] + \mathcal{D}[\rho], \tag{3.6}$$

where H is the Hamiltonian (3.2), and $\mathcal{D}[\cdot]$ has the form of a dissipative term (2.20).

First of all, we consider "collective" effects, i.e. dissipative effects affecting the boson and the total spin. The first one is the bosonic decay into a continuum of modes. This can represent photon losses in cavity realizations [24], or a cooling of the phonon degrees of freedom in trapped ion scenarios [59]. Such a process is modeled via the introduction of a jump operator $L = \sqrt{\gamma}a$, so that the dissipator reads

$$\mathcal{D}_\gamma[\rho] = \gamma \left(a\rho a^\dagger - \frac{1}{2}\{a^\dagger a, \rho\} \right). \tag{3.7}$$

The second effect is the total spin decay that can represent collective decay of atoms. This is modeled by the jump operator $L = \sqrt{\Gamma} S^-$, giving rise to a dissipator of the form

$$\mathcal{D}_\Gamma[\rho] = \Gamma \left(S^- \rho S^+ - \frac{1}{2}\{S^+ S^-, \rho\} \right). \tag{3.8}$$

It can be shown [28] that the Dicke model (3.2) in the presence of boson decay and total spin decay still undergoes a superradiant phase transition at the critical point

$$g_c = \frac{1}{2}\sqrt{\frac{\omega + \gamma^2}{\omega}\frac{\Omega + \Gamma^2}{\Omega}}. \tag{3.9}$$

The critical exponents characterizing such a dissipative system are the same of the CPT of the isolated system. As a result, the open quantum Dicke model with boson and total spin decay belongs to the same universality class of the finite-temperature Dicke model (3.2).

Besides collective effects, there are also single spin dissipative processes that can be taken into account, such as single decay and dephasing. These are modeled via the introduction of the jump operators $L_i = \sqrt{\Gamma_\downarrow} s_i^-$ and $L_i = \sqrt{\Gamma_\phi} s_i^z$, respectively, and give rise to the dissipative terms

$$\mathcal{D}_\downarrow = \sum_{i=1}^{N} \Gamma_\downarrow \left(s_i^- \rho s_i^+ - \frac{1}{2}\{s_i^+ s_i^-, \rho\} \right), \tag{3.10}$$

$$\mathcal{D}_\phi = \sum_{i=1}^{N} \Gamma_\phi \left(s_i^z \rho s_i^z - \rho \right). \tag{3.11}$$

It has been shown that, while adding any dephasing to the model prevents the occurrence of the superradiant phase transition, the latter survives in the presence of spin decay [27]. If this is the case, and when adding also the single boson decay, the critical point of the superradiant phase transition reads

$$g_c = \frac{1}{2}\sqrt{\frac{(\omega + \gamma^2)(\Omega + \Gamma_T^2)}{-2\langle s_z \rangle \Omega \omega}}, \tag{3.12}$$

where $\Gamma_T = \Gamma_\downarrow + \Gamma_\phi$ and $\langle s_z \rangle$ is the expectation value in the stationary state.

3.3 Disordered Dicke model

We will now consider a generalization of the multi-mode Dicke model (3.1) that takes into account the role of disorder, the latter being defined in terms of spin-boson dependent coupling strengths. The Hamiltonian reads

$$H = \sum_{\mu=1}^{p} \omega_\mu a_\mu^\dagger a_\mu + \Omega \sum_{i=1}^{N} s_i^z + \sum_{\mu=1}^{p}\sum_{i=1}^{N} \tilde{g}_{i\mu}(a_\mu^\dagger + a_\mu)(s_i^+ + s_i^-), \tag{3.13}$$

where the interaction coupling $\tilde{g}_{i\mu}$ can be further written as $\tilde{g}_{i\mu} = Gg_{i\mu}/\sqrt{N}$ where G is an overall coupling strength, and the parameters $g_{i\mu}$ are treated as indepentent identically distributed random variables, with mean value J_0 and variance J^2. This model, initially introduced in the context of BEC in multi-mode cavities [18,60], was later investigated in relation to the superradiant phase transition of the original Dicke model [19,29,30]. In general, it is possible to show that in the weak disordered regime, i.e. for large values of the ratio J_0/J, the model (3.13) undergoes a superradiant phase transition both at zero temperature [29] and at finite temperature [30], between a normal phase, that occurs at weak coupling and high temperature, and a superradiant phase occurring at strong coupling and low temperature.

3.3.1 From the equilibrium disordered Dicke model to the Hopfield neural network

The central focus of this Section is on the fact that there exists a relation between the above described superradiant phase transition occurring in the multi-mode, disordered Dicke model and the second order phase transition that describes the retrieval of memories in a stochastic HNN as described in Ch. 1. Such a result is explained in detail in Ref. [31] for the general case of the Hamiltonian (3.13) at finite temperature.

First of all, in the fully-commuting case $\Omega = 0$, the partition function takes the form $Z = Z_{FB}Z_I$, being Z_{FB} the partition function of a free boson, and Z_I the partition function of an Ising model with all-to-all interactions,

$$Z_I = \mathrm{Tr}[e^{-\beta H_I}] = \mathrm{Tr}[e^{\beta \sum_{ij} J_{ij}\sigma_i\sigma_j}]. \tag{3.14}$$

Here, H_I is the Ising model for the classical spins $\{\sigma_i\}$, and the interaction couplings J_{ij} read

$$J_{ij} = -\frac{G^2}{N}\sum_{\mu=1}^{p}\frac{g_{i\mu}g_{j\mu}}{\omega}. \tag{3.15}$$

On the one hand, this result implies that, when tracing away the bosonic field, the latter mediates a long-range interaction among the spins that is modeled via an effective fully connected Ising model. On the other hand, when comparing the Ising model (3.14) with the energy function (1.10) and the interaction couplings (3.15) with the Hebb's storage prescription (1.4), the disordered couplings $g_{i\mu}$ may take a form reminiscent of memory patterns. Indeed, this similarity emerges when the couplings $g_{i\mu}$ are chosen so that they take the values ± 1, since patterns are special configurations and, as such, N-uples of ± 1s.

Remarkably this analogy between the HNN and the effective spin model derived from the Dicke Hamiltonian remains unaltered even in the case of

a non-vanishing Ω. In this case, one can estimate the partition function and thus the free energy density of the spin-boson model with Hamiltonian (3.13). Such calculation becomes exact in the thermodynamic limit and if the number of patterns is sub-extensive, $p/N \to 0$. By introducing the vector $\vec{m} = (m^1, ..., m^p)^T$, where m^μ represents the average number of bosons for the μ-th mode, normalized by N, the free energy density is minimized by the solutions of the equation

$$m^\mu = \frac{G^2}{2} \left\langle \left\langle \frac{(\vec{g} \cdot \vec{m}) g_\mu}{\mu(\vec{g})} \tanh\left[\beta \mu(\vec{g})\right] \right\rangle \right\rangle , \tag{3.16}$$

where $\mu(\vec{g}) = (\Omega^2 + G^2(\vec{g} \cdot \vec{m})^2)^{\frac{1}{2}}$, and $\langle\langle \cdot \rangle\rangle$ represents the average over the disorder distribution of the couplings, and we have fixed, without loss of generality, $\omega = 1$. In the limit $\Omega \to 0$, Eq. (3.16) resembles the MF equations obtained for the Hopfield model (1.23), provided that the disordered couplings $g_{i\mu}$ play the role of the patterns $\xi_{i\mu}$. Such similarity is made more manifest by taking the disorder distribution of the couplings to be the bimodal distribution as defined by Eq. (1.2). In the normal phase, the only solution of Eq. (3.16) is a "paramagnetic" state, where $m^\mu = 0 \; \forall \mu$. The superradiant phase corresponds to a broken symmetry phase where, in resemblance with the retrieval phase of the HNN, there are $2p$ non-vanishing solutions of Eq. (3.16), of the type

$$\vec{m}_{(\mu)} = (\underbrace{0, 0, ..., 0}_{\mu - 1 \, times}, \underbrace{\pm m, 0, ..., 0}_{p - \mu + 1 \, times}), \tag{3.17}$$

for $\mu = 1, ..., p$.

The above described result shows the relation between the multimodal disordered Dicke model and the stochastic HNN at equilibrium. Starting from this work, our interest is in analyzing the out-of-equilibrium properties of a disordered Dicke model, with particular focus on the dynamical evolution towards a steady state. This investigation will be the central topic of Part III of this thesis.

Part II

An open quantum generalization of classical spin models

Chapter 4

Quantum accelerated approach to the thermal state of classical spin systems with applications to pattern-retrieval in the Hopfield neural network

A fundamental question that is currently triggering much attention in the quantum information, quantum many-body and computer science communities is whether quantum effects may lead to advantages in solving computational problems [10, 61–65]. Several quantum algorithms have been proposed which can outperform their best classical counterparts, such as in the paradigmatic examples of integer factorization [3] and database search problems [4]. Fluctuations due to quantum effects can moreover be employed to improve the performance of classical optimization algorithms by opening "tunnelling" paths through high potential barriers that could otherwise trap a classical system in configurations potentially very different from the sought solution. This is the case, for instance, of quantum annealing [5] which seeks to find the state of minimum energy within the energy landscape of e.g. a highly-connected spin system with random couplings [6–9]. More recently, a further paradigm emerged seeking to exploit the intrinsic open nature of quantum systems for quantum computing [13]. Its underlying idea is to encode the result of a computation in the stationary state of a suitably engineered [16, 17] quantum dissipative evolution of a many-body (spin) system [15].

Starting from these considerations, in this Chapter we explore the question of whether quantum effects in a purely dissipative dynamics can be advantageous for an accelerated approach to the thermal state of an interacting

system. For defining the latter, we will mainly focus our attention on a fully connected Ising model, and secondarily on the HNN that has been treated in Ch. 1. Analogously to the above-mentioned annealing or quantum computation protocols, the equilibrium state of the dynamics may encode the solution of a computational problem or the result of an optimization protocol. Our construction is based on a dissipative – yet quantum – generalization of a classical equilibrium Markov process. The corresponding dynamics has a pure stationary state which yields expectation values for classical observables that are identical to those of a thermal ensemble [66]. We show that the stationary state is invariant under a set of unitary transformations which, however, affect the dynamics in a non-trivial way [67,68]. This freedom permits a (quantum) speedup of the approach towards stationarity in comparison with the classical dynamics. We illustrate this in the case of a fully connected Ising model and show that similar results hold for a HNN [14, 35], which hints at the possibility of using quantum effects for the accelerated retrieval of patterns.

The work discussed in this Chapter appears in the publication:

"Quantum accelerated approach to the thermal state of classical spin systems with applications to pattern-retrieval in the Hopfield neural network"
E. Fiorelli, M. Marcuzzi, P. Rotondo, J.P. Garrahan, I. Lesanovsky
Physical Review A **99**, 032126 (2019).

4.1 Quantum generalization of classical stochastic processes

In the following we will focus for simplicity on equilibrium spin models. In this Section, starting from classical descriptions of the latter, we will build a quantum generalization with the aim of comparing the possibly different dynamical approach to the stationary state.

At the classical level, a spin model is described by a set of configurations $\{\vec{\sigma}\} = \{\sigma_1, \sigma_2, \ldots, \sigma_N\}$ with N the number of classical spins, $\sigma_i = \pm 1$ being an Ising spin variable. An instance of an equilibrium classical spin model is given in Sec. 1.2 of Ch. 1, for describing the finite-temperature HNN. Similarly to the introduction of the energy function (1.10), each equlibrium classical spin model is defined in terms of an energy (or "cost") function $E(\vec{\sigma})$. In hard optimization problems [69], these functions are typically defined so that their global minima correspond to the sought solutions in configuration space. Similarly to what has been illustrated in Sec. 1.2.3 of Ch. 1 for

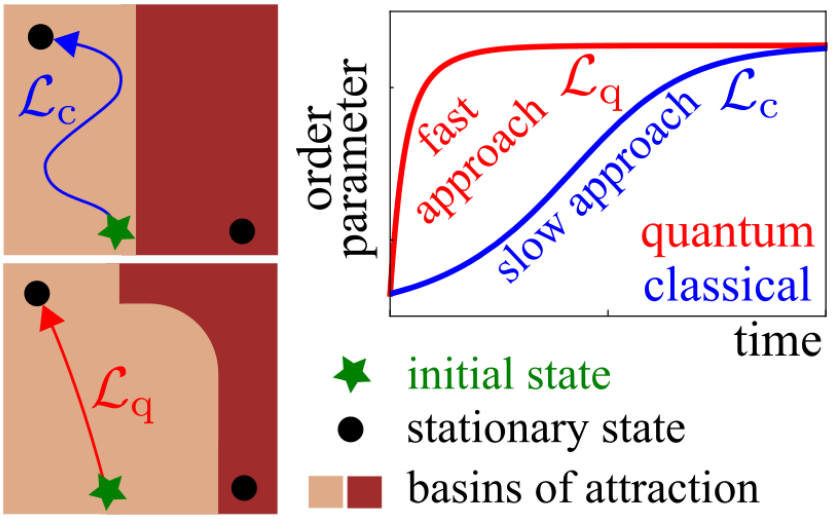


Figure 4.1: **Quantum accelerated approach towards stationarity.** We consider a purely dissipative open quantum evolution which reproduces the stationary state properties of an equilibrium stochastic dynamics (with generator $\mathcal{L}_c$). The quantum dynamics (generated by the operator $\mathcal{L}_q$) will result generally in different dynamical timescales and may lead to an accelerated approach of the order parameter towards stationarity with respect to the classical evolution. The acceleration emerges from the unitary transformation of the dynamics that leaves the stationary states invariant but may change the structure of their basins of attraction.

the HNN dynamics, it can be shown that under any single-spin-flipping (or, more generally, ergodic) dynamics which satisfies the detailed balance condition (1.15), the probability $P(\vec{\sigma}, t)$ of being in a given configuration $\vec{\sigma}$ at time t will approach, in the limit $t \to \infty$, the Gibbs distribution. This reads

$$P_{\rm eq}(\vec{\sigma}) = e^{-\beta E(\vec{\sigma})}/Z(\beta), \tag{4.1}$$

where β is the inverse temperature and $Z(\beta)$ the partition function.

In order to define a quantum generalization of such a classical spin process, we first promote the classical variables σ_i to quantum spins σ_i^z and encode the corresponding configurations in quantum states $|\vec{\sigma}\rangle$ such that $\sigma_i^z |\vec{\sigma}\rangle = \sigma_i |\vec{\sigma}\rangle$. In the following, we shall refer to this as the "classical basis" and to observables diagonal in this basis as "classical observables". Secondly, we will focus on an open quantum system, so that its state is described by a density operator ρ that is, in general, a mixed one. Among the possible open dynamics, we restrict for simplicity to a markovian and purely dissipative one. That is, the state ρ evolves according to a GKSL equation (2.19) which reads

$$\dot{\rho} = \mathcal{L}\rho = \sum_j \left(L_j \rho L_j^\dagger - \frac{1}{2} \left\{ L_j^\dagger L_j, \rho \right\} \right), \tag{4.2}$$

where $\mathcal{L}$ denotes the generator of the time evolution and the operators L_j are jump operators. In order to fully specify the dynamics (4.2), we need to fix the form of the jump operators. To this end, we define the pure state

$$|\Psi_{\rm ss}\rangle = \sum_{\{\vec{\sigma}\}} \sqrt{P_{\rm eq}(\vec{\sigma})}\,|\vec{\sigma}\rangle \tag{4.3}$$

and require it to be a so-called *dark state* of the dynamics, i.e. a state such that $L_j\,|\Psi_{\rm ss}\rangle = 0\,\forall j$. As a result, the density operator $\rho_{\rm ss} = |\Psi_{\rm ss}\rangle\langle\Psi_{\rm ss}|$ is a stationary state of Eq. (4.2), and its matrix representation on the classical basis $\{|\vec{\sigma}\rangle\}$ reproduces on its diagonal the equilibrium thermal distribution of the corresponding classical spin model. In other words, any expectation value of a classical observable on the stationary state $\rho_{\rm ss}$ corresponds to the (classical) thermal average

$$\langle O_{\rm cl}\rangle = {\rm Tr}(\rho_{\rm ss}O_{\rm cl}) = \sum_{\{\vec{\sigma}\}} e^{-\beta E(\vec{\sigma})}\,\langle\vec{\sigma}|O_{\rm cl}|\vec{\sigma}\rangle\,/Z(\beta). \tag{4.4}$$

As a consequence of the above construction, any classical property can be equivalently retrieved from the stationary state of the open quantum system. Conversely, quantum fluctuations can affect the typical timescales of the dynamics. It is worth noticing that, by imposing the dark state property $L_j\,|\Psi_{\rm ss}\rangle = 0\,\forall j$, the "global" stationary state property $\mathcal{L}\rho_{\rm ss} = 0$ is "locally" satisfied by each jump operator. This is reminiscent of the *frustration-free* property typically associated to special (Rokhsar-Kivelson) systems [70].

On the one hand we have seen that the dark-state property allows us to fix the stationary state. On the other hand, it does not uniquely fix the jump operators. Indeed, let us consider a given set of L_j and second one, L'_j, derived from the former set by applying a set of unitary transformations u_j, i.e. $L'_j = u_j L_j$, with $u_j^\dagger u_j = \mathbb{I}$. The dynamics generated by $\mathcal{L}'$, which is given in terms of the set of jump operators L'_j, would still have $\rho_{\rm ss}$ as a stationary state, since $L'_j\,|\Psi_{\rm ss}\rangle = 0\ \forall j$. It is worth noticing that it is the "frustration-free" property of the dark state that allows one to choose different unitary operators u_j for different j. In the following we will exploit the freedom in the choice of the unitary transformations: as illustrated in Fig. [4.1], it allows us to construct and explore different dynamics, all sharing the same stationary state(s). Generically, the typical timescales of the dynamics will change for different u_j, yielding in some cases a faster, in others a slower approach to stationarity.

In order to go ahead with the characterization of the quantum Markov process (4.2), let us outline the construction of a set of jump operators. The technical details of this derivation can be found in Appendix A.1. Firstly, we define $\vec{\sigma}_{\{i\}}$ as the list of Ising variables excluding the i-th one. Furthermore, we denote by $D_i(\vec{\sigma}_{\{i\}}) = [E(\vec{\sigma}_{\{i\}}, \sigma = -1) - E(\vec{\sigma}_{\{i\}}, \sigma = +1)]/2$ half

the energy cost for flipping the i-th spin down, leaving the configuration of the remaining spins fixed. From D_i we define an operator ΔE_i obtained by taking the functional form of D_i and replacing every σ_j ($j \neq i$) with the corresponding Pauli matrix σ_j^z. For example, for $D_i = (1/N)\sum_{j\neq i}\sigma_j$ one would get $\Delta E_i = (1/N)\sum_{j\neq i}\sigma_j^z$. The N jump operators (one per site) are then constructed according to

$$L_i = \alpha_i^- n_i - \alpha_i^+ \sigma_i^+, \quad \text{with} \quad \alpha_i^\pm = \frac{\mathrm{e}^{\pm\frac{\beta}{2}\Delta E_i}}{[2\cosh(\beta\Delta E_i)]^{\frac{1}{2}}}, \tag{4.5}$$

where $\sigma_i^\pm = (\sigma_i^x \pm i\sigma_i^y)/2$ are the Pauli raising and lowering operators, $n_i = (\sigma_i^z + \mathbb{I}_2)/2$, and the dependence of ΔE_i on all spins but the i-th one is implicit. This particular form of the jump operators is convenient, because it will allow us, in the examples discussed further below, to directly relate the purely-dissipative quantum dynamics (4.2) to the corresponding classical Glauber dynamics with energy function $E(\vec{\sigma})$.

To conclude the construction of the jump operators we use the freedom given by the unitaries u_j. For the sake of simplicity we choose local unitaries parametrized by the two angles θ and ϕ as

$$u_j(\theta,\phi) = e^{i\phi\frac{\sigma_i^z}{2}} e^{i\theta\sigma_i^y} e^{-i\phi\frac{\sigma_i^z}{2}}. \tag{4.6}$$

4.2 Fully connected quadratic models

In this Section, we study the dependence of the relaxation timescales under the angles (θ,ϕ), focusing on classical fully connected models, which are generically described by the energy function

$$E(\vec{\sigma}) = -\sum_{i,j} J_{ij}\sigma_i\sigma_j, \tag{4.7}$$

with J_{ij} being a symmetric real $N \times N$ matrix. This will allow us to study the dynamics in terms of semi-classical collective variables. The equations of motion for the local operators $\sigma_i^{x,y,z}$ generated by the dynamics (4.2) with jump operators (4.5) read (see Appendix A.2)

$$\begin{aligned}
\dot{\sigma}_i^x &= -A_i^x - \frac{\beta}{2}\sum_{k\neq i} J_{ki}\mathrm{sech}(\beta\Delta E_k)\sigma_k^y\sigma_i^y + \frac{\mathrm{sech}(\beta\Delta E_i)}{2}, \\
\dot{\sigma}_i^y &= -A_i^y + \frac{\beta}{2}\sum_{k\neq i} J_{ki}\mathrm{sech}(\beta\Delta E_k)\sigma_k^y\sigma_i^x, \\
\dot{\sigma}_i^z &= -A_i^z + \frac{1}{2}\tanh(\beta\Delta E_i).
\end{aligned} \tag{4.8}$$

Here we have defined $A_i^\alpha = \{f_\alpha\left[\mathrm{sech}(\beta\Delta E_i)\sigma_i^x + \tanh(\beta\Delta E_i)\sigma_i^z - 1\right] + \sigma_i^\alpha\}/2$ ($\alpha = x,y,z$), which depends on the angles (θ,ϕ) through the functions

$f_x(\theta,\phi) = -\sin(2\theta)\cos(\phi)$, $f_y(\theta,\phi) = \sin(2\theta)\sin(\phi)$, $f_z(\theta) = \cos(2\theta)$. It is worth noticing that for $\theta = \pi/4$ [i.e. $f_z(\pi/4) = 0$] the last equation is defined entirely in terms of combinations of σ^z matrices. Further below, we shall use this choice (together with $\phi = \pi/2$) as a classical reference case, as it will yield, for the z-component of spin operator, the same dynamics one would derive from a purely-classical Glauber dynamics. We stress that this particular choice, although reproducing the same equations of motions for the order parameter of the classical case, is not strictly equivalent to it. Away from this classical limit the dynamics of σ^z becomes coupled to the quantum coherences (represented by σ^x and σ^y), and this coupling is controlled by the angles θ and ϕ. In this sense these two parameters control the "quantumness" of the dynamics.

4.2.1 Fully connected Ising model

As a first example we consider the fully connected Ising model, i.e. we choose spin-independent couplings $J_{ij} = 1/N$. The first step is constructing a set of semiclassical collective variables that allow to reduce the problem to a system of $3N$ coupled ordinary differential equations. Indeed, we consider the variables $s^\alpha = (1/N)\sum_{i=1}^N \sigma_i^\alpha$ ($\alpha = x, y, z$). Furthermore, since their commutator reads $\left[s^\alpha, s^\beta\right] = 2i\epsilon_{\alpha\beta\gamma}s^\gamma/N$, it vanishes in the thermodynamic limit $N \to \infty$. Thus, we can effectively replace them with their expectation values $s^\alpha \approx \langle s^\alpha \rangle \equiv m^\alpha$. The equations of motion read

$$\begin{aligned}
\dot{m}^x &= -A_x + \frac{1}{2}\mathrm{sech}(\beta m^z) - \frac{\beta}{2}\mathrm{sech}(\beta m^z)(m^y)^2, \\
\dot{m}^y &= -A_y + \frac{\beta}{2}\mathrm{sech}(\beta m^z) m^y m^x, \\
\dot{m}^z &= -A_z + \frac{1}{2}\tanh(\beta m^z),
\end{aligned} \tag{4.9}$$

where $A_\alpha = \{f_\alpha\left[m^x\mathrm{sech}(\beta m^z) + m^z\tanh(\beta m^z) - 1\right] + m^\alpha\}/2$ ($\alpha = x, y, z$). As in the case of Eqs. (4.8), the choice $\theta = \pi/4$ decouples the third equation from the others, implying that the dynamics of m^z proceeds independently from the one of $m^{x,y}$. Furthermore, the equation for m^z is equivalent to the mean-field evolution equation of the order parameter of a classical Ising model under a continuous-time Glauber dynamics. We thereby consider this angle $\theta = \pi/4$ our *classical* reference point (the specific choice of ϕ will not affect the evolution of m^z).

The stationary state structure can be extracted by setting the l.h.s. of Eqs. (4.9) to zero. As a result, we obtain that in the high temperature regime $\beta \leq 1$, the equations admit a single solution $m^z = m^y = 0$, $m^x = 1$. We will refer to this case as the *paramagnetic* one. In the low temperature regime

$\beta > 1$, the paramagnetic solution becomes unstable. Here, two stable solutions satisfying $m^z \neq 0$ appear, obeying $m^z = \tanh(\beta m^z)$. We will refer to this case as the *ferromagnetic* one.

The aim of the next paragraphs is comparing the timescales of the quantum dynamics with the one of our classical reference point. To this end, in Fig. [4.2a] we show the "quantum" (red square and red dashed lines) and "classical" (blue circle) evolution of the order parameter $m^z(t)$ in the ferromagnetic phase for a specific choice of θ and ϕ and fixed initial conditions. Here, it is worth noticing that the observed acceleration away from the classical limit arises in the early stages of the dynamics, whereas the long-time, asymptotic behavior is exponential with the same rate for both curves [panel (b)]. The onset of this exponential decay is thus shifted in time, leading to a speedup.

To quantify this accelerated approach to stationarity, we define the relaxation time $\bar{t}$ as the time it takes the order parameter to approach its stationary value within the threshold $\epsilon = 10^{-3}$. The choice of this threshold is arbitrary; however, for most values of θ and ϕ the asymptotic approach to stationarity is exponential with the *same* rate for both quantum and classical dynamics (see A.3 for more details), as in Fig. [4.2b]. Hence, the specific value of ϵ is not relevant to determine the presence of a speedup. Some small regions where the quantum dynamics is asymptotically slower than the classical one exist, but they are included within regions where the early-time dynamics is slowed down as well. In Fig. [4.2c] we show $\bar{t}/\bar{t}_c$ — which is the relaxation time normalized by the classical relaxation time $\bar{t}_c$ (at $\theta = \pi/4$ and $\phi = \pi/2$) — in the (θ, ϕ)-plane for a given choice of very small initial conditions. The plot shows large regions of accelerated relaxation separated by two narrow strips, close to the "classical" regime, where the quantum dynamics experiences instead a slowdown. The shape of these strips shows only a weak dependence on the initial conditions.

This robustness is a consequence of the fact that, while the stationary states are independent of the angles θ and ϕ, their respective basins of attraction change (see sketch in Fig. [4.1]). As can be gleaned from Eqs. (4.9), $m^z = 0$ identifies an invariant subspace under the classical dynamics (i.e., $m^z = 0 \Rightarrow \dot{m}^z = 0$). Hence, by choosing the initial conditions $|m^\alpha| \ll 1$ the initial dynamics in the z-direction will necessarily be slow (due to the almost vanishing derivative). By changing the angles (and thereby the shape of the attraction basins), the same initial condition will generically not be close to such an invariant manifold and the quantum dynamics will start faster, leading to the observed accelerated early-time dynamics. Indeed, the instances in which it is slower [bright regions in panel (c)] correspond to regions where the dynamics swaps from reaching one ferromagnetic sta-

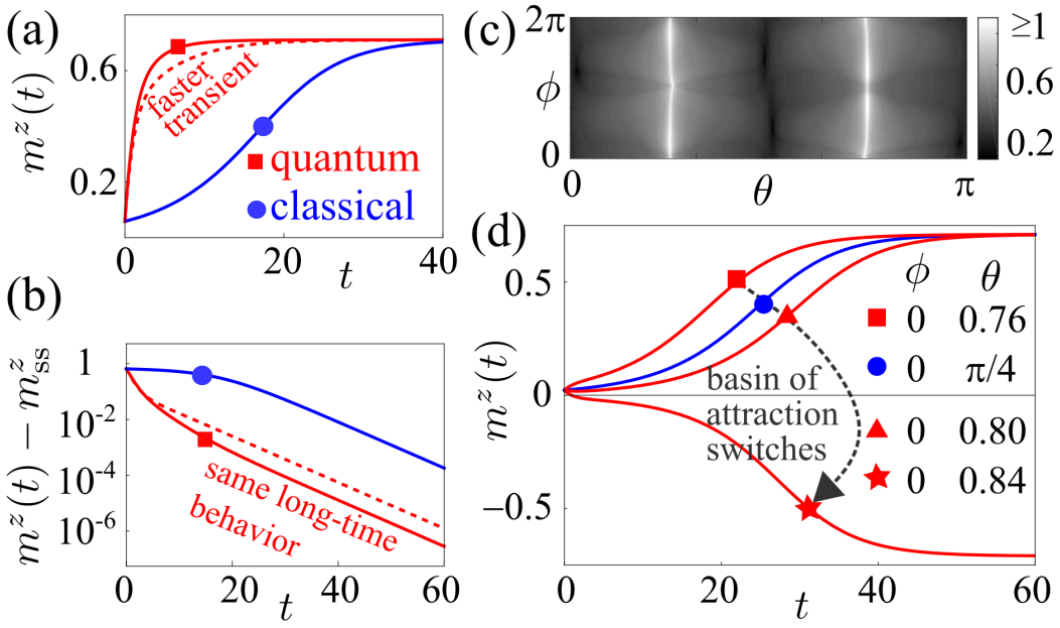


Figure 4.2: **Comparison between the "classical" and "quantum" dynamics of a fully connected Ising model.** (a) Magnetization m^z as a function of time t. (b) Logarithmic plot of $m^z(t) - m^z(t \to \infty)$ displaying the exponential approach towards the stationary value of the magnetization. The equal slope of all curves highlights that the asymptotic rate is the same for all choices of the angles (θ, ϕ). (c) Density plot of the ratio $\bar{t}/\bar{t}_c$ in the (θ, ϕ)-plane. Here $\bar{t}$ is the relaxation time at given θ, ϕ-values and $\bar{t}_c$ is the relaxation time in the classical limit (at $\theta = \pi/4$). (d) Magnetization m^z for selected angles [see panel (c)]. In panels (a) and (b) blue circle denotes the classical case $\theta = \pi/4$; dashed line and red square correspond to the choices $(\theta, \phi) = (3, 0)$ (dashed) and $(\theta, \phi) = (0.3, 4)$ (square). In all panels, $\beta^{-1} = 0.8$ and the initial conditions are randomly chosen such that $|m^\alpha(0)| \ll 1$ $(\alpha = x, y, z)$.

tionary state to its opposite [panel (d)]. Hence, for most choices of θ and ϕ the quantum dynamics will be faster than the classical one independently of the initial conditions as long as $|m^\alpha(0)| \ll 1$.

4.2.2 Application to the Hopfield neural network

In this Section, we focus on the HNN that has been considered in Ch. 1. Referring to the energy funciton (4.7), the coupling matrix reads $J_{ij} = (1/N) \sum_{\mu=1}^{p} \xi_i^\mu \xi_j^\mu$, where ξ_i^μ are the patterns defined in Sec. 1.2. as independent, identically distributed random variables, with a certain probability distribution. To make a brief recap, we have seen that the energy function of the HNN is minimized by choosing configurations $\sigma_i = \xi_i^\mu \, \forall i$ for any fixed μ. Hence, a stochastic Glauber dynamics has the patterns as stationary states, as long as the number of patterns obeys $p/N \ll 1$ [2, 39]. More generally,

as seen in Sec. 1.2.3, at finite temperature two phases emerge: for $\beta < 1$ the system is in a paramagnetic phase where the typical configurations have no extensive overlap with any of the patterns, $\lim_{N\to\infty}(1/N)\sum_i \xi_i^\mu \langle\sigma_i\rangle = 0\,\forall\mu$. Instead, $\beta > 1$ identifies a retrieval phase where the system picks one of the patterns (say, the ν-th) and acquires a non-vanishing overlap with it, $\lim_{N\to\infty}(1/N)\sum_i \xi_i^\nu \langle\sigma_i\rangle \neq 0$.

In the corresponding quantum model, this overlap is generalized to

$$m_\mu^\alpha = \frac{1}{N}\sum_{i=1}^{N} \xi_i^\mu \langle\sigma_i^\alpha\rangle\,, \tag{4.10}$$

with $\langle\cdot\rangle = \mathrm{Tr}\,\{(\cdot)\rho(t)\}$ representing the quantum expectation value at time t, and $\alpha = x, y, z$. However, in contrast to the fully connected Ising model, the equations of motion do not straightforwardly close in the collective variables (overlaps) m_μ^α and further approximations are required: since the stationary state should yield the same expectation values as a classical HNN, it is natural to think that, at least not too far from the stationary points, the dynamics will be mostly determined by the properties of the overlaps m_μ^α. We thus perform the approximation $\langle\sigma_i^\alpha\rangle \approx \xi_i^\mu m_\mu^\alpha$. Moreover, we exploit the self-averaging property defined by Eq. (1.22): for large N we can perform the substitution $(1/N)\sum_i F(\vec{\xi}_i) \to \overline{F(\vec{\xi})}$, where $\overline{(\cdot)}$ denotes the average over the disorder distribution of the patterns. This reduces the equations of motion (see Appendix A.4) to

$$\begin{aligned} \dot{m}_\mu^{x,y} &= -\bar{A}_\mu^{x,y}(\beta), \\ \dot{m}_\mu^{z} &= -\bar{A}_\mu^{z}(\beta) + \frac{1}{2}\overline{\xi^\mu \tanh\beta\vec{\xi}\cdot\vec{m}^z}, \end{aligned} \tag{4.11}$$

where $\bar{A}_\mu^\alpha = \left[f_\alpha m_\mu^x \overline{\mathrm{sech}(\beta\vec{\xi}\cdot\vec{m}^z)} + m_\mu^\alpha\right]/2$ $(\alpha = x, y, z)$. These equations close in the $3p$ variables $m_\mu^{x,y,z}$ and can be solved numerically, the averages being calculated according to their definition $\overline{F(\vec{\xi})} = \frac{1}{2^p}\sum_{\xi^1=\pm1}\cdots\sum_{\xi^p=\pm1} F(\vec{\xi})$.

As for the example of the fully connected Ising model treated in Sec. 4.2.1, the choice $\theta = \pi/4$ decouples the equations for the z-component and makes them equivalent to the classical (mean-field) dynamics. Unlike in the previous case, however, the order parameters [the overlaps $m^\alpha(t)$] are not necessarily known (one would have to know the patterns ξ^μ to derive them from the spin configurations) and therefore an averaging over initial conditions is required.

We focus on initial conditions representing "corrupted memories", i.e., we pick the initial (random) overlaps $m_\mu^z(0)$ uniformly over a small interval $[-0.01, 0.01]$ with the exception of a single one (without loss of generality, we fix $\mu = p$) $m_p^z(0) = Z_0 \pm 0.01$, which is instead centered around a non-vanishing value $Z_0 \neq 0$. This mimics a case where a classical memory en-

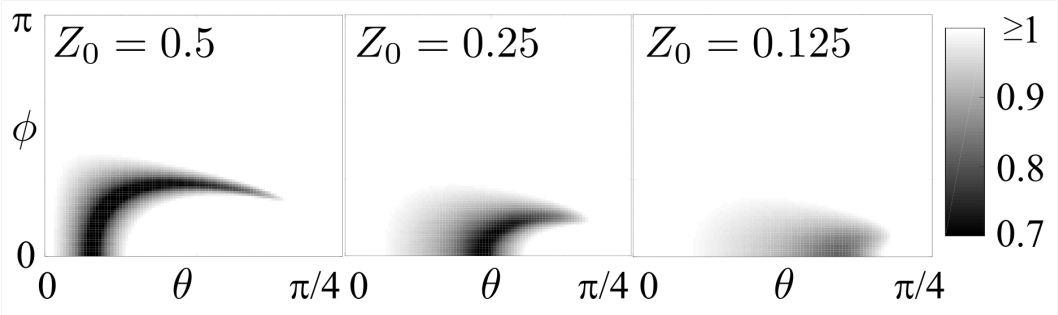


Figure 4.3: **Comparison between the "classical" and "quantum" dynamics of a HNN.** Density plot of the ratio $\bar{t}/\bar{t}_c$, averaged over 200 realizations (for protocol see text). The initial conditions are fixed such that $|m^z_\mu(0)|$ is uniformly distributed in the interval $[-0.01, 0.01]$ $\forall \mu = 1, ..., p-1$, whereas $m^z_p(0) \in [Z_0 - 0.01, Z_0 + 0.01]$ with $Z_0 = 0.5$, 0.25 and 0.125. The remaining components $m^x(0)$ and $m^y(0)$ are randomly chosen in $[-0.01, 0.01]$. For the "quantum" case the rotation $m^z(0) \to m^x(0)$, $m^x(0) \to -m^z(0)$ is performed before running the dynamics. The remaining parameters, common to all panels, are $p = 3$ (number of patterns), $\beta^{-1} = 0.8$. These plots display one eighth of the entire (θ, ϕ)-plane (corresponding to the bottom-left corner of Fig. [4.2c]), but the remainder can be reconstructed by symmetry arguments via the transformations $\phi \to 2\pi - \phi$, $\theta \to \pi/2 - \theta$ and $(\theta, \phi) \to (\pi - \theta, \phi + \pi)$ (see Appendix A.4.2 for more details).

codes a portion of a given pattern and the task of the neural network is to reconstruct the remainder.

Notably, merely changing θ and ϕ does not lead to any speedup as in the Ising case. To find a regime where quantum acceleration occurs, a possible protocol is the following:

(i) for each random choice of the initial conditions a spin rotation is performed which maps the overlaps' x-components in z-components and vice versa $[m^x_\mu(0) \to -m^z_\mu(0), m^y_\mu(0) \to m^y_\mu(0), m^z_\mu(0) \to m^x_\mu(0)]$.

(ii) Afterwards the quantum dynamics is switched on. To quantify the speedup the timescale $\bar{t}$ is measured analogously to the Ising case and compared with the classical value $\bar{t}_c$ (see Appendix A.4.1). The ratios $\bar{t}/\bar{t}_c$ corresponding to different initial conditions are subsequently averaged. The results are shown in Fig. [4.3], where this ratio is displayed in the (θ,ϕ)-plane for three choices of Z_0. We can identify choices of the angles for which an accelerated pattern retrieval is indeed achieved. In particular, the gain is more significant for less corrupted initial memories, i.e. larger Z_0.

4.3 Summary and outlook

We investigated how quantum effects can accelerate the approach towards stationarity of a classical fully connected stochastic system. Our results suggest that, for the analyzed models, complementary methods to the established quantum annealing techniques [9,61–65] may be exploited to enhance pattern retrieval in neural networks. It is worth remarking that the problem of retrieval in associative memories such as the Hopfield network we considered here is solvable in linear (in the size N of the network) time $t = \alpha N$ by any standard gradient descent method. Technically what we found here is that we can manipulate the additional degrees of freedom of our open quantum dynamics in order to produce a protocol that speeds up the retrieval at the level of the prefactor, i.e. the time needed for the retrieval is $t = \alpha_q N$ with $\alpha_q < \alpha$.

Part III

Out of equilibrium dynamics of disordered, dissipative spin-boson models

Chapter 5

Dynamics of strongly coupled disordered dissipative single-mode spin-boson systems

Prominent platforms for quantum simulation, such as cavity, circuit [71] or waveguide quantum electrodynamics [72] as well as trapped ions [73,74] can be modeled by ensembles of two-level systems interacting with bosonic degrees of freedom (electromagnetic modes or phonons) according to the Dicke Hamiltonian (3.1), as it has been highlighted in Ch. 3. The theoretical understanding of such models can thus give a significant boost in the realization and control of quantum devices. However, while the weak coupling regime of spin-boson models is relatively well understood and can be treated by a perturbative integration of the bosonic degrees of freedom, the strong coupling limit is far more challenging [75].

An additional layer of complexity is added by the presence of disorder, i.e. when individual spins couple to the bosons at different strengths. Beside the fact that some degree of quenched disorder may affect realistic systems, there is also an increasing interest in engineering non-uniform couplings for practical applications. Indeed, systems characterized by tunable quasi-random couplings form the basis for physical implementations of complex optimization problems, which may for instance be solved via quantum annealing protocols [6,9,76].

Disordered spin-boson systems have only recently moved into the focus of theoretical investigations. Some of them explore the emergence of glassiness when many electromagnetic modes interact at different strength with an ensemble of qubits [29,77]. As highlighted in Sec. 3.3, Refs. [30,31] deal with the same system showing that it effectively realizes, at equilibrium, an associative memory. Most of the techniques employed to explore these systems, however, cannot be straightforwardly generalized to study open quan-

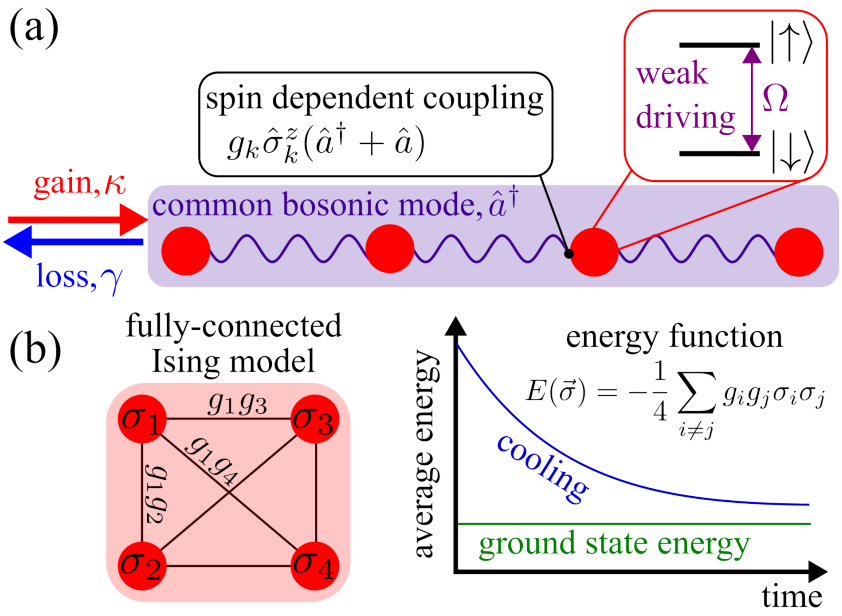


Figure 5.1: **Dissipative spin-boson system.** (a) N weakly driven (at strength Ω) two-level systems (spins) are strongly coupled to a single bosonic mode with couplings g_k ($k=1,\ldots,N$). Gain and loss of the bosons occur at rates κ and γ, respectively. (b) The resulting effective dissipative dynamics of the spins is related to a fully connected Ising energy function ($\sigma_k=\pm1$), $E(\vec{\sigma})$ [Eq. (5.6)], in which the interaction strength between spins i and j is proportional to the product of the coupling constants, g_ig_j. The effective dynamics features regimes which permit cooling of the many-body spin state, i.e. significant population of the low-energy configurations.

tum dynamics in the strong coupling regime, and only a few studies deal with disordered open quantum systems [14,28,78]. This topic acquires further relevance in the light of recent experimental progress in multimodal cavity QED, which realizes tunable range [79] and sign-changing [80,81] photon-mediated atomic interactions.

In this Chapter, we investigate a disordered and dissipative system in which weakly driven spins are strongly coupled to a bosonic mode, as it is illustrated in panel (a) of Fig. [5.1]. We employ a perturbative approach which relies on the weakness of the driving rather than of the spin-boson coupling. We find that the effective spin dynamics is governed by a rate equation that depends on a fully connected Ising energy function as sketched in the left-hand panel (b) of Fig. [5.1]. Depending on the rates of bosonic loss and gain we identify several distinct dynamical regimes: two of them are high-temperature ones, in which the stationary state of the system is fully mixed. A further one mimics an effective low-temperature dynamics, which permits cooling of the spin system. Outside these the dynamics is

generally non-thermal and detailed balance is broken. This link between an open, strongly coupled spin-boson system and the physics of disordered Ising spin systems opens up the possibility of engineering complex classical energy landscapes - with importance in the context of associative memories - together with a cooling protocol.

The work presented in this Chapter appears in the publication:

"Dynamics of strongly coupled disordered dissipative spin-boson systems"
E. Fiorelli, P. Rotondo, F. Carollo, M. Marcuzzi, I. Lesanovsky
Physical Review Research **2**, 013198 (2020).

5.1 Non-equilibrium spin-boson model

We consider an ensemble of N two-level systems interacting with a single bosonic mode described by the Dicke Hamiltonian

$$H = \omega a^\dagger a + \sum_{i=1}^{N} g_i \sigma_i^z (a^\dagger + a) + \Omega \sum_{i=1}^{N} \sigma_i^x. \tag{5.1}$$

Here, $\sigma_i^{x,y,z}$ are the Pauli operators and a and $a^\dagger$ the bosonic annihilation and creation operators. The parameters ω and Ω denote the fundamental frequency of the boson, and the coherent coupling strength between the two spin states, respectively. The spin-boson couplings g_i will be modeled here as a set of independent, identically-distributed real random variables. In the following we shall consider two cases: as a representative of distributions centered around zero, we first take a uniform one with weight $1/(2g_0)$ between $-g_0$ and g_0 and zero elsewhere. We then consider a bimodal distribution which peaks around two opposite values $\pm g_0$. This choice mimics the two-value distribution defined by Eq. (1.2) often encountered in associative memory models. More precisely, we superpose two Gaussians, each of variance s^2, centered around $\pm g_0$. In both cases the mean is zero and we denote the variance by g^2.

We also include dissipation on the bosonic degree of freedom in the form of markovian gain and loss processes. The state of the system, encoded in a density matrix ρ, thus evolves under the action of a GKSL-like equation

$$\dot{\rho} = \mathcal{L}\rho = -i[H, \rho] + \sum_{n=l,g} L_n \rho L_n^\dagger - \frac{1}{2}\{L_n^\dagger L_n, \rho\} \tag{5.2}$$

with the jump operators $L_l = \sqrt{\gamma} a$, $L_g = \sqrt{\kappa} a^\dagger$ where γ (κ) is the loss (gain) rate and $\gamma > \kappa \geq 0$.

Let us at this point briefly discuss the validity of the employed GKSL master equation description. This is a formalism widely-employed for dissipative light-matter systems [27, 54, 56, 82]. Formally, it is derived from a

setting in which work is performed upon the environment so that its correlation with the system is very quickly erased (on timescales smaller than the ones at which correlations are built between different subsystems, in this case spins and bosons). Equivalently, one can imagine that the system is coupled in succession to a plethora of equal copies of the environment [83]. Constant contact with a single environment would eventually correlate system and bath degrees of freedom; in the system dynamics, this would be reflected in the emergence of non-local terms. For instance, in our description this would produce dissipation on the spins as well, neglecting which would cause apparent violations of the second law of thermodynamics [84].

A physical realization of the Dicke model can for instance be achieved on trapped-ion quantum simulators, as it has been addressed both theoretically [26,85] and experimentally [86,87]. Following the scheme represented in Fig. [5.1], such a system would consist of N ions coupling to the centre-of-mass phonon mode of the lattice. As it has been shown for the quantum Rabi model [88] and eventually generalized to the Dicke model [26], the application of multiple laser fields on the ions yields both the spin dependent coupling $g_k\sigma_k^z(a+a^\dagger)$ and the weak driving term, $\Omega\sigma_k^x$ entering Eq. (5.1). Finally, as illustrated in panel (a) of Fig. [5.1], the gain and loss dynamics can be achieved by applying lasers on the ions on the edge of the chain, as discussed in Ref. [89]. Since this ion is coupled to the same phonon mode as the other ions this effectively implements jump operators of the form introduced in Eq. (5.2).

5.1.1 Spin dynamics at strong coupling

We explore the dynamics (5.2) in the strong coupling regime, i.e. when the driving acting on the spins is much weaker than the spin-boson interaction ($\Omega \ll g$). In the following we sketch the perturbative technique we employ for this purpose, whose details can be found in Appendix B.1. First, we split the Lindblad superoperator according to $\mathcal{L} = \mathcal{L}_0 + \mathcal{L}_1$, where $\mathcal{L}_1(\cdot) = -i\Omega[\sum_i \sigma_i^x, \cdot]$ can be regarded as a small perturbation. Focusing now on $\mathcal{L}_0$, we notice that each σ_i^z commutes with all jump operators and Hamiltonian terms in it, implying that the z-components of the spins constitute N independent conserved quantities [90]. Hence, the dynamics can be separated in 2^N independent sectors labeled by the classical spin configurations $\vec{\sigma} = (\sigma_1, \ldots, \sigma_N)$, $(\sigma_i \in \{-1, 1\})$, where $\sigma_i^z |\vec{\sigma}\rangle = \sigma_i |\vec{\sigma}\rangle$; in other words, states belonging to different sectors never mix under the action of $\mathcal{L}_0$. In each sector, the bosonic mode evolves according to a reduced Lindbladian $\mathcal{L}_0(\sigma_i^z \to \sigma_i)$ in which each Pauli matrix is replaced with the corresponding eigenvalue extracted from the chosen label. For any such choice of classi-

cal configuration, the reduced Lindbladian is quadratic in the bosonic operators and thus describes a damped quantum harmonic oscillator with a (spin-configuration-dependent) spatial displacement. This admits a single (bosonic) stationary state, denoted by $\rho_{\vec{\sigma}}$. We assume that, due to the random and independent nature of the couplings g_i, no additional symmetries are present which could protect more complex subspaces. Hence, for any initial state ρ_0 of the spin-boson system the corresponding stationary states under $\mathcal{L}_0$ is of the form $\rho_{\text{stat}} = \sum_{\vec{\sigma}} p_{\vec{\sigma}} \rho_{\vec{\sigma}} \otimes |\vec{\sigma}\rangle \langle\vec{\sigma}|$, where the coefficients $p_{\vec{\sigma}}$ form a set of classical probabilities.

The perturbation $\mathcal{L}_1$ couples sectors corresponding to different classical spin configurations $\vec{\sigma}$. Its action can be incorporated perturbatively [68, 91] as long as Ω is small compared to the typical rate at which coherences between sectors decay (estimated further below). We define the projector P onto the stationary manifold of $\mathcal{L}_0$ according to

$$P\rho(t) = \sum_{\vec{\sigma}} \text{Tr}_B \left\{ \langle\vec{\sigma}| \rho(t) |\vec{\sigma}\rangle \right\} \rho_{\vec{\sigma}} \otimes |\vec{\sigma}\rangle \langle\vec{\sigma}| , \tag{5.3}$$

where Tr_B denotes the partial trace over the bosonic mode, and use it to define a projected dynamics for $P\rho(t)$. This is a particular example of a Nakajima-Zwanzig projection scheme that has been introduced in Ch. 2. In our case, this reduction yields a considerable simplification: from Eq. (5.3) we see in fact that the time dependence of the reduced state is entirely encoded in the coefficients $p_{\vec{\sigma}}(t) = \text{Tr}_B \left\{ \langle\vec{\sigma}| \rho(t) |\vec{\sigma}\rangle \right\}$ which constitute a list of classical probabilities. These evolve according to a master equation

$$\dot{p}_{\vec{\sigma}} = \sum_{\vec{\sigma}'} W_{\vec{\sigma}' \to \vec{\sigma}} p_{\vec{\sigma}'} - W_{\vec{\sigma} \to \vec{\sigma}'} p_{\vec{\sigma}}, \tag{5.4}$$

where $W_{\vec{\sigma}' \to \vec{\sigma}}$ is the rate for switching from configuration $\vec{\sigma}'$ to $\vec{\sigma}$. Note that, up to second order in Ω, the corresponding stochastic process includes only single spin flips (i.e., $W_{\vec{\sigma}' \to \vec{\sigma}} \neq 0$ only if $\vec{\sigma}$ and $\vec{\sigma}'$ differ by a single spin). The rates read

$$\begin{aligned} W_{\vec{\sigma} \to \vec{\sigma}'} &= \frac{2\Omega^2}{\omega} \int_0^\infty d\tau e^{-\frac{2g_i^2 \nu}{\omega^2}(f(\tau)+\tau)} \cos\left[16 \tfrac{\Delta E_i \tau - g_i^2 s(\tau)}{\omega^2(\eta^2+4)}\right], \\ f(\tau) &= \frac{8-2\eta^2}{\eta\left(\eta^2+4\right)} \left[1 - e^{-\frac{\eta}{2}\tau} \cos(\tau)\right] - \frac{8 e^{-\frac{\eta}{2}\tau}}{\eta^2+4} \sin(\tau), \\ s(\tau) &= \frac{4\eta \left[e^{-\frac{\eta}{2}\tau} \cos(\tau) - 1\right] + \left[\eta^2 - 4\right] e^{-\frac{\eta}{2}\tau} \sin(\tau)}{\eta^2+4}, \end{aligned} \tag{5.5}$$

where the index i denotes which spin is being flipped and changes sign between configurations $\vec{\sigma}$ and $\vec{\sigma}'$.

In Eq. (5.5) we have introduced for brevity the (scaled) difference between loss and gain rates $\eta = (\gamma - \kappa)/\omega \equiv \gamma/\omega(1-\theta)$, the ratio $\theta = \kappa/\gamma \in [0, 1)$

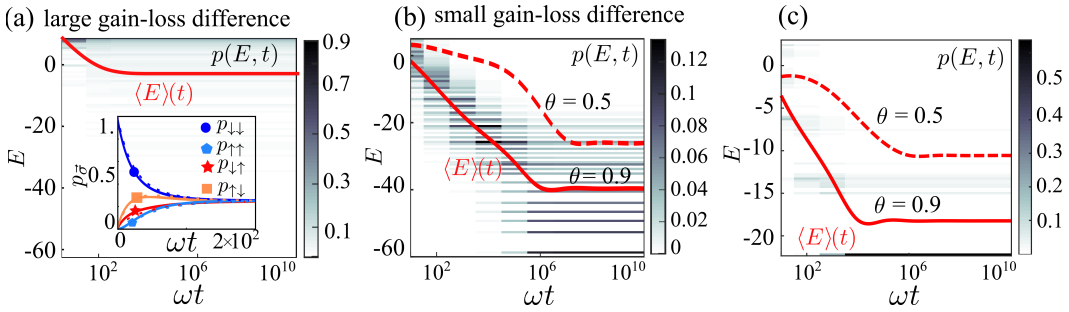


Figure 5.2: **Regimes of effectively thermal spin dynamics.** We set $\Omega = 0.1$, $\omega = 1$. (a) Statistical energy distribution versus time for $N = 10$ spins for large gain-loss difference η, starting from an initial state where all spins point down. The superposed red solid line displays the evolution of the average energy, $\langle E\rangle(t)$ as a function of time, whereas the shading represents the probability of being in a configuration with energy E at time t. We set $\eta = 10$ and $\theta = 1/11$ and we select the couplings g_i from a uniform distribution in $[-g_0, g_0]$ with $g_0 = 3$. Inset: evolution of the probabilities p_σ for a system of two spins with the same parameters. We compare the effective model (solid lines) with the numerically-exact diagonalization of the full open quantum problem (dashed lines), highlighting good agreement. (b) Statistical energy distribution versus time for $N = 10$ spins and corresponding evolution of the average energy, $\langle E\rangle(t)$ for $\eta = 0.1$ and $\theta = 0.9$ for the red solid line and $\theta = 0.5$ for the red dashed line. We select the couplings g_i as in (a). The shading represents the probability density of the energy levels and refers to the latter case ($\theta = 0.9$). (c) The same analysis of (b) has been performed with g_i having been selected from a bimodal distribution given by the symmetric superposition of two Gaussians centered in $\pm g_0 = \pm 1$ and variance $s = 0.25$. Again, the dynamics tends to preferentially populate the low-energy configurations at long times, and the more so the closer θ is to 1. As for (b), the shading relates to the $\theta = 0.9$ case.

and the parameter $\nu = 4(1+\theta)\eta/[(\eta^2+4)(1-\theta)]$. Importantly, the sole dependence on the spin configuration is through the quantity $\Delta E_i = g_i\sigma_i \sum_{l\neq i} g_l\sigma_l$, which can be interpreted as an energy difference, as it will clarified further below. Note that there is a characteristic scale of exponential suppression of the integrand of $W_{\vec{\sigma}\to\vec{\sigma}'}$. This corresponds to the typical timescale involved in the loss of coherence between sectors belonging to different classical spin configurations. Since the function $f(\tau)$ is bounded, and thereby $f(\tau)+\tau \sim \tau$ for $\tau \to \infty$, we can estimate this timescale as $t_{\rm L} = \tau_L/\omega \approx \omega/(2g^2\nu)$. Our perturbative expansion thus holds as long as $\Omega \ll 1/t_{\rm L}$.

In the following we perform a detailed investigation of the effective spin dynamics. It turns out that the loss-gain parameter η is central in determining the qualitative dynamical behavior: we will identify an effective high-temperature regime in the asymptotic limits $\eta \to \infty$ and $\eta \to 0^+$. Furthermore, we find an effective low-temperature (cooling) dynamics when $\eta < 1$ and θ is close to unity.

5.2 Large η: infinite temperature dynamics

As remarked above, the quantity ΔE_i can be interpreted as the change in the energy function

$$E(\vec{\sigma}) = -\frac{1}{4}\sum_{i\neq j} g_i g_j \sigma_i \sigma_j \,, \tag{5.6}$$

occurring when the i-th spin is flipped, i.e. $\Delta E_i = E(-\sigma_i) - E(\sigma_i)$. For a large gain-loss difference, $\eta \gg 1$, we find that in Eq. (5.5) $f(\tau) \sim s(\tau) \sim O(1/\eta)$. Therefore both functions are approximately zero and the parameter $\nu \approx 4\frac{1+\theta}{1-\theta}\eta^{-1}$ determines the leading behavior of the timescale $t_{\rm L}$. The validity of the perturbative requirement thus imposes an upper bound to the loss-gain difference, which must satisfy $1 \ll \eta \ll \frac{4g^2(1+\theta)}{\omega\Omega(1-\theta)}$.

With the above approximations the rate $W_{\vec{\sigma}\to\vec{\sigma}'}$ acquires a considerably simpler form: having neglected $s(\tau)$, it no longer depends on the sign of ΔE_i, implying that the rates for inverse processes $\sigma \to \sigma'$ and $\sigma' \to \sigma$ are equal. This gives rise to an infinite-temperature dynamics which populates all configurations uniformly. This behavior is highlighted in panel (a) of Fig. [5.2] for an example using couplings g_i extracted from a uniform distribution: we show that the average energy $\langle E\rangle(t)$ approaches (up to small corrections) zero, its infinite-temperature average, as a consequence of reaching an approximately equal population of all spin configurations at stationarity.

5.3 Small η: approximate low-temperature dynamics

We now consider the opposite case $0 < \eta \ll 1$; as we discuss further below, a regime can be found in which the rate equation dynamics mimics, to an extent, a thermal process with finite temperature. To start, we keep θ as an independent parameter and consider couplings extracted from the same uniform distribution employed above. As shown in panel (b) of Fig. [5.2], in this regime the stationary average of the energy function (5.6) generally approaches values distinctively lower than the infinite temperature one found in the previous Section. Moreover, our numerical exploration of this parameter regime suggests that this "cooling" tendency is enhanced as θ approaches its upper limit 1. An effect of this can be gleaned from the two curves for $\theta = 0.5$ (dashed line) and 0.9 (solid line) displayed in Fig. [5.2], panel (b), where the former clearly decreases to a lower value than the latter. From a physical standpoint, recalling that $\theta = \kappa/\gamma$ describes the relative strength of losses and gains, this suggests that the bosonic mode cools the spins more effectively when higher bosonic numbers are present.

In the third panel of Fig. [5.2] we repeat the same analysis for a set of couplings g_i produced from a different distribution. In this case, we take a symmetric, bimodal one, in order to mimic an associative memory model such as those described in Ch. 1. However, the following important differences are considered: first, as pointed out in previous works [30, 31], accounting for a single bosonic mode implies that only a single pattern (and its complementary, where all spins are flipped) can be stored in the system. Second, in previous works the couplings can only take two possible values $\pm g_0$ with equal probability. For consistency with our assumptions that no higher symmetries than the ones we identified at the beginning are present, in our work we cannot allow the couplings to be equal in pairs (otherwise the total spin on the pair of sites would be conserved). Hence, we broaden the peaks into two Gaussians, identical up to a translation, centered at $\pm g_0$ with variance s^2. In other words, if we denote by

$$\mathcal{N}_{g_0,s}(g) = (2\pi s^2)^{-1/2} \exp\left[-(g-g_0)^2/(2s^2)\right] \tag{5.7}$$

a generic normal distribution, we generate our couplings from

$$P(g) = \frac{1}{2}\left[\mathcal{N}_{g_0,s}(g) + \mathcal{N}_{-g_0,s}(g)\right]. \tag{5.8}$$

With this choice, the cooling behavior is still present and displays the same qualitative features highlighted for the uniform case, i.e. the dynamics tends to explore lower energies for values of θ closer to 1.

A naive comparison of panels (b) and (c) of Fig. [5.2] suggests that the bosons are more effective in their cooling action on the spins when the spin-boson couplings are bimodally distributed. In fact, one can notice a sharper contrast between the shading (proportional to the population) of the ground state with respect to the other energy levels in (c) than in (b). However, the two distributions have different variances and the scale of the shading is different in the two panels. In order to more properly address this difference, we have compared the bimodal distribution used in (c) with a uniform one with the same variance, i.e. with $g_0 = \sqrt{51}/4$. Figure [5.3] displays a counting diagram of the stationary ground state population for 1000 realizations of either distribution of the couplings. Here, one can notice that the bimodal case has, statistically speaking, a distinctively higher ground state population than the uniform case, peaking beyond 0.5. Uniformly-distributed couplings, in contrast, give rise to dynamics which typically populate the ground state much less, with a finite probability of having less than 5% population at long times.

5.4 Thermal versus non-thermal rates

In order to obtain some insights on this cooling mechanism we extract now some approximate expressions for the transition rate, which, for simplicity, we treat as a function of the energy difference ΔE, now regarded as a continuous parameter. Additionally, to simplify the treatment we restrict to the case where η is made smaller by bringing $\gamma \to \kappa^+$, while keeping κ and ω constant, so that $\theta = (1+\eta\omega/\kappa)^{-1}$ increases towards unity as η is decreased. Despite being a restriction, this allows us to explore the most interesting regime, i.e. the one where the dynamics seems to achieve the most efficient cooling. The details of the calculations can be found in Appendix B.2.

First, we note that, for sufficiently small η, the integrand defining $W_{\vec{\sigma}\to\vec{\sigma}'}$ is rapidly suppressed for $\tau > 0$ due to a fast initial increase of $f(\tau) \approx 2(1-\cos\tau)/\eta$. Thus, the integral is dominated by the contribution close to $\tau = 0$. Hence, one can expand all arguments in powers of τ. Setting for simplicity $\omega = \kappa = 1$ and keeping for brevity only the leading orders in $\eta \to 0$, one obtains $\tau + f(\tau) \approx \tau^2/\eta - \tau^3/6$, $\nu \approx 2$ and $s(\tau) \approx -\tau + \tau^3/6$. This implies that the suppression of the integrand occurs on a timescale $\tau \sim \sqrt{\eta/(4g_i^2)}$, whereas the cosine term oscillates with a frequency which is approximately $\Gamma_i = 4(\Delta E + g_i^2)$. We thereby identify (i) a regime of "small energy jumps", where $\Gamma_i^2 \ll 4g_i^2/\eta$ and (ii) a "large energy jumps" one with $\Gamma_i^2 \gg 4g_i^2/\eta$. In

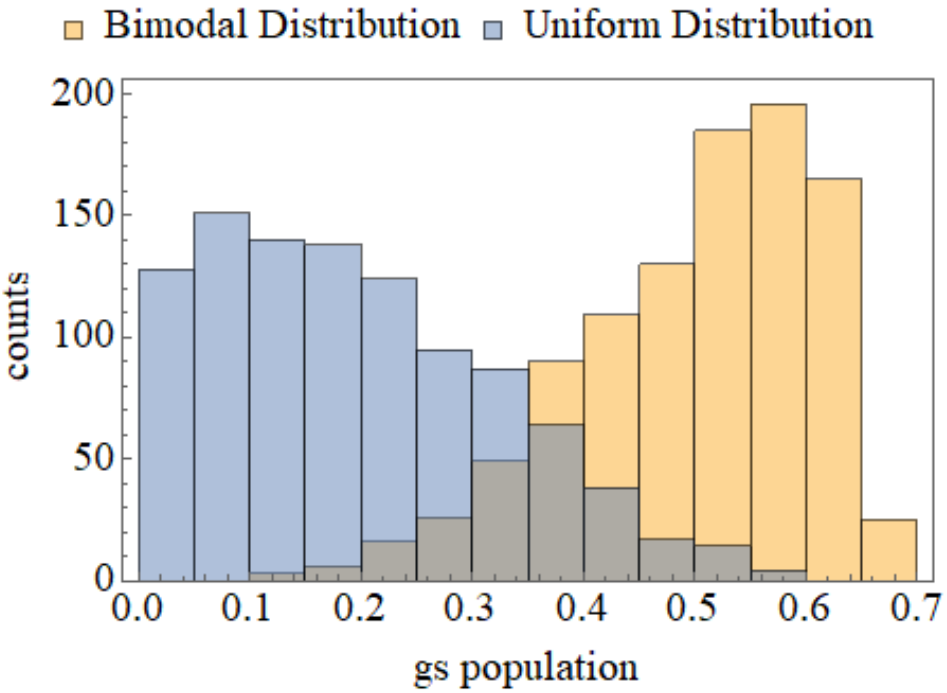


Figure 5.3: **Ground state population for two different distributions of the spin-boson couplings.** Histogram of the stationary ground state (gs) population for 1000 realizations of either distributions. Blue (yellow) columns refer to the uniform (bimodal) case. Both distributions have zero mean and variance $g^2 = 17/16$. The physical parameters are $\omega = 1$, $\eta = 0.1$, $\theta = 1/(\eta + 1) \approx 0.909$, $\Omega = 1$ for a system of $N = 10$ spins. The bimodal distribution data peaks beyond 0.5; the extracted mean is approximately 50% with a standard deviation of 11%, implying half of the final population typically lies in the ground state; the tails show a negligible probability of it being smaller than 20%. Conversely, the uniform distribution generates a slightly broader profile, with an average of approximately 20% and a standard deviation of 13%, implying that the ground state is populated much less in proportion.

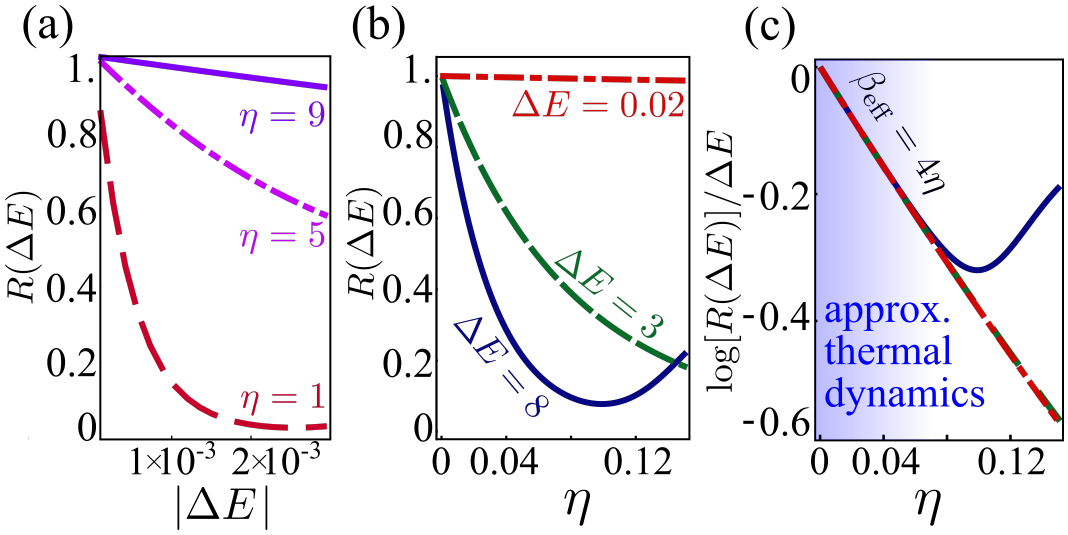


Figure 5.4: **Asymmetry of the rates.** We set $\Omega = 0.1, \omega = 0.1, \kappa = 1$. (a) Ratio $R_i(\Delta E) = W_i(\Delta E)/W_i(-\Delta E)$ versus energy difference $|\Delta E|$. For small values of η the rate $W_i(\Delta E)$ is strongly asymmetric with respect to ΔE, whereas for large η we have $W_i(\Delta E) \approx W_i(-\Delta E)$. (b) The ratio $R_i(\Delta E)$ is shown for three different values of $\Delta E = 0.02, 3, 8$ and the values of g_k are drawn from a uniform distribution with support in $[-g_0, g_0]$ with $g_0 = 6$. At small η, the ratio $R_i(\Delta E)$ approaches one, indicating that configurations are visited with equal probability as for large η. (c) The three curves in (b) are rescaled according to $\log R_i(\Delta E)/\Delta E$. Their asymptotic collapse in the limit $\eta \to 0$ highlights the existence of a unique inverse temperature $\beta_{\rm eff}$ which governs the dynamics when η is sufficiently small.

case (i), we obtain

$$W_i(\Delta E) \approx \frac{\Omega^2}{2}\sqrt{\frac{\pi\eta}{g_i^2}}e^{-\frac{\eta}{g_i^2}(\Delta E + g_i^2)^2}, \tag{5.9}$$

where the index i reminds us of which spin is being flipped [1]. The rate reaches its maximum when $\Delta E = -g_i^2 \leq 0$ and, in general, $W_i(|\Delta E|) < W_i(-|\Delta E|)$. This means that spin flips which lower the energy are favored, consistently with the picture of a cooling dynamics. Case (ii) can be analyzed using the asymptotic expansion of Fourier integrals [92]. To leading order this yields a power-law decay $W_i(\Delta E) \approx 8\Omega^2 g_i^2 \Gamma_i^{-4}$, which shares the same "cooling" properties, i.e. it corresponds to a rate that is is larger when ΔE is negative. A numerical integration suggests that $W_i(|\Delta E|) < W_i(-|\Delta E|)$ holds also in between the asymptotic cases (i) and (ii).

To shed further light on the cooling dynamics we analyze this asymmetry of the rates through the ratio $R_i(\Delta E) = W_i(\Delta E)/W_i(-\Delta E)$. This is depicted in Fig. [5.4(a,b)] as a function of ΔE and η, respectively. In regime (i) we

[1] Note, that in this notation if $W_{\vec{\sigma}\to\vec{\sigma}'} \equiv W_i(\Delta E)$ then $W_{\vec{\sigma}'\to\vec{\sigma}} \equiv W_i(-\Delta E)$).

have $R_i(\Delta E) \approx e^{-4\eta\Delta E}$, which implies a thermal dynamics with an effective inverse temperature $\beta_{\text{eff}} = 4\eta$. Note that the r.h.s. has no dependence on the index i, implying the existence of a unique, well-defined temperature for all spin-flip processes. In Fig. [5.4c] we display the ratio $\log[R_i(\Delta E)]/\Delta E$ for different values of ΔE and show that different curves collapse to a single (negative) inverse temperature $-\beta_{\text{eff}}$ up to the edge of case (i). At $\eta = 0$ we find that β_{eff} approaches zero, leading to an infinite-temperature dynamics. This is reasonable, since in this limit the bosonic gain rate approaches the loss rate. This implies the population of arbitrarily high Fock states, effectively heating the bosons. The latter then act as a high-temperature bath on the spins. If, on the other hand, $1/\beta_{\text{eff}}$ remains small or comparable with the energy gap from the ground states of (5.6) — which on average is of order g^2, meaning $4\eta g^2 \geq 1$) — an effective low-temperature dynamics is realized.

In case (ii), the ratio $R_i(\Delta E) \approx (\Delta E - g_i^2)^4/(\Delta E + g_i^2)^4$ tends to increase towards 1 as ΔE grows. Typically, the available ΔE_is populate both range (i) and (ii), implying the presence of type (ii) processes which do not follow the same low-temperature rules obeyed by the "small-jump" ones. Provided the number of spins N is not too large, these non-thermal processes constitute, however, a small perturbation for the following two reasons: first, the distribution of energy jumps is peaked around 0, implying that, if the parameters are adequately chosen, most jumps lie in regime (i). Second, since the rates are decreasing functions of $|\Delta E + g_i^2|$, type (ii) processes occur at smaller rates than the type (i), thermal ones. A numerically exact analysis of the classical master equation for $N = 10$, displayed in Fig. [5.2(b,c)], indeed shows that the effect of the non-thermal processes is sufficiently weak to avoid having a significant population of high-energy states in the long-time limit. The statistical energy distribution tends instead to become concentrated on low-energy configurations, highlighting a clear bias of the dynamics towards cooling, as compared e.g., to the $\eta \gg 1$ case in panel (a).

We remark that our considerations above are qualitatively independent of the choice of distribution for the couplings. The latter can influence instead the quantitative aspects, in particular the distribution of the energy jumps, and in turn what portion of them belongs to either the thermal of the non-thermal type. This can shed some light on the difference highlighted in Fig. [5.3]: in fact, it is reasonable to expect, among the two distributions with equal variance, that the uniform one will typically produce smaller (in modulus) couplings than the bimodal one, which is peaked instead away from the origin. Intuitively, the energies (5.6) and the energy jumps, quadratic in the couplings, will generically be smaller (in modulus) in the former than in the latter. Given that the parameter $\eta = 0.1$, and hence the effective (inverse) temperature $\beta_{\text{eff}} = 4\eta$, is the same for both cases displayed in Fig. [5.3], it

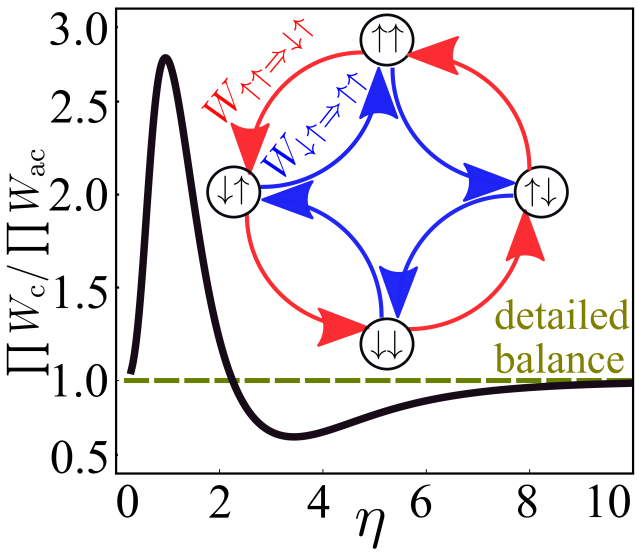


Figure 5.5: **Non-equilibrium regime.** Kolmogorov criterion in a two-spin subspace with uniformly distributed couplings; the displayed quantity is the ratio of the product $\prod W_c$ of the four rates encountered when performing the loop clockwise (blue arrows) divided by the analogous counter-clockwise (red arrows) product $\prod W_{ac}$, plotted as a function of η. This ratio is 1 (signalling detailed balance conditions) only for large and very small values of η. The intermediate point $\eta \approx 2$ where $\prod W_c = \prod W_{ac}$ can be safely ignored for the following reason: for systems with more than two spins there are multiple loops in configuration space and Kolmogorov's criterion is never satisfied simultaneously for all of them (except in the extremal limits $\eta \to 0$ and $\eta \to \infty$) and the dynamics does not obey detailed balance. The parameters are: $\omega = 1$, $\Omega = 0.1$, $\kappa = 1$ and $g_0 = 4$.

follows that the proportion in which higher-energy states will be populated will typically be greater for uniformly-distributed couplings than for the bimodal ones. The population of the ground state reflects this, being smaller in the former case than in the latter.

5.5 Breakdown of detailed balance

Outside the thermal regimes the dynamics is not an equilibrium one, i.e. it does not obey detailed balance. This can be proved via Kolmogorov's criterion [93] which we analyze for the loop formed in the configuration space of a two-spin system (see Fig. [5.5]): $(\uparrow\uparrow) \to (\uparrow\downarrow) \to (\downarrow\downarrow) \to (\downarrow\uparrow) \to (\uparrow\uparrow)$. To this end we investigate the ratio between the product of the rates for the clockwise (blue arrows) cycle and the corresponding product for the counter-clockwise (red arrows) one. This ratio goes to 1 when $\eta \to \infty$ and also when $\eta \to 0$, signalling the emergence of the infinite-temperature dy-

namics. For different values η the ratio is typically different from one, which indicates the persistence of probability currents in the stationary state and the absence of detailed balance.

5.6 Summary and outlook

We have studied a disordered dissipative spin-boson system in the limit of strong coupling and weak driving, which can for example be implemented on trapped ion quantum simulators. Many aspects of the emerging physics can be understood in terms of a disordered fully connected Ising model whose state evolves according to a rate equation. In general the dynamics violates detailed balance, and the system is thus out of equilibrium. However, we could identify parameter regimes in which the evolution is effectively thermal. Among them there is one where predominantly low-energy configurations are populated, which mimics the action of a low-temperature dynamics. We have compared two cases in which the couplings have been randomly generated from either a uniform or a bimodal distribution. The latter case typically displays a more effective ability to cool the spins, typically achieving more than 50% population of the ground state in the stationary limit. In the future it would be interesting to see whether this effective cooling mechanism permits to access low-energy states or even ground states of complex spin networks. This might open an elegant way for encoding and solving computationally hard problems [94] or associative memories [35] through Ising energy functions and an appropriate (thermal) dynamics on quantum simulators.

Chapter 6

Signatures of associative memory behavior in a multi-mode spin-boson model

As discussed in Ch. 3, the Dicke model under equilibrium conditions, and for large number of spins $N \to \infty$, displays a quantum phase transition from a dark to a superradiant phase: for weak spin-boson coupling the average occupation number of bosons is sub-extensive (it grows slower than N with the number of spins), whereas it is extensive ($\propto N$) above a critical threshold.

While originally predicted for a single bosonic degree of freedom, this phase transition was eventually generalized to a multi-mode scenario, where each spin interacts with several different bosonic modes. Interesting phenomena can emerge in this setting, in particular when the spin-boson couplings are non-uniform, disordered, and depend on both the specific spin and the specific boson. In this case the superradiant phase features glassy behavior [29, 30, 77] as well as an energy landscape that shares similarities with simple neural networks [31, 76, 80].

In the following, we deal with the multi-mode generalization of the model treated in Ch. 5, taking into account a driven-dissipative multi-mode spin-boson model, which is sketched in panel (a) of Fig. [6.1]. We show that its stationary properties resemble those of the HNN presented in Ch. 1. More precisely, we identify a crossover between a disordered "paramagnetic" phase and an ordered "ferromagnetic" one, as schematically illustrated in Fig. [6.1], panel (b); the latter appears to be closely related to the retrieval phase of the HNN, characterized in turn by the ability to recall previously stored information. We furthermore explore the impact of fluctuating spin-boson coupling constants on this crossover. Our results show that analogies between multi-mode spin-boson systems and phases of the HNN are not

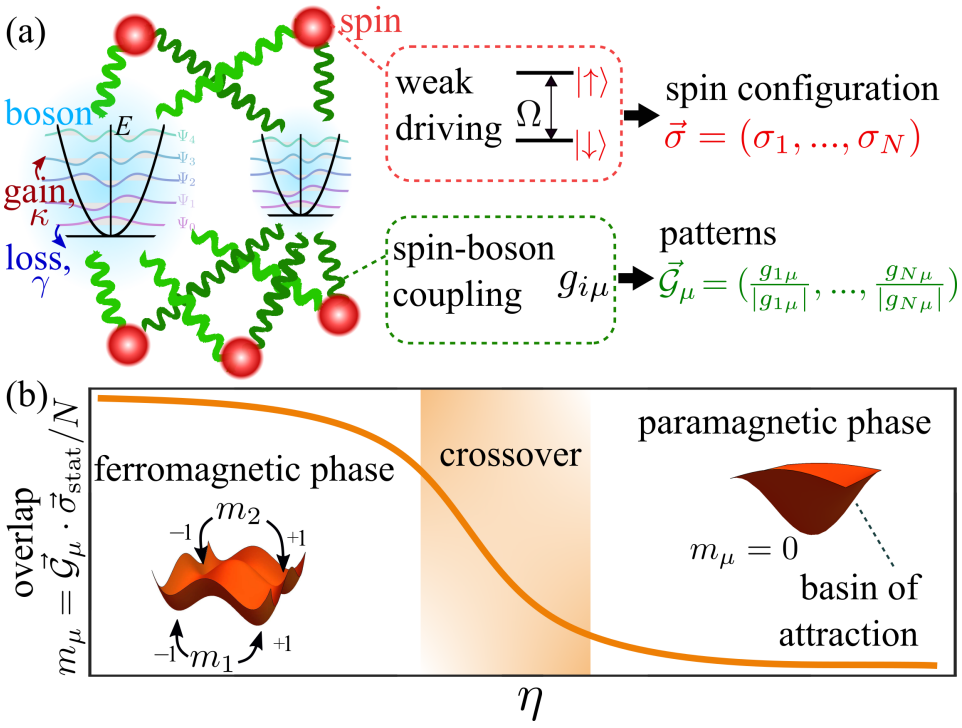


Figure 6.1: **Disordered, dissipative spin-boson system.** (a) N spin-1/2 particles are strongly coupled to two bosonic modes with couplings $g_{i\mu}$ ($i = 1, ..., N$, $\mu = 1, 2$). The spins are weakly driven at a strength $\Omega \ll g_{i\mu}$. Each bosonic mode is subjected to two dissipative processes, gain and loss, occuring at rates κ and γ respectively. Patterns are encoded in the couplings between the spins and the bosons, corresponding to $\vec{\mathcal{G}}_\mu = [\text{sign}(g_{1\mu}), ..., \text{sign}(g_{N\mu})]^T$ ($\mu = 1, 2$). (b) Phase diagram of the overlap $m_\mu = (\mathcal{G}_\mu \cdot \vec{\sigma}_{\rm stat})/N$ between the classical, stationary spin configuration and the pattern as a function of the parameter $\eta = (\gamma - \kappa)/\omega$ (for details see text). A smooth transition between two phases occurs, these being characterized by the presence of several (ferromagnetic or "retrieval" phase) and one (paramagnetic one) basins of attraction. The insets show qualitative sketches of the effective free energy landscape.

limited to equilibrium settings that have been considered in Sec. 3.3.

The work presented in this Chapter appears in the publication:

"Signatures of Associative Memory Behavior in a Multimode Dicke Model"
E. Fiorelli, M. Marcuzzi, P. Rotondo, F. Carollo, I. Lesanovsky
Physical Review Letters **125**, 070604 (2020).

6.1 Non-equilibrium multi-mode spin-boson model

In this Section we briefly introduce the generalization of the single spin-boson system that has been treated in Sec. 5.1 to the multi-mode case. The

system is made of N spin-$1/2$ particles that interact with M independent bosonic modes, according to the Dicke-like Hamiltonian

$$H = \sum_{\mu=1}^{M} \omega_\mu a_\mu^\dagger a_\mu + \sum_{\mu=1}^{M}\sum_{i=1}^{N} g_{i\mu}\sigma_i^z(a_\mu^\dagger + a_\mu) + \Omega \sum_{i=1}^{N} \sigma_i^x. \tag{6.1}$$

The interaction coupling $g_{i\mu}$ are now spin and boson dependent, and we assume them to be independent, identically-distributed, real random variables. Additionally, the system exchanges bosons with a markovian bath, so that the system state ρ evolves according to a GKSL equation of type (2.19). This reads

$$\dot{\rho} = \mathcal{L}\rho = -i[H,\rho] + \sum_{\mu,n=l,g} L_{n,\mu}\rho L_{n,\mu}^\dagger - \frac{1}{2}\{L_{n,\mu}^\dagger L_{n,\mu}, \rho\}, \tag{6.2}$$

where the jump operators $L_{l,\mu} = \sqrt{\gamma_\mu}a_\mu$, $L_{g,\mu} = \sqrt{\kappa_\mu}a_\mu^\dagger$ describe independent processes of loss and gain of bosons at rates $\gamma_\mu > \kappa_\mu \geqslant 0$.

Similarly to the case of a single boson case, we can obtain an effective master equation restricted to the spin degrees of freedom only: Up to order Ω^2 the reduced spin dynamics is encoded in the classical rate equation

$$\dot{p}_{\vec{\sigma}} = \sum_{\vec{\sigma}'} \left(W_{\vec{\sigma}'\to\vec{\sigma}}p_{\vec{\sigma}'} - W_{\vec{\sigma}\to\vec{\sigma}'}p_{\vec{\sigma}}\right), \tag{6.3}$$

with $p_{\vec{\sigma}}$ the probability to find the spins in the configuration $\vec{\sigma}$ and $W_{\vec{\sigma}\to\vec{\sigma}'}$ the transition rate for switching from configuration $\vec{\sigma}$ to $\vec{\sigma}'$. Due to the structure of the perturbative term, the only allowed elementary processes are single spin flips, i.e. $W_{\vec{\sigma}\to\vec{\sigma}'} \neq 0$ exclusively when $\vec{\sigma}$ and $\vec{\sigma}'$ differ by a single spin. Restricting for simplicity to $\gamma_\mu \equiv \gamma$, $\kappa_\mu \equiv \kappa$, $\omega_\mu \equiv \omega$, $\forall\mu$, the derivation of Eq. (6.3) can be found in Appendix B.1. We also set $\omega = 1$.

6.1.1 Energy function, overlaps and coupling distribution

Remarkably, when generalizing the result (5.6) derived for the single-mode case, it turns out that the transition rates only depend on the spin configuration through the quantity $\Delta E_i = \sigma_i \sum_{\mu,j\neq i} g_{i\mu}g_{j\mu}\sigma_j$, which can be regarded as the cost $\Delta E_i = E(-\sigma_i) - E(\sigma_i)$ of flipping the i-th spin given an energy function of the form

$$E(\vec{\sigma}) = -\frac{1}{4}\sum_{\mu}\sum_{i\neq j} g_{i\mu}g_{j\mu}\sigma_i\sigma_j. \tag{6.4}$$

Equation (6.4) bears a clear resemblance to the Hopfield energy (1.10) if one replaces the patterns $\xi_{i\mu}$ with the spin-boson couplings $g_{i\mu}$. With this analogy in mind, we interpret the spin-boson couplings as "noisy patterns". Specifically, we pick the coupling constants $g_{i\mu}$ from a bimodal distribution

as the one defined by Eq. (5.8) and peaked around ± 1; i.e. we consider $\mathcal{P}(g) = \frac{1}{2}[\mathcal{N}_{+1,s}(g) + \mathcal{N}_{-1,s}(g)]$, given by the symmetric superposition of two Gaussians $\mathcal{N}_{g_0,s}(g)$ as defined by Eq. (5.7). From this perspective, it is natural to introduce, as prospective order parameters, and in analogy to the HNN, the *overlaps*

$$m_\mu = \sum_{i=1}^{N} \text{sign}(g_{i\mu})\sigma_i/N \equiv \vec{\mathcal{G}}_\mu \cdot \vec{\sigma}/N, \tag{6.5}$$

where $\vec{\mathcal{G}}_\mu = [\text{sign}(g_{1\mu}), ..., \text{sign}(g_{N\mu})]^T$ represent the "noiseless" patterns.

For the sake of simplicity, and in analogy with the previous Chapter, we focus on the behavior of m_μ upon varying only the parameter $\eta = \gamma - \kappa$ that quantifies the net bosonic loss rate. As we show further below, this parameter controls, to some extent, effective thermal fluctuations. We further fix $\kappa/\gamma = 0.9$, $N = 50$, $M = 2$. Finally, as transition rates are $\propto \Omega^2$, we rescale the time accordingly and effectively set $\Omega = 1$.

6.2 Non-equilibrium dynamics

We simulate the dynamics (6.3) via kinetic Monte Carlo methods [95–97]. For convenience, we call different realizations of the stochastic process "trajectories", reserving "realizations" for different random choices of the couplings.

As a starting point of the analysis we consider that, as discussed in Ch. 1, the HNN dynamics within the retrieval phase is characterized by the presence of multiple basins of attractions, labeled by the solutions in Eq. (1.25). On the other hand, the paramagnetic phase is characterized by the presence of a single basin of attraction, which is labeled by the solution of Eq. (1.24). Two trajectories (at fixed coupling realization) of the stochastic process (6.3) are shown in panel (a) of Fig. [6.2] for two distinct η regimes. In both cases, the initial configuration is obtained by flipping 20% of the $N = 50$ spins with respect to the first pattern; that is, the initial configuration is 80% aligned with the first pattern implying $m_1(t = 0) = 0.6$. For ease of visualization we apply a gauge transformation $\sigma_i \to \mathcal{G}_{i,1}\sigma_i$, $\mathcal{G}_{i,\mu} \to \mathcal{G}_{i,1}\mathcal{G}_{i,\mu}$ which aligns all the components of the first pattern, $\mathcal{G}_{i,1}\xi_i^1 > 0$, $\forall i$. The components are then re-ordered to bring all the positive components of the second pattern on one side and all the negative ones on the other. In the small-η regime (left-hand side) the dynamics is trapped for long times in configurations close to either pattern; these long-lasting periods are separated by fast switching from one pattern to the other, a behavior commonly seen in finite-size versions of systems undergoing spontaneous symmetry breaking. Phenomenologically (see panel (b) of Fig. [6.1]), the free energy landscape over the space of con-

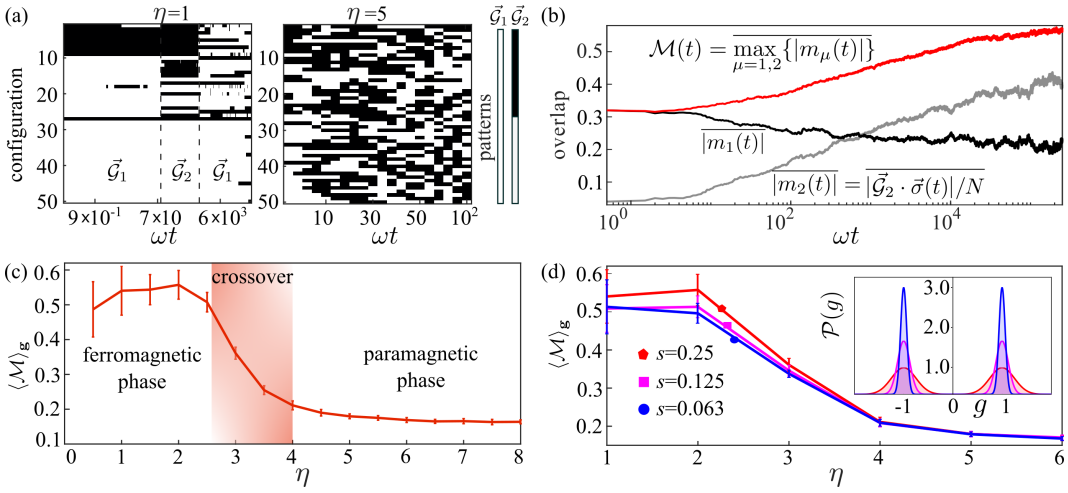


Figure 6.2: (a)-(b) **Stochastic dynamics.** We select the spin-boson couplings from a bimodal distribution given by two superposed Gaussians centered at $g_0 = \pm 1$ and standard deviation $s = 0.25$. (a) Time evolution of a spin configuration at fixed disorder realization. The two patterns $\vec{\mathcal{G}}_{1,2}$ are represented in the legend. At the initial time, the overlap between the spin configuration and $\mathcal{G}_1$ is $m_1(0) = 0.6$. The left-hand side panel shows the time evolution at $\eta = 1$, whereas the right-hand side shows the time evolution at $\eta = 5$. (b) Time evolution of order parameter and overlaps as a function of time, at $\eta = 1$. The overlaps are shown in terms of the absolute values averaged over $N_{\rm traj} = 200$ realizations of the stochastic process (6.3). The initial configuration is chosen randomly. (c)-(d) **Stationary properties.** Disorder-averaged order parameter $\langle\mathcal{M}\rangle_{\rm g}$ as a function of η and its standard deviation (half error bars) $\pm(\langle\mathcal{M}^2\rangle_{\rm g} - \langle\mathcal{M}\rangle_{\rm g}^2)^{1/2}$, resulting after the average over $N_{\rm distr} = 30$ disorder realizations of the (symmetrized) order parameter $\mathcal{M}$. The specific times at which the points are taken differ at different η since, as can be gleaned from Fig. [6.2a], the dynamical timescales differ greatly in the opposite regimes of small and large η. Lines are guides for the eyes. (c) The interaction coupling are selected from a bimodal distribution given by superposing two Gaussians centered in $g_0 = \pm 1$ and with standard deviation $s = 0.25$. (d) Plots of the symmetrized order parameter against η for three values of the standard deviation $s = 0.25$ (red star), $s = 0.125$ (magenta square), and $s = 0.063$ (blue circle), as reported in the legend. Different Gaussian distributions are represented in the inset. Other parameters are $N = 50$, $M = 2$, $\omega = 1$, $\kappa/\gamma = 0.9$.

figurations breaks into different, approximate basins of attraction (BA); the dynamics tends to remain confined in one such "potential well" until a rare, sufficiently large fluctuation is able to overcome the barrier, after which the dynamics is trapped again for long times in the new BA. A similar behavior would also be observed, at finite size, in the thermal dynamics of the HNN within the retrieval phase. For large η (right-hand side), instead, memory of the initial state is quickly lost; the dynamics does not appreciably approach either pattern, implying $m_1 \approx m_2 \approx 0$ and corresponding to a case with a single, trivial BA, analogous to the paramagnetic phase of the HNN.

The emergence of multiple BAs for small η, in which the configuration tends to fluctuate close to one of the recorded patterns, shows that, in spite of the dissipation, the system is still dynamically capable of retrieving part of the stored information. In order to quantify this very capacity, we consider averages over a number N_{traj} of trajectories, which we denote by $\overline{O(t)}$ for an observable O at time t. Panel (b) of Fig. [6.2] shows the typical evolution of the average overlaps $\overline{|m_\mu(t)|}$ (grey and black curves) at fixed coupling realization, $\eta = 1$ and $N_{\mathrm{traj}} = 200$, where the absolute value is taken to avoid averaging to zero due to the $\vec{\sigma} \leftrightarrow -\vec{\sigma}$ symmetry of the model. These quantities clearly assume finite values at long times. These values, however, are not indicative of the overlaps that can be actually achieved in any given trajectory. This is because, once the dynamics starts exploring different BAs, at most one overlap will be appreciably different from zero at any given time. We clarify this with an example: say that, at a large time t, pN_{traj} trajectories (with $p < 1$) align with the first pattern giving $|m_1(t)| = m$, whereas the others align with the second one ($m_1(t) \approx 0$). Then, $\overline{|m_1(t)|} \approx pm < m$. To obviate this reduction, we also study the averaged maximum

$$\mathcal{M}(t) = \overline{\max(|m_1(t)|, |m_2(t)|)}, \tag{6.6}$$

which constitutes a one-component order parameter symmetric under sign change $\vec{\sigma} \leftrightarrow -\vec{\sigma}$ and pattern permutation ($1 \leftarrow 2$); this symmetrization makes $\mathcal{M}(t)$ a more reliable estimate of the overlap that can be achieved within individual trajectories on either pattern.

6.3 Stationary properties

To estimate the extent of the retrieval regime, we now focus on the stationary (long-time) properties and study $\mathcal{M}(t \to \infty)$ as a function of η. We additionally account for the fact that this quantity depends on the specific realization of the couplings and is thus a random variable. We thereby denote by $\langle \mathcal{M} \rangle_{\mathbf{g}}$ its average over the previously-defined doubly-peaked distribution of the $g_{i\mu}$s and plot it against η in panel (c) of Fig. [6.2].

As discussed in Ch. 5, when considering the large and the small η limits, effectively thermal regimes can occur. At large η, an infinite temperature scenario emerges. The finite value taken by the disorder-averaged $\langle \mathcal{M} \rangle_{\mathbf{g}}$ in this regime is due to the finite size of the system. As η is decreased, a crossover emerges towards larger and larger values and for $\eta \approx O(1)$ it seems to reach a maximum of approximately 0.5, meaning 75% of the configuration spins are aligned with a pattern. In this regime, the error bars get larger as well, implying that the system becomes more sensitive to the specific values taken by the spin-boson couplings. Combining these results with the dynamical ones from the previous Section, showing the emergence of several approximate BAs, suggests that the two regimes, η large and small, reproduce to an extent the physics of the paramagnetic and retrieval phases of a HNN, with η playing the role of an effective temperature. Future investigations at variable system size will shed further light on the features of the crossover. In order to provide some insights on the role of quantum fluctuations, a comparison with a simpler model is performed in Appendix B.4.

6.4 Influence of pattern noise

We recall that, in order to connect the physics of the HNN to our model, we considered the couplings $\vec{g}_\mu$ as noisy patterns, and $\vec{\mathcal{G}}_\mu$ as the noiseless ones. One can thus distinguish between two sources of fluctuations: (i) the randomness of the patterns, whose components can be either ± 1 with equal probability , and (ii) the noise due to the finite width s of the distribution peaks around ± 1.

It is worth noticing that, while (i) is present in the HNN as well, (ii) represents an additional source of noise specific to our model. For this reason, we wish to better understand its impact on the retrieval ability of the dynamics, reporting the result in panel (d) of Fig. [6.2]. After having excluded the rightmost points $\eta > 6$, we compare the data used for the curve in panel (c), corresponding to $s = 0.25$ (red) to two additional data sets analogously obtained for $s = 0.125$ (magenta) and 0.063 (blue). Interestingly, reducing s does not seem to affect the standard deviation (i.e. the error bars); instead, one can spot a decrease in the average values $\langle \mathcal{M} \rangle_{\mathbf{g}}$. This suggests that small amounts of noise over the patterns can very slightly improve the retrieval of stored information. Although the cause is not entirely clear, it is worth mentioning that a similar effect can be observed in the HNN too (see Appendix B.3 for further details), where, at finite size, the introduction of disorder over the patterns induces a broadening of the order parameter profile. This broadening results in an effective increase of the overlaps close

to the critical point; as one moves deeper in the retrieval phase, however, the effect is reversed and the average overlap decreases at larger noise levels.

6.5 Summary and outlook

We have investigated the dynamics and the stationary phases of a dissipative multi-mode spin-boson model, highlighting analogies between this many-body system and the HNN, such as a pattern retrieval dynamics and a crossover between a retrieval and a paramagnetic phase. Beyond mimicking the HNN, physical realizations of this spin-boson Hamiltonian, e.g. atom-cavity setups, have the potential to systematically probe the quantum regime, i.e. go beyond the perturbative limit considered here. Increasing the degree of "quantumness", i.e. adding the possibility to host superpositions and entanglement offers intriguing potential for exploring quantum effects in the context of machine learning.

Conclusions

In this thesis we have dealt with two different aspects concerning the implementation of HNN via open quantum systems. First, we have investigated an open quantum generalization of HNNs, asking whether this description could lead to a speed-up in reaching a retrieval state, with respect to the classical counterpart. Second, we have considered a practically relevant many-body system (spin-boson) that naturally implements a HNN dynamics, and may be thus considered as a quantum generalization of a HNN.

As the HNN is modeled in terms of a classical spin network ruled by a stochastic dynamics, we first considered the issue of dealing with a meaningful generalization of this kind of systems in terms of quantum mechanics. To this end, in Chapter 4 we explored the question as to whether quantum effects can yield a speed-up of the non-equilibrium evolution of fully connected quadratic spin models towards a classical thermal state. In our approach, we exploited the fact that the thermal state of a spin system can be mapped onto a node-free quantum state whose coefficients are given by thermal weights. This perspective permits the construction of a dissipative – yet quantum – dynamics which encodes in its stationary state the thermal state of the original problem. We have shown for the case of an all-to-all connected Ising spin model that an appropriate transformation of this dissipative dynamics allows the system to interpolate between a regime in which the order parameter obeys the classical equations of motion under Glauber dynamics, to a quantum regime with an accelerated transient timescale before approaching stationarity. Furthermore, we have shown that this effect enables in principle a speedup of pattern retrieval in a HNN.

In order to deal with feasible physical realizations of quantum systems showing HNN-like properties, we have then focused on spin-boson Hamiltonians that are described by the Dicke model. The latter are indeed an effective description for numerous quantum many-body systems such as atoms coupled to cavity modes, quantum electrodynamics in circuits and trapped ion systems. In equilibrium, these systems often feature a radical change in their behavior when switching from weak to strong spin-boson interaction. This usually manifests in a transition from a “normal" to a “superradi-

ant" phase. However, understanding the out-of-equilibrium physics of these models is extremely challenging, and even more so for strong spin-boson coupling. While reaching the latter limit is possible in current experiments, the theoretical analysis of the physics in this parameter regime, when both disorder and dissipation are taken into account, is a challenge.

In Chapter 5, we have investigated a regime where the many-body spin dynamics can be related to an Ising energy function defined in terms of the spin-boson couplings. While in the coherent weak coupling regime it is known that an effective description in terms of a spin Hamiltonian is possible, we have shown that a similar viewpoint can be adopted in the presence of dissipation and strong couplings. The resulting many-body dynamics features approximately thermal regimes, separated by out-of-equilibrium ones in which detailed balance is broken. Moreover, we have shown that under appropriately chosen conditions one can even achieve cooling of the spin degrees of freedom. In Chapter 6 we have generalized such a result, showing that the non-equilibrium multi-mode Dicke model at strong coupling can mimic some fundamental properties of an associative memory. Patterns have been encoded in the couplings between spins and bosons, and we have discussed the dynamics of the spins from the perspective of pattern retrieval in HNN models. We identified two phases, a “paramagnetic" and a “ferromagnetic" one, and a crossover behavior between these regimes. The “ferromagnetic" phase is reminiscent of pattern retrieval. We have highlighted similarities and differences with the thermal dynamics of a HNN and shown that indeed elements of associative memory behavior emerge in the strongly coupled multi-mode Dicke model.

Appendices

Appendix A

Technical details for Part II

A.1 Construction of the jump operators

In this Section we provide details on how Eq. (4.5) can be obtained. Our starting point is to consider a classical spin model defined in terms of an energy function $E(\vec{\sigma})$ and an equilibrium probability distribution $P_{\rm eq}(\vec{\sigma}) = e^{-\beta E(\vec{\sigma})}/Z(\beta)$, with $\{\vec{\sigma}\} = \{\sigma_1, \sigma_2, ..., \sigma_N\}$ a set of configurations of the classical spins, being $\sigma_i = \pm 1$ a classical Ising variable. As a preliminary step, we promote the classical variables σ_i to quantum spins σ_i^z and the corresponding classical configurations $\{\vec{\sigma}\}$ to quantum states $|\vec{\sigma}\rangle$ such that $\sigma_z^i |\vec{\sigma}\rangle = \sigma_i |\vec{\sigma}\rangle$.

Once having set these definitions, we require the pure state

$$|\Psi_{\rm ss}\rangle = \frac{1}{\sqrt{Z(\beta)}} \sum_{\{\vec{\sigma}\}} e^{-\frac{\beta}{2}E(\vec{\sigma})} |\vec{\sigma}\rangle \tag{A.1}$$

to be a dark state of the dynamics defined in Eq. (4.2) , i.e. $L_k |\Psi_{\rm ss}\rangle = 0 \ \forall k$. In order to get an explicit form for the jump operator L_k, we consider the k-th spin state $|\psi\rangle_k = \frac{1}{N(\beta)} e^{-\frac{\beta}{2}E(\vec{\sigma}_{\{k\}},\sigma_k=1)} |\uparrow\rangle_k + e^{-\frac{\beta}{2}E(\vec{\sigma}_{\{k\}},\sigma_k=-1)} |\downarrow\rangle_k$, where $\vec{\sigma}_{\{k\}} = (\sigma_1, ..\sigma_{k-1}, \sigma_{k+1}, ..., \sigma_N)$ and $N(\beta)$ is a normalization factor. It is worth noticing that the state $|\psi\rangle_k$ represents a local dark state of the dynamics, i.e. $L_k |\psi\rangle_k = 0$ with respect to the jump operator defined in Eq. (4.5). Therefore, applying the jump operator (4.5) to the state (A.1) we find

$$\begin{aligned} L_k |\Psi_{\rm ss}\rangle =& L_k \frac{1}{Z(\beta)^{1/2}} \sum_{\vec{\sigma}_{\{k\}}} (e^{-\frac{\beta}{2}E(\vec{\sigma}_{\{k\}},\sigma_k=1)} |\uparrow\rangle_k + \\ &+ e^{-\frac{\beta}{2}E(\vec{\sigma}_{\{k\}},\sigma_k=-1)} |\downarrow\rangle_k) \otimes e^{-\frac{\beta}{2}\vec{\sigma}_{\{k\}}} |\vec{\sigma}_{\{k\}}\rangle = \\ &\frac{1}{Z(\beta)^{1/2}} \sum_{\vec{\sigma}_{\{k\}}} L_k |\psi\rangle_k \otimes e^{-\frac{\beta}{2}\vec{\sigma}_{\{k\}}} |\vec{\sigma}_{\{k\}}\rangle = 0. \end{aligned} \tag{A.2}$$

A.2 Derivation of the equations of motion

This Section is devoted to provide details on how Eq. (4.8) can be derived. We first consider the equations of motion generated by the markovian and purely dissipative dynamics defined in Eq. (4.2) with the jumps operators (4.5), corresponding to the case $\theta = 0$. We shall account for the additional unitary transformation $u_i(\theta, \phi)$, instead, further below. We thereby evolve generic operators O via the adjoint Lindblad equation $\dot{O} = \sum_k L_k^\dagger O L_k - \frac{1}{2}\{L_k^\dagger L_k, O\}$.

In particular, this can be applied to the Pauli matrices σ_i^γ, $\gamma = +, -, z$, according to

$$\dot{\sigma}_i^\gamma = \sum_k L_k^\dagger \sigma_i^\gamma L_k - \frac{1}{2}\{L_k^\dagger L_k, \sigma_i^\gamma\}. \tag{A.3}$$

We consider first the σ_i^z operator. Since the "couplings" $\alpha_k^\pm$ appearing in the jump operators only depend on operators σ^z, we have that $[\alpha_k^\pm, \sigma_i^z] = 0$ $\forall k, i$. This, in turn, implies that $[L_k, \sigma_i^z] = 0$ $\forall k \neq i$ and therefore all terms arising from the sum over $k \neq i$ vanish, and Eq. (A.3) reads

$$\dot{\sigma}_i^z = -\frac{1}{2}\mathrm{sech}(\beta \Delta E_i)\sigma_i^x + \frac{1}{2}\left[1 + \tanh(\beta \Delta E_i)\right](1 - \sigma_i^z), \tag{A.4}$$

where we recall that we are denoting $2n_i = 1 + \sigma_i^z$ and we have used the identities $n_i^2 = n_i$, $n_i \sigma_i^+ = \sigma_i^+$, $\sigma_i^- n_i = \sigma_i^-$.

We now shift our attention to the equation of motion for σ_i^+ (the one for σ_i^- can then be obtained directly via hermitian conjugation). The term obtained for $k = i$ is

$$-\frac{\sigma_i^+}{2} + \frac{\alpha_i^- \alpha_i^+}{2}. \tag{A.5}$$

Regarding the terms arising for $k \neq i$, it is useful to introduce some shorthand notation. First, we note that any function $F(\{\sigma_k^z\}_k)$ regular enough to have a Taylor series expansion can be commuted with σ_i^+ at the price of inverting the sign of σ_i^z, i.e. $\sigma_i^+ F(\{\sigma_k^z\}_k) = F(\{\sigma_k^z\}_{k\neq i}, -\sigma_i^z)\sigma_i^+$. Accordingly,

$$\sigma_i^+ \alpha_k^+ = \frac{e^{\frac{\beta}{2}\sum_{j\neq i} J_{kj}\sigma_j^z} e^{-\frac{\beta}{2} J_{ki}\sigma_i^z}}{\sqrt{2\cosh(\beta \sum_{j\neq i} J_{kj}\sigma_j^z - \beta J_{ki}\sigma_i^z)}} \sigma_i^+ \equiv \alpha_{ki}^+ \sigma_i^+. \tag{A.6}$$

Similarly, we define

$$\alpha_{ki}^- = \frac{e^{-\frac{\beta}{2}\sum_{j\neq i} J_{kj}\sigma_j^z} e^{\frac{\beta}{2} J_{ki}\sigma_i^z}}{\sqrt{2\cosh(\beta \sum_{j\neq i} J_{kj}\sigma_j^z - \beta J_{ki}\sigma_i^z)}}. \tag{A.7}$$

This allows us to compactly write the following commutation relations

$$\begin{aligned}
&\sigma_i^+(\alpha_k^+)^2 = (\alpha_{ki}^+)^2\sigma_i^+, \\
&\sigma_i^+\alpha_k^- = \alpha_{ki}^-\sigma_i^+, \\
&\sigma_i^+(\alpha_k^-)^2 = (\alpha_{ki}^-)^2\sigma_i^+.
\end{aligned} \tag{A.8}$$

Calculating the contribution coming from the sum over $k \neq i$ in the equation of motion for σ_i^+ and collecting all terms, we can thus write

$$\begin{aligned}
\dot{\sigma}_i^+ = &-\frac{\sigma_i^+}{2} + \frac{\alpha_i^-\alpha_i^+}{2} + \sum_{k\neq i}\frac{1}{2}\Big[-\left(\alpha_k^- - \alpha_{ki}^-\right)^2 n_k - \\
&-(\alpha_k^+ - \alpha_{ki}^+)^2\sigma_k^-\sigma_k^+ + (\alpha_k^+ - \alpha_{ki}^+)(\alpha_k^-\sigma_k^+ - \alpha_{ki}^-\sigma_k^-) - \\
&-(\alpha_k^- - \alpha_{ki}^-)(\alpha_{ki}^+\sigma_k^+ - \alpha_k^+\sigma_k^-)\Big]\,\sigma_i^+.
\end{aligned} \tag{A.9}$$

In order to simplify this last equation, we now wish to exploit our assumption on the classical energy function $E(\vec{z}) = -\sum_{i,j} J_{ij}z_iz_j$, which describes a fully connected model. We recall that in Sec. 4.1 we defined $2\Delta E_i = E(\{\, z_k \to \sigma_k^z \,\}_{k\neq i}, z_i = -1) - E(\{\, z_k \to \sigma_k^z \,\}_{k\neq i}, z_i = +1)$. In order to have an energy function which is extensive in the system size, we ask that $J_{ki} \sim 1/N$. Considering the thermodynamic limit and performing a series expansion in $1/N$ it is

$$\alpha_k^\pm - \alpha_{ki}^\pm = \pm\alpha_k^\pm\left[1 \mp \tanh\left(\beta\sum_j J_{kj}\sigma_j^z\right)\right]\beta J_{ki}\sigma_i^z + O\left(N^{-2}\right). \tag{A.10}$$

We note now that this difference is $O(N^{-1})$. Since in the thermodynamic limit we neglect everything beyond this perturbative order, we can approximate any terms multiplying $(\alpha_k^\pm - \alpha_{ki}^\pm)$ with their $O(1)$ contribution. In particular, $(\alpha_k^\pm - \alpha_{ki}^\pm)\alpha_{ki}^\pm \to (\alpha_k^\pm - \alpha_{ki}^\pm)\alpha_k^\pm$. Equation (A.9) then reads, at leading order,

$$\begin{aligned}
\dot{\sigma}_i^+ = &-\frac{\sigma_i^+}{2} + \frac{\alpha_i^-\alpha_i^+}{2} + \sum_{k\neq i}\alpha_k^+\alpha_k^-\beta J_{ki}(i\sigma_k^y)\sigma_i^+ = \\
&-\frac{\sigma_i^+}{2} + \frac{1}{4}\mathrm{sech}(\beta\Delta E_i) + i\frac{\beta}{2}\sum_{k\neq i}\mathrm{sech}(\beta\Delta E_k)\sigma_k^y\sigma_i^+,
\end{aligned} \tag{A.11}$$

where we use the identities $\sigma_k^y = -i(\sigma_k^+ - \sigma_k^-)$ and $\sigma_i^z\sigma_i^+ = \sigma_i^+$ and make the products $\alpha_k^+\alpha_k^-$ explicit.

The dynamical equations for $\sigma_i^{x,y}$ are thus

$$\begin{aligned}
\dot{\sigma}_i^x &= -\frac{\sigma_i^x}{2} + \frac{1}{2}\mathrm{sech}(\beta\Delta E_i) - \frac{\beta}{2}\sum_{k\neq i} J_{ki}\mathrm{sech}(\beta\Delta E_k)\sigma_k^y\sigma_i^y, \\
\dot{\sigma}_i^y &= -\frac{\sigma_i^y}{2} + \frac{\beta}{2}\sum_{k\neq i} J_{ki}\mathrm{sech}(\beta\Delta E_k)\sigma_k^y\sigma_i^x,
\end{aligned} \tag{A.12}$$

A.2.1 Unitary transformation of the jump operators

As we explain in Sec. 4.1, the stationary state of the dynamics given by Eq. (4.2) does not change under applying unitary transformations u_i to the jump operators according to $L_i \to u_i L_i \equiv L'_i$. One can therefore generalize the dynamics to a class of processes "spanned" by the parameters entering these u_is. For simplicity, we restrict to unitaries such that u_i acts solely on the i-th spin. In each of the local subspaces, we choose

$$L'_i \equiv u_i L_i = \alpha_i^- u_i n_i - \alpha_i^+ u_i \sigma_i^+, \tag{A.13}$$

We choose to generalize the jump operators with the following equal spin rotation on all sites

$$u_i = \begin{pmatrix} \cos\theta & e^{i\phi}\sin\theta \\ -e^{-i\phi}\sin\theta & \cos\theta \end{pmatrix}, \tag{A.14}$$

where the matrix representation is given in the eigenbasis of σ_i^z.

Similarly, we represent $L_i^\dagger L_i$ as a matrix with operatorial entries

$$L_i^\dagger L_i = \begin{pmatrix} \alpha_i^- & 0 \\ -\alpha_i^+ & 0 \end{pmatrix} \begin{pmatrix} \alpha_i^- & -\alpha_i^+ \\ 0 & 0 \end{pmatrix} = \begin{pmatrix} (\alpha_i^-)^2 & -\alpha_i^-\alpha_i^+ \\ -\alpha_i^-\alpha_i^+ & (\alpha_i^+)^2 \end{pmatrix}. \tag{A.15}$$

The dynamical equation for σ_i^z reads

$$\dot\sigma_i^z = L_i'^\dagger \sigma_i^z L'_i - \frac{1}{2}\{L_i'^\dagger L'_i, \sigma_i^z\} = L_i'^\dagger \sigma_i^z L'_i - \frac{1}{2}\{L_i^\dagger L_i, \sigma_i^z\}, \tag{A.16}$$

where the first term on the right-hand side reads

$$L_i'^\dagger \sigma_i^z L'_i = L_i^\dagger u_i^\dagger \sigma_i^z u_i L_i = f_z L_i^\dagger L_i, \tag{A.17}$$

with the definition $f_z(\theta) \equiv \cos(2\theta)$.

The dynamical equation for σ_i^+ in the thermodynamic limit is instead

$$\begin{aligned} \dot\sigma_i^+ =& L_i'^\dagger \sigma_i^+ L'_i - \frac{1}{2}\{L_i^\dagger L_i, \sigma_i^+\} + \\ &+ \sum_{k\neq i} L_k'^\dagger \sigma_i^+ L'_k - \frac{1}{2}\{L_k^\dagger L_k, \sigma_i^+\}, \end{aligned} \tag{A.18}$$

where

$$\begin{aligned} L_i'^\dagger \sigma_i^+ L'_i &= L_i^\dagger u_i^\dagger \sigma_i^+ u_i L_i = -\cos(\theta)\sin(\theta) e^{-i\phi} L_i^\dagger L_i, \\ L_k'^\dagger \sigma_i^+ L'_k &= L_k^\dagger u_k^\dagger \sigma_i^+ u_k L_k = L_k^\dagger \sigma_i^+ L_k. \end{aligned} \tag{A.19}$$

Collecting all terms, the dynamical equations for generic (θ, ϕ) are

$$\begin{aligned} \dot\sigma_i^x =& -A_i^x(\beta) - \frac{\beta}{2}\sum_{k\neq i} J_{ki}\,\mathrm{sech}(\beta\Delta E_k)\sigma_k^y\sigma_i^y + \frac{\mathrm{sech}(\beta\Delta E_i)}{2}, \\ \dot\sigma_i^y =& -A_i^y(\beta) + \frac{\beta}{2}\sum_{k\neq i} J_{ki}\,\mathrm{sech}(\beta\Delta E_k)\sigma_k^y\sigma_i^x, \\ \dot\sigma_i^z =& -A_i^z(\beta) + \frac{1}{2}\tanh(\beta\Delta E_i), \end{aligned} \tag{A.20}$$

where we have defined $f_x(\theta,\phi) \equiv -\sin(2\theta)\cos(\phi)$, $f_y(\theta,\phi) \equiv \sin(2\theta)\sin(\phi)$ and $A_i^\alpha(\beta) = \{f_\alpha\,[\mathrm{sech}(\beta\Delta E_i)\sigma_i^x + \tanh(\beta\Delta E_i)\sigma_i^z - 1] + \sigma_i^\alpha\}/2$, $\alpha = x,y,z$. We observe that if one takes $f_x = 0$, i.e. $\theta_i = \frac{\pi}{4}\ \forall i$, the equation for σ_z^i decouples from the other operators and reads $\dot{\sigma}_i^z = \frac{1}{2}[-\sigma_i^z + \tanh(\beta\Delta E_i)]$. This allows us to compare the quantum dynamics with the classical one.

A.3 Stability analysis of the fully connected Ising model

We consider here the fully connected Ising model discussed in Section 4.2.1 of Chapter 4, obtained for $J_{ij} = 1/N$, $\forall i,j$, or equivalently for an energy function $E = -\frac{1}{N}\sum_{i,j}\sigma_i\sigma_j$. In the thermodynamic limit, the $3N$ equations of motions (4.8) are reduced to the closed set of 3 equations (4.9) for the collective operators $m^\alpha = \langle s^\alpha\rangle = 1/N\sum_{i=1}^N\langle\sigma_i^\alpha\rangle$, $\alpha = x,y,z$. For the reader's convenience we repeat them below:

$$\begin{aligned}
\dot{m}^x &= -A_x + \frac{1}{2}\mathrm{sech}(\beta m^z) - \frac{\beta}{2}\mathrm{sech}(\beta m^z)(m^y)^2,\\
\dot{m}^y &= -A_y + \frac{\beta}{2}\mathrm{sech}(\beta m^z)m^y m^x,\\
\dot{m}^z &= -A_z + \frac{1}{2}\tanh(\beta m^z),
\end{aligned} \tag{A.21}$$

where $A_\alpha = \{f_\alpha\,[m^x\mathrm{sech}(\beta m^z) + m^z\tanh(\beta m^z) - 1] + m^\alpha\}/2$, $\alpha = x,y,z$ and $f_x = -\sin(2\theta)\cos(\phi)$, $f_y = \sin(2\theta)\sin(\phi)$ and $f_z = \cos(2\theta)$.

The stationary solutions $\bar{m}^\alpha$ of interest of these equations obey $\bar{m}^x = \mathrm{sech}(\beta\bar{m}^z)$, $\bar{m}^y = 0$ and $\bar{m}^z = \tanh(\beta\bar{m}^z)$. In order to analyze their stability we consider a small shift away from them, i.e. we set $m^\alpha = \bar{m}^\alpha + \delta m^\alpha$ and expand the equations perturbatively in δm^α up to linear order. We analyze the timescales that characterize the long-time approach of m^α to the "ferromagnetic" stationary solution that appears for $\beta > 1$, comparing the quantum case (generic θ and ϕ) with the classical one ($\theta = \pi/4$). As we are considering the dynamics near to the stationary solution, we perform a first order expansion of Eqs. (A.21) around the fixed points, say $\bar{m^\alpha}$, so that $m^\alpha \sim \bar{m}^\alpha + \delta m^\alpha$. It is worth noting that the stationary solution itself is independent on the unitary transformation that has been applied on the jump operators, i.e. on the angles θ and ϕ, hence we can get the stationary solution $\bar{m}^\alpha$ fixing the values of θ and ϕ. For the sake of simplicity, we set $\theta = \pi/4$, $\phi = 0$ getting $\bar{m}^x = \mathrm{sech}(\beta\bar{m}^z)$, $\bar{m}^y = 0$ and $\bar{m}^z = \tanh(\beta\bar{m}^z)$.

This yields a linear equation of the form

$$\begin{pmatrix}\delta\dot{m}^x\\ \delta\dot{m}^y\\ \delta\dot{m}^z\end{pmatrix} = S\begin{pmatrix}\delta m^x\\ \delta m^y\\ \delta m^z\end{pmatrix}, \tag{A.22}$$

where the matrix elements of S are

$$\begin{aligned}
S_{11} =& -\frac{1}{2}(f_x \mathrm{sech}(\beta\bar{m}^z)+1), \quad S_{12}=S_{32}=0,\\
S_{13} =& \frac{1}{4}\mathrm{sech}^2(\beta\bar{m}^z)\left[f_x g(m^x,m^z)\ -2\beta\sinh(\beta\bar{m}^z)\right],\\
S_{21} =& -\frac{f_y}{2}\mathrm{sech}(\beta\bar{m}^z), \quad S_{31}=-\frac{f_z}{2}\mathrm{sech}(\beta\bar{m}^z),\\
S_{22} =& \frac{1}{2}[-1+\beta\mathrm{sech}(\beta\bar{m}^z)\bar{m}^x],\\
S_{23} =& \frac{f_y}{4}\mathrm{sech}^2(\beta\bar{m}^z)(g(m^x,m^z)-\sinh(2\beta\bar{m}^z))\\
S_{33} =& \frac{\mathrm{sech}^2(\beta\bar{m}^z)}{4}\left[f_z g(m^x,m^z)\ +2\beta\right]-\frac{1}{2}.
\end{aligned} \tag{A.23}$$

where $g(m^x,m^z) = (2\beta\bar{m}^x\sinh(\beta\bar{m}^z)-2\beta\bar{m}^z-\sinh(2\beta\bar{m}^z))$

It is not difficult to see that

$$S\begin{pmatrix}0\\1\\0\end{pmatrix}=\begin{pmatrix}0\\S_{22}\\0\end{pmatrix}, \tag{A.24}$$

implying that S_{22} is one of the eigenvalues of S. As it does not depend on the angles (θ,ϕ), this eigenvalue is the same in both the quantum ($\theta\neq\pi/4$) and classical ($\theta=\pi/4$) regimes.

We can immediately see that when substituting the stationary values of $\bar{m}^x$ in S_{22}, which is an eigenvalue of S, this is equal to the classical one obtained fixing $\theta=\pi/4$. A second important observation is that in the classical regime $f_z=0$ and therefore

$$S_{33}(\theta=\pi/4)=\frac{1}{2}\left[-1+\beta\mathrm{sech}^2(\beta\bar{m}^z)\right] \tag{A.25}$$

is also an eigenvalue of S and, since $\bar{m}^x=\mathrm{sech}(\beta\bar{m}^z)$, $S_{33}(\theta=\pi/4)=S_{22}$. This implies that, in the long-time limit, the quantum dynamics is dominated either by the same timescale or by a longer one than the classical dynamics. Therefore, the faster approach towards the stationary state of the quantum case over the classical one, which occurs for some value of θ and ϕ as reported in Ch. 4, is only due by the early stages of the dynamics.

A.4 Dynamical equations for the p memory case

In this Section we provide the main steps of the derivation of the equations of motion (4.11) in the case of a Hopfield network. We recall the definition of the overlap operators $s^\alpha_\mu \equiv \frac{1}{N}\sum_{i=1}^N \xi_i^{(\mu)}\sigma_i^\gamma, \alpha=x,y,z$. Their evolution in the Heisenberg picture depend explicitly on the patterns ξ_i^μ, which in turn are classical, discrete, independent identically distributed random variables

taking the values ± 1 with equal probability. We now note that (i) again, the stationary solution is independent on the unitary transformation, therefore it is the same obtained in the classical case $\theta = \pi/4$; (ii) the stationary dark state reproduces in its diagonal elements the probability distribution of a classical Hopfield NN; (iii) given any operator $O(\sigma^z)$ that is diagonal on the σ_i^z basis, the expectation value on the stationary state is the classical average value, being the correspondent weights the thermal ones, i.e. $\langle O(\sigma_z)\rangle = \mathrm{Tr}(\rho_{SS} O(\sigma_z)) = \frac{1}{Z(\beta)} \sum_{\vec{\sigma}} e^{-\beta E(\vec{\sigma})} \langle \vec{\sigma}|O(\sigma^z)|\vec{\sigma}\rangle$.

The previous considerations lead us to argue that the dynamics of the expectation value of spin operators will be mostly determined by the properties of the overlap and therefore we employ the following approximation,

$$\langle \sigma_i^\alpha \rangle \sim \xi_i^\mu m_\mu^\alpha, \ \alpha = x, y, z, \tag{A.26}$$

where $m_\mu^\alpha = \langle s_\mu^\alpha \rangle$ represents the expectation value calculated on the instantaneous quantum state. We assume now that the equations satisfy a self-averaging property, i.e. we substitute $\frac{1}{N}\sum_i f(\vec{\xi_i}) \to \overline{f(\vec{\xi})}$, where $\overline{(\cdot)}$ denotes the average over the pattern distribution.

Performing a mean field approximation, i.e. neglecting the correlations among the overlaps, we thus get

$$\begin{aligned} \dot{m}_\mu^{x,y} &= -\bar{A}_\mu^{x,y}(\beta), \\ \dot{m}_\mu^{z} &= -\bar{A}_\mu^{z}(\beta) + \frac{1}{2}\overline{\xi^\mu \tanh \beta \vec{\xi}\cdot\vec{m}^z}, \end{aligned} \tag{A.27}$$

where $\bar{A}_\mu^\alpha = \left[f_\alpha m_\mu^x \overline{\mathrm{sech}(\beta\vec{\xi}\cdot\vec{m}^z)} + m_\mu^\alpha \right]/2$, $\alpha = x, y, z$, $\vec{\xi} = (\xi^1, ..., \xi^p)^T$, and $\vec{m}^\alpha = (m_1^\alpha, ..., m_p^\alpha)^T$.

As a first consistency check for the approximations employed, we have verified that the stationary state is invariant under change of the angles (θ, ϕ) and that its qualitative structure is consistent with the classical one, i.e. only a paramagnetic stable solution appears at $\beta < 1$, whereas several retrieval solutions emerge at $\beta > 1$.

Second, we checked the results of these equations for small β with a high temperature expansion of Eqs. (A.27), obtaining agreement both in the early and late stages of the dynamics.

A.4.1 Stability analysis

Similarly to the Ising case, we sketch here the stability analysis of Eqs. (4.11), expanding them around the stationary solutions of the overlaps for $\beta > 1$ up to the first order. For the sake of simplicity, we fix $\theta = \pi/4$, $\phi = \pi/2$ in order to get the stationary solutions which read $\bar{m}_\nu^{x,y} = 0$, $\bar{m}_\nu^z = \overline{\xi^\nu \tanh(\beta\vec{\xi}\cdot\vec{\bar{m}}^z)}$. The expressions of the overlaps are thus taken to be

$$
\begin{aligned}
&m_\nu^{x,y} \approx \delta m_\nu^{x,y} \quad \forall \nu, \\
&m_\mu^z \approx \bar{m}_\mu^z + \delta m_\mu^z, \quad m_\nu^z \approx \delta m_\nu^z \, \forall \nu \neq \mu,
\end{aligned}
\tag{A.28}
$$

and we get $\begin{pmatrix} \delta \dot{m}_\mu^x \\ \delta \dot{m}_\mu^y \\ \delta \dot{m}_\mu^z \end{pmatrix} = S \begin{pmatrix} \delta m_\mu^x \\ \delta m_\mu^y \\ \delta m_\mu^z \end{pmatrix}$, with

$$
S = \begin{pmatrix} -\frac{1}{2}\left[f_x \mathrm{sech}(\beta \bar{m}_\mu^z) + 1\right] & 0 & 0 \\ -\frac{f_y}{2}\mathrm{sech}(\beta \bar{m}_\mu^z) & -\frac{1}{2} & 0 \\ -\frac{f_z}{2}\mathrm{sech}(\beta \bar{m}_\mu^z) & 0 & \frac{1}{2}\left[\frac{\beta}{\cosh^2(\beta \bar{m}_\mu^z)} - 1\right] \end{pmatrix}. \tag{A.29}
$$

Due to the triangular structure of this matrix, the eigenvalues can be directly read off the diagonal. We note that S_{33} is now independent of θ and ϕ, implying that, as in the Ising case, the asymptotic timescales of the quantum dynamics are either the same or longer than those of the classical dynamics ($\theta = \pi/4$). Hence, the net gain observed in the quantum dynamics arises only from the initial transient.

A.4.2 Symmetries within the θ-ϕ plane

We discuss here the three symmetries we exploit which allow us to focus on a portion (one eighth) of the θ-ϕ plane in Fig. [4.3] of Ch. 4. The first one is a symmetry of the dynamics, which is invariant under the involutive transformation $(\theta, \phi) \to (\pi - \theta, \phi + \pi)$ (remembering that θ is defined modulo π and ϕ modulo 2π). For any given choice of the initial conditions, the dynamics at (θ, ϕ) exactly matches the one at $(\pi - \theta, \phi + \pi)$ and the timescales involved are therefore also the same.

The other symmetries of the plot are not symmetries of the dynamics, and are only recovered upon averaging over the initial conditions. The first one involves the substitution $\phi \to \pi - \phi$ (which changes the sign of f_y) and $\vec{m}^y \to -\vec{m}^y$, which leaves the equations invariant. Therefore, any trajectory $\vec{m}^{x,y,z}(t)$ obtained at (θ, ϕ) is equivalent to one obtained at $(\theta, \pi - \phi)$ where the y component is simply inverted. Clearly, this does not affect the timescales of the dynamics. Since we are sampling over a symmetric distribution of initial conditions on $\vec{m}^y$, averages must be symmetric under $\phi \to \pi - \phi$.

Finally, we consider the transformation $\theta \to \pi/2 - \theta$ and $\vec{m}^z \to -\vec{m}^z$, which also leaves the equations invariant. For "quantum" trajectories the argument follows the same steps employed above: since the initial condition is generated symmetrically in m^z, averages should be symmetric under $\theta \to \pi/2 - \theta$. For the classical trajectories, since the initial conditions are biased by a fixed amount Z_0 this does not hold. However, the classical case ($\theta = \pi/4$) is special since θ gets simply mapped onto itself (and in fact $\vec{m}^z \to$

$-\vec{m}^z$ represents by itself a symmetry of the equations). Hence, the average dynamical timescales are symmetric under $\theta \to \pi/2 - \theta$ as well.

Appendix B

Technical details for Part III

B.1 Rate equation for a strongly coupled spin-boson model

In this Appendix we provide details on how Eq. (5.5) is derived. We consider the more general case of a multi-mode Dicke model with dissipation, which is the focus of Chapter 6. However, the result can be easily specialized to the single-mode case treated in Chapter 5. The state of the system, $\rho(t)$, evolves according to the Lindblad equation $\dot{\rho}(t) = \mathcal{L}[\rho(t)] = -i[H, \rho(t)] + \sum_{\mu=1}^{M} \sum_{n=l,g} L_{\mu,n}\rho(t)L_{\mu,n}^{\dagger} - \frac{1}{2}\{L_{\mu,n}^{\dagger}L_{\mu,n}, \rho(t)\}$. In order to obtain an effective description of the spin dynamics at strong coupling, we consider the evolution of the state as $\dot{\rho} = \mathcal{L}_0(\rho) + \mathcal{L}_1(\rho)$, with $\mathcal{L}_0 = \mathcal{L} - \mathcal{L}_1$ and $\mathcal{L}_1(\cdot) = -i\Omega[\sum_i \sigma_i^x, \cdot]$.

We first focus on the dynamics generated by $\mathcal{L}_0$. It is worth noticing that each spin operator σ_i^z is a conserved quantity under the action of the superoperator $\mathcal{L}_0$. As a result, the eigenstates of σ_i^z operators, $|\vec{\sigma}\rangle = |(\sigma_1, ..., \sigma_N)^T\rangle$, with $\sigma_i^z |\vec{\sigma}\rangle = \sigma_i |\vec{\sigma}\rangle$ and th $\sigma_i = \pm 1$, identify 2^N spin sectors. These are spanned by the combination $|\vec{\sigma}\rangle\langle\vec{\sigma}|$ and represent 2^N degenerate stationary subspaces. Thus, we can assume the stationary state of $\mathcal{L}_0$ of the form $\rho_{\text{stat}} = \sum_{\vec{\sigma}} p_{\vec{\sigma}}\rho_{\vec{\sigma}} |\vec{\sigma}\rangle\langle\vec{\sigma}|$, where $p_{\vec{\sigma}}$ are a set of classical probabilities and ρ_σ is the corresponding bosonic state, that we take to be a Gaussian state.

Secondly, we consider the superoperator $\mathcal{L}_1$, which mixes different spin sectors, as a perturbation with respect to $\mathcal{L}_0$, i.e. we consider $\Omega \ll g$. Indeed, projecting the dynamics onto the stationary manifold of $\mathcal{L}_0$, we exploit the Nakajima-Zwanzig formalism, up to the order $O(\Omega^2)$, to write the evolution

of the spins as

$$
\begin{aligned}
P\dot{\rho}^{\text{spin}}(\tau) &= \text{Tr}_B \int_0^{+\infty} d\tau' P\mathcal{L}_1 e^{\mathcal{L}_0\tau'}\mathcal{L}_1\rho_{\text{stat}}(\tau) \\
&= \Omega^2 \sum_{\{\vec{\sigma}\}} p_{\vec{\sigma}}(\tau) \sum_i \int_0^{+\infty} d\tau' \sum_{j=\pm} \text{Tr}_B \left[e^{\mathcal{V}^j_{\vec{\sigma},i}\tau'}(\rho_{\vec{\sigma}})\right] \\
&\times \left(\sigma_i^x \left|\vec{\sigma}\right\rangle \left\langle\vec{\sigma}\right| \sigma_i^x - \left|\vec{\sigma}\right\rangle \left\langle\vec{\sigma}\right|\right),
\end{aligned}
\tag{B.1}
$$

where $P\dot{\rho}^{\text{spin}}(\tau) = \text{Tr}_B[\dot{\rho}_{\text{stat}}(\tau)] = \sum_{\vec{\sigma}} \dot{p}_{\vec{\sigma}}(\tau) \left|\vec{\sigma}\right\rangle \left\langle\vec{\sigma}\right|$, and Tr_B is the partial trace over the bosonic modes. Furthermore, we have defined the spin-configuration dependent superoperators

$$
\begin{aligned}
\mathcal{V}^{\pm}_{\vec{\sigma},i}(\cdot) = \sum_{\mu} \Big\{ &-i\omega_\mu[a_\mu^\dagger a_\mu, \cdot] + \mathcal{D}_{\gamma_\mu}(\cdot) + \mathcal{D}_{\kappa_\mu}(\cdot) - iM_{l\mu}\left[(a_\mu^\dagger + a_\mu), \cdot\right] \\
&\pm i g_{l\mu}\sigma_l \left\{(a_\mu^\dagger + a_\mu), \cdot\right\}\Big\},
\end{aligned}
\tag{B.2}
$$

with $M_{l\mu} = \sum_{n\neq l} g_{n\mu}\sigma_n$, and $\mathcal{D}_{\gamma_\mu}$, $\mathcal{D}_{\kappa_\mu}$ the dissipative terms representing loss and gain, respectively. By projecting Eq. (B.1) on a state $|\vec{\sigma}'\rangle$, the dynamics reduces to the evolution of the classical probabilities ruled by a master equation as

$$
\dot{p}_{\vec{\sigma}} = \sum_{\vec{\sigma}'} \left(W_{\vec{\sigma}'\to\vec{\sigma}} p_{\vec{\sigma}'} - W_{\vec{\sigma}\to\vec{\sigma}'} p_{\vec{\sigma}}\right)
\tag{B.3}
$$

where $W_{\vec{\sigma}\to\vec{\sigma}'} = \Omega^2 \int_0^{+\infty} d\tau \sum_{j=\pm} \text{Tr}_B \left[e^{\mathcal{V}^j_{\vec{\sigma},i}\tau}(\rho_{\vec{\sigma}})\right]$, is the transition rate for the switching $\vec{\sigma} \to \vec{\sigma}'$ and it allows only spin flip processes.

For going ahead in evaluating the rate expression, we exploit the superoperator properties and we write $\text{Tr}_B \left[e^{\mathcal{V}^{\pm}_{\vec{\sigma},i}}(\rho_{\vec{\sigma}})\right] = \text{Tr}_B \left[(e^{\mathcal{V}^{\pm,*}_{\vec{\sigma},i}}\mathbb{I})\rho_{\vec{\sigma}}\right]$, with $\mathcal{V}^{\pm,*}_{\vec{\sigma},i}$ the adjoint superoperator of $\mathcal{V}^{\pm}_{\vec{\sigma},i}$ and $\mathbb{I}$ the identity operator. Moreover, the identity operator can be expressed in terms of a generalized displacement operator of a multi-mode bosonic coherent state as $\mathbb{I} = \mathcal{D}(0)$, where $\mathcal{D}(\tau) = e^{\sum_\mu \alpha_\mu(\tau)a_\mu^\dagger - \beta_\mu(\tau)a_\mu} e^{-\sum_\mu \gamma_\mu(\tau)}$ with $\alpha_\mu(0) = \beta_\mu(0) = \gamma_\mu(0) = 0$, $\forall\mu$. The operator $\mathcal{D}$ can be written as $\mathcal{D}(\tau) = \prod_\mu D_\mu(\tau)e^{-\gamma_\mu(\tau)}$, where $D_\mu(\tau) = e^{\alpha_\mu(\tau)a_\mu^\dagger - \beta_\mu(\tau)a_\mu}$, due to the commutation of bosonic operators referring to different modes. We then verify that the displacement operator $\mathcal{D}(0)$ is mapped into the generalized one $\mathcal{D}(\tau)$ by applying the adjoint superoperator $\mathcal{V}^{\pm}_{\vec{\sigma},i}$. To this end, we consider the differential equation $\frac{d}{d\tau}\left[\mathcal{D}^{\pm}_{\vec{\sigma},i}(\tau)\right] = \mathcal{V}^{\pm *}_{\vec{\sigma},i}\left[\mathcal{D}^{\pm}_{\vec{\sigma},i}(\tau)\right]$ and we obtain the solutions for the functions $\alpha^+_{\sigma_i\mu}(\tau) = \alpha^-_{-\sigma_i\mu}(\tau)$, $\beta^+_{\sigma_i\mu}(\tau) = \beta^-_{-\sigma_i\mu}(\tau)$, $\gamma^+_{\sigma_i\mu}(\tau) = \gamma^-_{-\sigma_i\mu}(\tau)$. For initial conditions $\alpha^{\pm}_{\sigma_i\mu}(0) = \beta^{\pm}_{\sigma_i\mu}(0) = \gamma^{\pm}_{\sigma_i\mu}(0) = 0$, and considering, for the sake of simplicity, $\omega_\mu \equiv \omega$, $\gamma_\mu \equiv \gamma$, $\kappa_\mu \equiv \kappa$ $\forall\mu$, we

get

$$
\begin{aligned}
\alpha^{+}_{\sigma_i\mu}(t) &= [\beta^{+}_{\sigma_i\mu}(t)]^{*} = \frac{i4g_{i\mu}\sigma_i}{\omega(\eta-2i)}\left[1-e^{(i-\frac{\eta}{2})t}\right], \\
\gamma^{+}_{\sigma_i\mu}(t) &= \frac{2g^2_{i\mu}\nu}{\omega^2\eta}\left[f_1(t)+t\right] + \frac{ig_{i\mu}\sigma_i M_{i\mu}}{\omega^2(\eta^2+4)}[s(t)+t], \\
f_1(t) &= \frac{1-e^{\eta t}}{\eta} - \frac{4\eta[1-e^{-\frac{\eta}{2}t}\cos(t)] - 8e^{-\frac{\eta}{2}t}\sin(t)}{\eta^2+4}, \\
s(t) &= \frac{4\eta\left[e^{-\frac{\eta}{2}t}\cos(t)-1\right] + (\eta^2-4)\,e^{-\frac{\eta}{2}t}\sin(t)}{\eta^2+4},
\end{aligned}
\tag{B.4}
$$

where we have defined the dimensionless time $t = \tau\omega$, and $\eta = (\gamma-\kappa)/\omega$, $\theta = \kappa/\gamma \in [0,1)$, and $\nu = 4(1+\theta)\eta/[(\eta^2+4)(1-\theta)]$.

The previous steps allow us to write the partial trace over the boson as $\mathrm{Tr}_B[e^{\mathcal{V}^{\pm}_{\vec{\sigma},i}}(\rho_{\vec{\sigma}})] = e^{-\sum_\mu \gamma^{\pm}_{\sigma_i\mu}(t)}\mathrm{Tr}_B[\mathcal{D}^{\pm}_{\vec{\sigma},i}(t)\rho_{\vec{\sigma}}]$. Recalling that the bosonic state $\rho_{\vec{\sigma}}$ is a multi-mode Gaussian state, we recognize the quantity $\mathrm{Tr}_B[\mathcal{D}^{\pm}_{\vec{\sigma},i}(t)\rho_{\vec{\sigma}}]$ as the *characteristic function* $\chi^{\pm}_{\vec{\sigma},i}(t)$ of the state $\rho_{\vec{\sigma}}$. The expression of the characteristic function for a generic Gaussian state ρ_G of a p-mode bosonic field reads

$$
\begin{aligned}
\chi_{\rho_G} &= e^{\vec{\alpha}^T\mathbf{\Omega}\vec{a}_G - \frac{1}{4}\vec{\alpha}^T\mathbf{\Sigma}\vec{\alpha}} = e^{\sum_{\mu=1}^{p}[\alpha_\mu\langle a^\dagger\rangle_G - \alpha^*_\mu\langle a\rangle_G - \frac{1}{4}\vec{\alpha}^T_\mu\Sigma_\mu\vec{\alpha}_\mu]} \\
\mathbf{\Omega} &= \bigoplus_{\mu=1}^{p}\Omega_\mu,\ \Omega_\mu = \begin{pmatrix} 0 & 1 \\ -1 & 0 \end{pmatrix} \\
\mathbf{\Sigma} &= \bigoplus_{\mu=1}^{p}\Sigma_\mu,
\end{aligned}
\tag{B.5}
$$

where $\vec{\alpha}^T = (\alpha_1, \alpha_1^*, ..., \alpha_p, \alpha_p^*)$, $\vec{\alpha}^T_\mu = (\alpha_\mu, \alpha_\mu^*)$, $\vec{a}^T_G = (\langle a_1\rangle_G, \langle a_1^\dagger\rangle_G, ..., \langle a_p\rangle_G, \langle a_p^\dagger\rangle_G)$, and $\langle\cdot\rangle_G$ are the expectation values of bosonic operators on the Gaussian sate ρ_G, and Σ_μ is the single mode covariance matrix and reads

$$
2\begin{pmatrix} -(\langle a^2\rangle_G - \langle a\rangle^2_G) & \frac{1}{2}(\langle a^\dagger a\rangle_G + \langle aa^\dagger\rangle_G) - \langle a^\dagger\rangle_G\langle a\rangle_G \\ \frac{1}{2}(\langle a^\dagger a\rangle_c + \langle aa^\dagger\rangle_G) - \langle a^\dagger\rangle_G\langle a\rangle_G & -(\langle a^{\dagger\,2}\rangle_G - \langle a^\dagger\rangle^2_G) \end{pmatrix},
\tag{B.6}
$$

where we omit the bosonic mode label μ for the sake of a lighter notation. We apply the definition (B.5), with the expectation values of the bosonic operators obtained by considering the Lindblad operator $\mathcal{L}_0$. The characteristic function reads

$$
\chi^{\pm}_{\vec{\sigma},i}(t) = \exp\left\{\sum_\mu\left[-\frac{1+\theta}{2(1-\theta)}|\alpha^{\pm}_{\sigma_i\mu}(t)|^2 + \frac{2ig_{i\mu}M_\mu}{\omega}\left(\frac{\alpha^{\pm}_{\sigma_i\mu}(t)}{\eta-2i} + \frac{\alpha^{\pm *}_{\sigma_i\mu}(t)}{\eta+2i}\right)\right]\right\},
\tag{B.7}
$$

where $M_\mu = \sum_l g_{l\mu}\sigma_l$. Thus, the final expression of the rate is

$$\begin{aligned} W_{\vec{\sigma}\to\vec{\sigma}'} &= \frac{\Omega^2}{\omega}\int_0^{+\infty} dt \sum_{j=\pm} e^{-\sum_\mu \gamma^j_{\sigma_i\mu}(t)}\chi^j_{\vec{\sigma},i}(t) \\ &= \frac{2\Omega^2}{\omega}\int_0^{\infty} dt e^{-\frac{2g_i^2\nu}{\omega^2}[f(t)+t]}\cos\left[16\frac{\Delta E_i t - g_i^2 s(t)}{\omega^2(\eta^2+4)}\right], \\ f(t) &= \frac{-2\eta^2+8}{\eta\left(\eta^2+4\right)}\left[1-e^{-\frac{\eta}{2}t}\cos(t)\right] - \frac{8e^{-\frac{\eta}{2}t}}{\eta^2+4}\sin(t)\,, \end{aligned} \tag{B.8}$$

where $g_i^2 \equiv \sum_{\mu=1}^M g_{i\mu}^2$ and the quantity $\Delta E_i = \sum_\mu g_{i\mu}\sigma_i \sum_{l\neq i} g_{l\mu}\sigma_l$ encodes the entire dependence on the spin configuration. By considering the rate expression in the case $M = 1$, one obtains the single-mode case rate, which is defined by Eq. (5.5).

B.2 Approximate expression of the rate for η small

For sufficiently small $\eta \ll 1$, the exponent appearing in $W_{\vec{\sigma}\to\vec{\sigma}'}$ is dominated by

$$f(\tau) \approx \frac{2}{\eta}(1-\cos(\tau)), \tag{B.9}$$

implying that the integrand is quickly suppressed as τ grows. We therefore perform an expansion around $\tau = 0$ which yields

$$\tau + f(\tau) = (\eta^2+4)\left(\frac{1}{4\eta}\tau^2 - \frac{1}{24}\tau^3 - \frac{4-\eta^2}{192\eta}\tau^4\right) + O(\tau^5) \tag{B.10}$$

and

$$s(\tau) = -\tau + \frac{\eta^2+4}{24}\tau^3 - \eta\frac{\eta^2+4}{96}\tau^4 + O(\tau^5). \tag{B.11}$$

From the first term in Eq. (B.10) we see that the integrand is strongly suppressed on scales $\tau \gtrsim \sqrt{\eta}$. Noticing that in the Taylor expansion of $\tau + f(\tau)$ odd coefficients are finite, whereas even ones are $O(1/\eta)$ for $\eta \to 0$ and introducing the rescaled integration variable $z = \tau\sqrt{\eta}$ we see that higher orders are perturbations of order $O(\eta^{n+1/2}z^{2n+1}, \eta^{n-1}z^{2n})$ and can be neglected. Similar considerations can be applied to $s(\tau)$, which can be therefore also approximated with its leading order $-\tau$. In the following, for simplicity we set $\omega = 1$, remembering that our "energy" ΔE_i is actually measured by construction in units of ω^2. Additionally, we introduce the shorthand

$$\Gamma_i = \frac{16}{\eta^2+4}(\Delta E_i + g_i^2), \tag{B.12}$$

so that, by keeping only the lowest orders of the expansion in τ, we can approximate our rate as

$$W_{\vec{\sigma}\to\vec{\sigma}'} \approx 2\Omega^2\int_0^\infty d\tau\, e^{-2\frac{g_i^2(2\kappa+\eta)}{\eta}\tau^2}\cos\left(\Gamma_i\tau\right), \tag{B.13}$$

which can be integrated to give the closed expression

$$W_{\vec{\sigma}\to\vec{\sigma}'} \approx \Omega^2 \sqrt{\frac{\pi\eta}{2g_i^2\,(2\kappa+\eta)}}\, e^{-\frac{\eta\Gamma_i^2}{8g_i^2(2\kappa+\eta)}}. \tag{B.14}$$

It is worth remarking that the exponent can be rewritten as

$$\begin{aligned} -\frac{\eta\Gamma_i^2}{8g_i^2\,(2\kappa+\eta)} &= \frac{128\eta}{(2\kappa+\eta)(\eta^2+4)^2}\left[-\frac{(\Delta E_i+g_i^2)^2}{4g_i^2}\right] = \\ &= \frac{128\eta}{(2\kappa+\eta)(\eta^2+4)^2}\left[E(\vec{\sigma})-\frac{\sum_j g_j^2}{4}\right] = \beta_{\text{eff}}E(\vec{\sigma}) - const.\,, \end{aligned} \tag{B.15}$$

highlighting the "thermal" structure of the rates. Note that, in order to obtain the approximation (B.13), we have assumed that we can resum the Taylor expansion of the original cosine to the function $\cos(\Gamma_i\tau)$, whose series only coincides with the former up to $O(\tau^2)$. This is only valid as long as the cosine does not oscillate significantly before the other Gaussian term suppresses the integrand; in other words, Eq. (B.14) should be valid up to values of Γ_i of the order of $\sim 1/\sqrt{\eta}$. Since we wish to understand the behavior of the rates as functions of the energy difference ΔE_i without restrictions imposed by the other parameters (like η), we need to account for energies which exceed this range. To do this, we extract the asymptotic behavior of the rate for $\Gamma_i \to \infty$. We start by rewriting the integrand in W as

$$I(\Gamma_i,\tau) \equiv \text{Re}\left\{e^{-2\frac{g_i^2\nu}{\omega^2}(f(\tau)+\tau)}e^{i\Gamma_i\tau-16i\frac{g_i^2}{\eta^2+4}(s(\tau)+\tau)}\right\} = \tag{B.16}$$

$$= \text{Re}\left\{A(\tau)e^{i\Gamma_i\tau}\right\}. \tag{B.17}$$

We now use the result that, if the function A admits a small τ expansion

$$A(\tau) = \sum_{n=0}^{\infty} a_n\tau^n, \tag{B.18}$$

then asymptotically in the limit $\Gamma_i \to \infty$ one finds

$$\int_0^\infty d\tau\, A(\tau)e^{i\Gamma_i\tau} = \sum_{n=0}^{\infty} i^n\, n!\, a_n\Gamma_i^{-n-1}. \tag{B.19}$$

The leading term in this expansion corresponds to the lowest n for which one finds a non-vanishing real part. In particular, we note that $\text{Re}[a_n i^{n+1}]$ equals $(-1)^{l+1}\text{Re}[a_{2l+1}]$ if $n = 2l+1$ is odd, and $(-1)^{l+1}\text{Im}[a_{2l}]$ if $n = 2l$ is even. For our function we find

$$a_0 = 1, \tag{B.20a}$$

$$a_1 = 0, \tag{B.20b}$$

$$a_2 = -2g_i^2\frac{2\kappa+\eta}{\eta}, \tag{B.20c}$$

$$a_3 = \frac{g_i^2}{3}\left[2\kappa+\eta-2i\right]. \tag{B.20d}$$

The leading behavior in the large Γ_i limit is therefore determined by $\mathrm{Re}[a_3]$, implying

$$W_{\vec{\sigma}\to\vec{\sigma}'} = 2\Omega^2 \int_0^\infty d\tau\, I(\Gamma_i,\tau) \approx 4\Omega^2 g_i^2(2\kappa+\eta)\left[\frac{\eta^2+4}{16(\Delta E_i + g_i^2)}\right]^4. \tag{B.21}$$

To provide a very crude estimate of where the change from the two regimes characterized by Eqs. (B.14) ("small Γ_i") and (B.21) ("large Γ_i") occurs, we evaluate the point where the two asymptotic expressions cross (for η sufficiently small): setting

$$4g_i^2(2\kappa+\eta)\Gamma_i^{-4} = \sqrt{\frac{\pi\eta}{2g_i^2\,(2\kappa+\eta)}}e^{-\frac{\eta\Gamma_i^2}{8g_i^2(2\kappa+\eta)}}, \tag{B.22}$$

we find

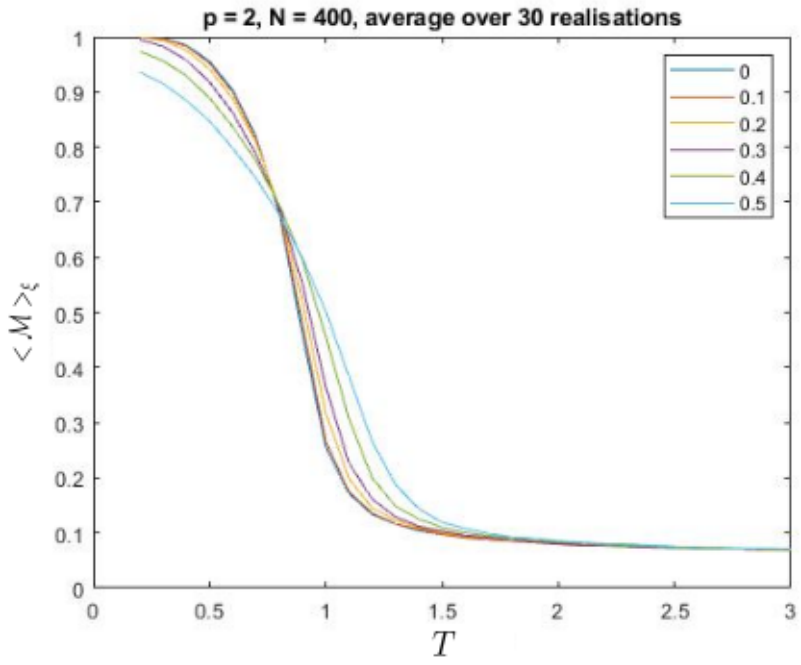
$$\Gamma_i^2 \approx \frac{4g_i^2(2\kappa+\eta)}{\eta}\left[\log A + 4\log\left(\frac{1}{2}\log A\right)\right], \tag{B.23}$$

where $A = 32g_i^2\pi(2\kappa+\eta)\eta^{-3}$.

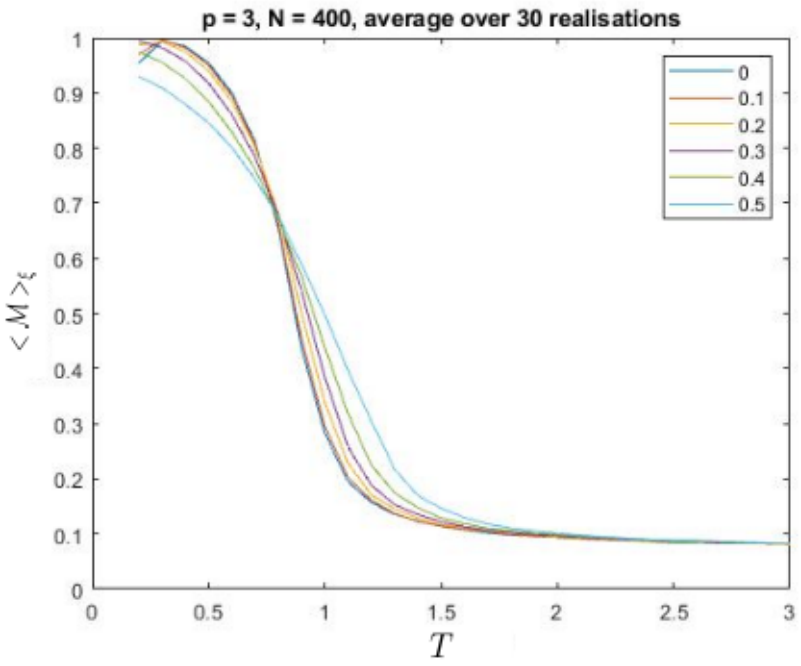
B.3 Impact of pattern noise in the Hopfield Neural Network

In this Section we compare the behavior of our spin-boson model to that of a HNN with noisy patterns. In particular, we generate the pattern components analogously to the spin-boson couplings, i.e. from a bimodal distribution consisting of the superposition of two Gaussians $\mathcal{P}(\xi) = \frac{1}{2}[\mathcal{N}_{+1,s}(\xi) + \mathcal{N}_{-1,s}(\xi)]$, with $N_{x_0,s}(x) = (2\pi s)^{1/2}\exp -(x-x_0)^2/(2s^2)$.

The results, reported in Fig. [B.1], have been obtained by means of a Monte Carlo sampling of the HNN's configurations at different temperatures. Denoting the the p overlaps for the HNN as $\zeta_\mu = \vec{\xi}_\mu \cdot \vec{\sigma}/N$, in Fig. [B.1(a,b)] we show the HNN disorder averaged order parameter, $\langle\mathcal{M}\rangle_\xi = \langle\max_{\mu=1,\dots,p}\overline{|\zeta_\mu|}\rangle_\xi$, as a function of the temperature T for $\mu = 1,\dots,p$ with $p = 2$ (two memory case) and a $p = 3$ (three memory case), respectively. Different lines correspond to different Gaussian widths, as reported in the legend. As can be seen from Fig. [B.1a], near the critical point $T = 1$, the order parameter increases with s. A similar behavior seems to be present as the number of memories increases, as displayed in Fig. [B.1b].



(a)



(b)

Figure B.1: **Impact of pattern noise on the phase transition in the HNN.** Order parameter as a function of the temperature. The disorder distribution of the patterns is a bimodal distribution consisting of two peaks, each of Gaussian shape, peaked at ± 1. Each line corresponds to a value of the Gaussian width s. The two panels report the results in (a) the two memory case, $p = 2$, and (b) the three memory case, $p = 3$.

B.4 Considerations on the reliability of the rate equation at long times

As illustrated by Fig. [6.2c] of Ch. 6, we find for the rate equation (6.3) parameter regimes with different stationary properties. Borrowing the terminology from the physics of the HNN, we observe a "paramagnetic" phase at large η and a "retrieval" one when η is small, but not too small ($\eta \sim O(1)$). This latter phase is characterized by the emergence of multiple approximate basins of attraction (BAs) which appear in the dynamics as metastable states separated by fast switching from one to the other. In this section, we offer a few considerations on whether our effective, classical approach does in fact capture the properties of the quantum dynamics and on whether the observed emergence of distinct (albeit approximate) attractors may be disrupted by the inclusion of higher order terms in the perturbative expansion ($\propto \Omega^4$ and higher).

The formalism we employ, details of which can be found in Refs. [68,91], is a perturbation around the stationary space of the $\Omega = 0$ dynamics. The three main assumptions behind it can be summarized as follows:

(i) the presence of a subspace which is "fully" absorbing for the $\Omega = 0$ dynamics, i.e. which is always reached independently of the initial condition and never left. In our work, that would be the subspace the projector P projects upon.

(ii) the presence of a finite gap (or, more precisely, a gap with finite real part) in the spectrum of the generator $\mathcal{L}_0$ of the $\Omega = 0$ dynamics. This implies the presence of a finite timescale τ_G (proportional to the inverse of the gap) beyond which all contributions coming from states not belonging to the stationary subspace are exponentially suppressed in time.

(iii) a small term (in our case, $\propto \Omega$) which connects the stationary subspace of the unperturbed dynamics to the remainder of the space of states, inducing a dynamics upon it. The assumption of smallness means that it must act on timescales greater than the unperturbed relaxation ones ($\Omega\tau_G \ll 1$).

As long as these conditions are satisfied, the resulting perturbation theory captures with reasonable accuracy the dynamical behavior of the system and the higher order terms can be safely discarded even at long times (as long as Ω remains perturbatively small).

The disordered, multi-mode Dicke model we discuss Ch. 6 is unfortunately too complicated to to perform simulations of the full quantum dy-

namics for a sensible system size. Hence, to provide some insights on the formation of distinct basins of attraction at finite size and to show how they can remain stable when quantum fluctuations are fully accounted for, we employ a toy example, consisting of a non-disordered, single-mode Dicke model with Hamiltonian

$$H = \omega a^\dagger a + \Omega S^x + g S^z (a + a^\dagger). \tag{B.24}$$

Here, $S^\alpha = \sum_{i=1}^N \sigma_i^\alpha/2$ is the global α component of the spin and dissipation is included, for simplicity, in the form of losses only with jump operator $L = \sqrt{\gamma} a$. Models of this kind have been studied in the recent literature [27, 28], providing strong evidence that they undergo, at sufficiently strong coupling g, a superradiant phase transition which breaks the Z_2 inversion symmetry $\sigma_i^z \to -\sigma_i^z$, $a \to -a$. Before proceeding, it is important to remark two important differences with respect to the model we discuss in Ch. 6: the first one is that currently there is not enough evidence to support the presence of a phase transition in the multi-mode, disordered case; the intricate form of the transition rates limits our simulations to sizes of about $N = 50$; as we mention in the main text, further efforts at higher N are required to understand how the crossover we find behaves. The second difference is that the simplified Dicke model of Eq. (B.24) cannot be treated within the same perturbative scheme used in Chs. 5 and 6, and illustrated in Appendix B.2; the issue is that having equal couplings introduces new symmetries, and indeed it is more convenient to describe the spins collectively as a "large spin" variable S^α. Under these conditions, the space of "diagonal" density matrices onto which P projects is no longer the full stationary space of the unperturbed dynamics. This violates assumption (i) above: the subspace we project onto would still be absorbing, but not "fully" so, i.e., there would be sets of stationary states outside it including non-zero off-diagonal coherences. Despite these two differences, the aspects under discussion here are sufficiently general to treat the results about the simplified model, presented below, as a reasonable indication of the behavior of the multi-mode, disordered one discussed in Ch. 6.

To formulate a comparison with the methodology used in the main text, which is based on sampling stochastic trajectories generated by the rate equation (6.3), the best framework to take is a quantum jump one, where the dissipative processes are constantly monitored [98]. We have employed a quantum-jump Monte Carlo (QJMC) algorithm to sample trajectories for the model defined around Eq. (B.24) above. We have set $N = 13$ and exploited the conservation of the total spin to restrict the state space to the highest spin representation $S^2 = N(N/2+1)/2 = 195/4$ (or $S = 13/2$ for short). In Fig. [B.2] below we show the average value of the z component,

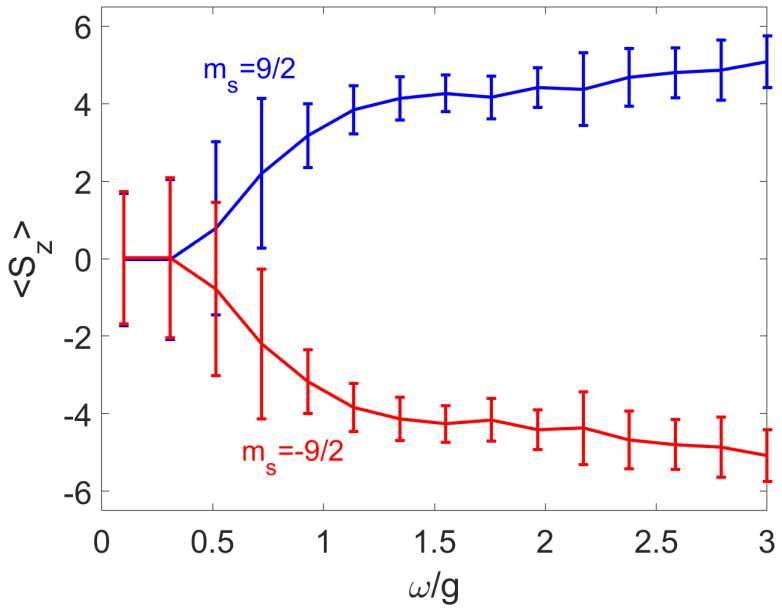


Figure B.2: **Quantum-jump Monte Carlo simulation of the simplified model.** Average value of the global spin z component $\langle S_z \rangle$ as a function of the dimensionless coupling ω/g, for two different initial conditions. The system parameters are all defined in terms of the coupling g according to $\Omega = 0.05g$, $\gamma = 2g$, $S = 13/2$ ($N = 13$ spins), and the plot shows $\langle S_z \rangle$ after a time $t_{final} = 2500g^{-1}$. The blue (red) curve is characterized by the initial z-component condition $m_s = 9/2$ ($m_s = -9/2$).

$\langle S^z \rangle$, for two different initial conditions ($|\psi(t=0)\rangle = |S = 13/2, S_z = m_S\rangle$ with $m_S = \pm 9/2$) after a long time $t_{final} = 2500 g^{-1}$ for various values of the dimensionless control parameter ω/g; note that increasing this parameter at fixed γ is similar to decreasing our parameter η in the main text at fixed ω. Each of the two curves is the result of averaging over 50 independent trajectories and the errorbars display plus or minus the corresponding standard deviation. The two initial conditions have been chosen with strong biases in either direction, therefore strongly breaking the Z_2 symmetry of the problem and, as expected, for sufficiently large ω/g this induces a distinctive bunching of QJMC trajectories around positive or negative values. Of course, at any finite size waiting for long enough would lead the dynamics to eventually restore the symmetry, but these simulations show that for rather long times the approximate basins of attractors remain stable, even under the action of quantum fluctuations. Whether increasing the system size would stabilize the approximate basins of attraction under our non-equilibrium dynamics, as it should under equilibrium conditions [29,31], remains for now an open question.

Bibliography

[1] Daniel J. Amit. *Modelling Brain Function: The World of Attractor Neural Networks*. Cambridge University Press, USA, 1st edition, 1992.

[2] Daniel J. Amit, Hanoch Gutfreund, and Haim Sompolinsky. Spin-glass models of neural networks. *Physical Review A*, 32:1007–1018, 1985.

[3] Peter W. Shor. Polynomial-time algorithms for prime factorization and discrete logarithms on a quantum computer. *SIAM Review*, 41(2):303–332, 1999.

[4] Lov K. Grover. Quantum mechanics helps in searching for a needle in a haystack. *Physical Review Letters*, 79:325–328, Jul 1997.

[5] Arnab Das and Bikas K. Chakrabarti. Colloquium: Quantum annealing and analog quantum computation. *Reviews of Modern Physics*, 80:1061–1081, Sep 2008.

[6] Edward Farhi, Jeffrey Goldstone, Sam Gutmann, Joshua Lapan, Andrew Lundgren, and Daniel Preda. A quantum adiabatic evolution algorithm applied to random instances of an np-complete problem. *Science*, 292(5516):472–475, 2001.

[7] Giuseppe E. Santoro, Roman Martoňák, Erio Tosatti, and Roberto Car. Theory of quantum annealing of an Ising spin glass. *Science*, 295(5564):2427–2430, 2002.

[8] Hidetoshi Nishimori and Kabuki Takada. Exponential enhancement of the efficiency of quantum annealing by non-stoquastic hamiltonians. *Frontiers in ICT*, 4:2, 2017.

[9] Vasil S. Denchev, Sergio Boixo, Sergei V. Isakov, Nan Ding, Ryan Babbush, Vadim Smelyanskiy, John Martinis, and Hartmut Neven. What is the computational value of finite-range tunneling? *Physical Review X*, 6:031015, Aug 2016.

[10] Jacob Biamonte, Peter Wittek, Nicola Pancotti, Patrick Rebentrost, Nathan Wiebe, and Seth Lloyd. Quantum machine learning. *Nature*, 549(7671):195–202, Sep 2017.

[11] Maria Schuld, Ilya Sinayskiy, and Francesco Petruccione. The quest for a quantum neural network. *Quantum Information Processing*, 13(11):2567–2586, 2014.

[12] Àngel Rivas and Susana F. Huelga. *Open Quantum Systems*. Springer Berlin Heidelberg, 2012.

[13] H. P. Breuer and F. Petruccione. *The theory of open quantum systems*. Oxford University Press, Great Clarendon Street, 2002.

[14] Pietro Rotondo, Matteo Marcuzzi, Juan P. Garrahan, Igor Lesanovsky, and Markus Müller. Open quantum generalisation of Hopfield neural networks. *Journal of Physics A: Mathematical and Theoretical*, 51(11):115301, 2018.

[15] Frank Verstraete, Michael M Wolf, and J Ignacio Cirac. Quantum computation and quantum-state engineering driven by dissipation. *Nature Physics*, 5(9):633–636, 2009.

[16] Sebastian Diehl, A Micheli, A Kantian, B Kraus, HP Büchler, and P Zoller. Quantum states and phases in driven open quantum systems with cold atoms. *Nature Physics*, 4(11):878, 2008.

[17] Markus Müller, Sebastian Diehl, Guido Pupillo, and Peter Zoller. Engineered open systems and quantum simulations with atoms and ions. In Paul Berman, Ennio Arimondo, and Chun Lin, editors, *Advances in Atomic, Molecular, and Optical Physics*, volume 61 of *Advances In Atomic, Molecular, and Optical Physics*, pages 1 – 80. Academic Press, 2012.

[18] Sarang Gopalakrishnan, Benjamin L. Lev, and Paul M. Goldbart. Emergent crystallinity and frustration with bose-einstein condensates in multimode cavities. *Nature Physics*, 5:845–850, 2009.

[19] Sarang Gopalakrishnan, Benjamin L. Lev, and Paul M. Goldbart. Frustration and glassiness in spin models with cavity-mediated interactions. *Physical Review Letters*, 107(27):277201, 2011.

[20] Robert H. Dicke. Coherence in spontaneous radiation processes. *Physical Review*, 93(1):99, 1954.

[21] Klaus Hepp and Elliott H Lieb. On the superradiant phase transition for molecules in a quantized radiation field: the Dicke maser model. *Annals of Physics*, 76(2):360 – 404, 1973.

[22] Yo K Wang and FT Hioe. Phase transition in the Dicke model of superradiance. *Physical Review A*, 7(3):831, 1973.

[23] Clive Emary and Tobias Brandes. Chaos and the quantum phase transition in the Dicke model. *Physical Review E*, 67:066203, Jun 2003.

[24] F. Dimer, B. Estienne, A. S. Parkins, and H. J. Carmichael. Proposed realization of the Dicke-model quantum phase transition in an optical cavity QED system. *Physical Review A*, 75:013804, Jan 2007.

[25] Dávid Nagy, Gábor Kónya, Gergely Szirmai, and Peter Domokos. Dicke-model phase transition in the quantum motion of a Bose-Einstein condensate in an optical cavity. *Physical Review Letters*, 104:130401, Apr 2010.

[26] Ibai Aedo and Lucas Lamata. Analog quantum simulation of generalized Dicke models in trapped ions. *Physical Review A*, 97:042317, 04 2018.

[27] Peter Kirton and Jonathan Keeling. Suppressing and restoring the Dicke superradiance transition by dephasing and decay. *Physical Review Letters*, 118:123602, Mar 2017.

[28] Emanuele G. Dalla Torre, Sebastian Diehl, Mikhail D. Lukin, Subir Sachdev, and Philipp Strack. Keldysh approach for nonequilibrium phase transitions in quantum optics: Beyond the Dicke model in optical cavities. *Physical Review A*, 87:023831, Feb 2013.

[29] Philipp Strack and Subir Sachdev. Dicke quantum spin glass of atoms and photons. *Physical Review Letters*, 107:277202, Dec 2011.

[30] Pietro Rotondo, Enrico Tesio, and Sergio Caracciolo. Replica symmetry breaking in cold atoms and spin glasses. *Physical Review B*, 91:014415, Jan 2015.

[31] Pietro Rotondo, Marco Cosentino Lagomarsino, and Giovanni Viola. Dicke simulators with emergent collective quantum computational abilities. *Physical Review Letters*, 114:143601, Apr 2015.

[32] John Hertz, Anders Krogh, and Richard G. Palmer. *Introduction to the Theory of Neural Computation*. Addison-Wesley, Redwood City, CA, 1991.

[33] Hidetoshi Nishimori. *Statistical Physics of Spin Glasses and Information Processing: an Introduction*. Oxford University Press, Oxford; New York, 2001.

[34] Warren S. McCulloch and Walter Pitts. A logical calculus of the ideas immanent in nervous activity. *Bulletin of Mathematical Biophysics*, pages 115–133, 1943.

[35] John J. Hopfield. Neural networks and physical systems with emergent collective computational abilities. *Proceedings of the National Academy of Sciences*, 79:2554–2558, 1982.

[36] Donald Olding Hebb. *The organization of behavior: a neuropsychological theory*. J. Wiley; Chapman & Hall, 1949.

[37] William A Little and Gordon L Shaw. Analytic study of the memory storage capacity of a neural network. *Mathematical biosciences*, 39(3-4):281–290, 1978.

[38] Roy J. Glauber. Time-dependent statistics of the Ising model. *Journal of Mathematical Physics*, 4(2):294–307, 1963.

[39] Daniel J. Amit, Hanoch Gutfreund, and Haim Sompolinsky. Storing infinite numbers of patterns in a spin-glass model of neural networks. *Physical Review Letters*, 55:1530–1533, Sep 1985.

[40] Daniel. J. Amit, Hanoch Gutfreund, and Haim Sompolinsky. Statistical mechanics of neural networks near saturation. *Annals of Physics*, 173:30–67, 1987.

[41] Michael A. Nielsen and Isaac L. Chuang. *Quantum computation and quantum information*. Cambridge University Press, Cambridge, 2000.

[42] Maciej Lewenstein, Dagmar Bruß, Juan Ignacio Cirac, Barbara Kraus, M. Kuś, J. Samsonowicz, Anna Sanpera, and R. Tarrach. Separability and distillability in composite quantum systems - a primer. *Journal of Modern Optics*, 47(14-15):2481–2499, 2000.

[43] Harold Ollivier and Wojciech H. Zurek. Quantum discord: A measure of the quantumness of correlations. *Physical Review Letters*, 88:017901, Dec 2001.

[44] Leah Henderson and Vlatko Vedral. Classical, quantum and total correlations. *Journal of Physics A: Mathematical and General*, 34(35):6899, 2001.

[45] Peter Štelmachovič and Vladimír Bužek. Dynamics of open quantum systems initially entangled with environment: Beyond the kraus representation. *Physical Review A*, 64:062106, Nov 2001.

[46] Karl Kraus, A. Böhm, J. D. Dollard, and W. H. Wootters, editors. *States, Effects, and Operations Fundamental Notions of Quantum Theory*. Springer Berlin Heidelberg, 1983.

[47] Vittorio Gorini, Andrzej Kossakowski, and E. C. G. Sudarshan. Completely positive dynamical semigroups of n-level systems. *Journal of Mathematical Physics*, 17(5):821–825, 1976.

[48] Goran Lindblad. On the generators of quantum dynamical semigroups. *Communications in Mathematical Physics*, 48(2):119–130, 1976.

[49] Herbert Spohn. An algebraic condition for the approach to equilibrium of an open n-level system. *Letters in Mathematical Physics*, 2(1):33–38, 1977.

[50] Sadao Nakajima. On quantum theory of transport phenomena: Steady diffusion. *Progress of Theoretical Physics*, 20(6):948–959, 1958.

[51] Robert Zwanzig. Ensemble method in the theory of irreversibility. *The Journal of Chemical Physics*, 33(5):1338–1341, 1960.

[52] E Brian Davies. Markovian master equations. *Communications in mathematical Physics*, 39(2):91–110, 1974.

[53] E Brian Davies. Markovian master equations. II. *Mathematische Annalen*, 219(2):147–158, 1976.

[54] Peter Kirton, Mor M. Roses, Jonathan Keeling, and Emanuele G. Dalla Torre. Introduction to the Dicke model: From equilibrium to nonequilibrium, and vice versa (adv. quantum technol. 1-2/2019). *Advanced Quantum Technologies*, 2(1-2):1970013, 2019.

[55] Barry M. Garraway. The Dicke model in quantum optics: Dicke model revisited. *Philosophical Transactions of the Royal Society A: Mathematical, Physical and Engineering Sciences*, 369(1939):1137–1155, 2011.

[56] Zhiqiang Zhang, Chern Hui Lee, Ravi Kumar, K. J. Arnold, Stuart J. Masson, A. L. Grimsmo, A. S. Parkins, and M. D. Barrett. Dicke-model simulation via cavity-assisted raman transitions. *Physical Review A*, 97:043858, Apr 2018.

[57] Peter Domokos and Helmut Ritsch. Collective cooling and self-organization of atoms in a cavity. *Physical Review Letters*, 89:253003, Dec 2002.

[58] Adam T. Black, Hilton W. Chan, and Vladan Vuletić. Observation of collective friction forces due to spatial self-organization of atoms: From Rayleigh to Bragg scattering. *Physical Review Letters*, 91:203001, Nov 2003.

[59] Juan Ignacio Cirac, Robert Blatt, Peter Zoller, and William D. Phillips. Laser cooling of trapped ions in a standing wave. *Physical Review A*, 46:2668–2681, Sep 1992.

[60] Sarang Gopalakrishnan, Benjamin L. Lev, and Paul M. Goldbart. Atom-light crystallization of Bose-Einstein condensates in multimode cavities: Nonequilibrium classical and quantum phase transitions, emergent lattices, supersolidity, and frustration. *Physical Review A*, 82(4):043612, 2010.

[61] Tadashi Kadowaki and Hidetoshi Nishimori. Quantum annealing in the transverse Ising model. *Physical Review E*, 58:5355–5363, Nov 1998.

[62] Satoshi Morita and Hidetoshi Nishimori. Mathematical foundation of quantum annealing. *Journal of Mathematical Physics*, 49(12):125210, 2008.

[63] Dorit Aharonov, Wim Van Dam, Julia Kempe, Zeph Landau, Seth Lloyd, and Oded Regev. Adiabatic quantum computation is equivalent to standard quantum computation. *SIAM Review*, 50(4):755–787, 2008.

[64] Sergio Boixo, Troels F Rønnow, Sergei V Isakov, Zhihui Wang, David Wecker, Daniel A Lidar, John M Martinis, and Matthias Troyer. Evidence for quantum annealing with more than one hundred qubits. *Nature Physics*, 10(3):218, 2014.

[65] Carlo Baldassi and Riccardo Zecchina. Efficiency of quantum vs. classical annealing in nonconvex learning problems. *Proceedings of the National Academy of Sciences*, 115(7):1457–1462, 2018.

[66] Robert Alicki. On the detailed balance condition for non-hamiltonian systems. *Reports on Mathematical Physics*, 10(2):249–258, 1976.

[67] Beatriz Olmos, Igor Lesanovsky, and Juan P. Garrahan. Out-of-equilibrium evolution of kinetically constrained many-body quan-

tum systems under purely dissipative dynamics. *Physical Review E*, 90:042147, Oct 2014.

[68] Matteo Marcuzzi, Jan Schick, Beatriz Olmos, and Igor Lesanovsky. Effective dynamics of strongly dissipative Rydberg gases. *Journal of Physics A: Mathematical and Theoretical*, 48(48):482001, 2014.

[69] Marc Mezard and Andrea Montanari. *Information, physics, and computation*. Oxford University Press, 2009.

[70] Claudio Castelnovo, Claudio Chamon, Christopher Mudry, and Pierre Pujol. From quantum mechanics to classical statistical physics: Generalized rokhsar-kivelson hamiltonians and the stochastic matrix form decomposition. *Annals of Physics*, 318(2):316 – 344, 2005.

[71] Alexandre Blais, Ren-Shou Huang, Andreas Wallraff, S. M. Girvin, and R. J. Schoelkopf. Cavity quantum electrodynamics for superconducting electrical circuits: An architecture for quantum computation. *Physical Review A*, 69:062320, Jun 2004.

[72] Huaixiu Zheng, Daniel J. Gauthier, and Harold U. Baranger. Waveguide-QED-based photonic quantum computation. *Physical Review Letters*, 111:090502, Aug 2013.

[73] Juan Ignacio Cirac and Peter Zoller. Quantum computations with cold trapped ions. *Physical Review Letters*, 74:4091–4094, May 1995.

[74] Dietrich Leibfried, Robert Blatt, Christopher Monroe, and David Wineland. Quantum dynamics of single trapped ions. *Reviews of Modern Physics*, 75:281–324, Mar 2003.

[75] Anton Frisk Kockum, Adam Miranowicz, Simone De Liberato, Salvatore Savasta, and Franco Nori. Ultrastrong coupling between light and matter. *Nature Reviews Physics*, 1(1):19, 2019.

[76] Valentin Torggler, Sebastian Krämer, and Helmut Ritsch. Quantum annealing with ultracold atoms in a multimode optical resonator. *Physical Review A*, 95:032310, Mar 2017.

[77] Sarang Gopalakrishnan, Benjamin L. Lev, and Paul M. Goldbart. Frustration and glassiness in spin models with cavity-mediated interactions. *Physical Review Letters*, 107:277201, Dec 2011.

[78] Michael Buchhold, Philipp Strack, Subir Sachdev, and Sebastian Diehl. Dicke-model quantum spin and photon glass in optical cavities:

Nonequilibrium theory and experimental signatures. *Physical Review A*, 87:063622, Jun 2013.

[79] Varun D. Vaidya, Yudan Guo, Ronen M. Kroeze, Kyle E. Ballantine, Alicia J. Kollár, Jonathan Keeling, and Benjamin L. Lev. Tunable-range, photon-mediated atomic interactions in multimode cavity QED. *Physical Review X*, 8:011002, Jan 2018.

[80] Sarang Gopalakrishnan, Benjamin L. Lev, and Paul M. Goldbart. Exploring models of associative memory via cavity quantum electrodynamics. *Philosophical Magazine*, 92(1-3):353–361, 2012.

[81] Yudan Guo, Ronen M. Kroeze, Varun D. Vaidya, Jonathan Keeling, and Benjamin L. Lev. Sign-changing photon-mediated atom interactions in multimode cavity quantum electrodynamics. *Physical Review Letters*, 122:193601, May 2019.

[82] Emanuele G. Dalla Torre, Yulia Shchadilova, Eli Y. Wilner, Mikhail D. Lukin, and Eugene Demler. Dicke phase transition without total spin conservation. *Physical Review A*, 94:061802, Dec 2016.

[83] Gabriele De Chiara, Gabriel Landi, Adam Hewgill, Brendan Reid, Alessandro Ferraro, Augusto J Roncaglia, and Mauro Antezza. Reconciliation of quantum local master equations with thermodynamics. *New Journal of Physics*, 20(11):113024, nov 2018.

[84] Amikam Levy and Ronnie Kosloff. The local approach to quantum transport may violate the second law of thermodynamics. *Europhysics Letters*, 107(2):20004, jul 2014.

[85] Diego Porras and Juan Ignacio Cirac. Effective quantum spin systems with trapped ions. *Physical Review Letters*, 92:207901, May 2004.

[86] Dingshun Lv, Shuoming An, Zhenyu Liu, Jing-Ning Zhang, Julen S. Pedernales, Lucas Lamata, Enrique Solano, and Kihwan Kim. Quantum simulation of the quantum Rabi model in a trapped ion. *Physical Review X*, 8:021027, Apr 2018.

[87] Arghavan Safavi-Naini, Robert J. Lewis-Swan, Justin G. Bohnet, Martin Gärttner, Kevin A. Gilmore, Judith E. Jordan, J. Cohn, James K. Freericks, Ana M. Rey, and John J. Bollinger. Verification of a many-ion simulator of the Dicke model through slow quenches across a phase transition. *Physical Review Letters*, 121:040503, Jul 2018.

[88] A Mezzacapo, U Las Heras, JS Pedernales, L DiCarlo, E Solano, and L Lamata. Digital quantum Rabi and Dicke models in superconducting circuits. *Scientific Reports*, 4:7482, 2014.

[89] G-D Lin, S-L Zhu, Rajibul Islam, Kihwan Kim, M-S Chang, Simcha Korenblit, Christopher Monroe, and L-M Duan. Large-scale quantum computation in an anharmonic linear ion trap. *Europhysics Letters*, 86(6):60004, 2009.

[90] Victor V. Albert and Liang Jiang. Symmetries and conserved quantities in Lindblad master equations. *Physical Review A*, 89:022118, Feb 2014.

[91] Peter Degenfeld-Schonburg and Michael J. Hartmann. Self-consistent projection operator theory for quantum many-body systems. *Physical Review B*, 89:245108, Jun 2014.

[92] Hui-Hui Dai and Derek Naylor. On an asymptotic expansion of Fourier integrals. *Proceedings of the Royal Society of London. Series A: Mathematical and Physical Sciences*, 436(1896):109–120, 1992.

[93] Royce K. P. Zia and Beate Schmittmann. Probability currents as principal characteristics in the statistical mechanics of non-equilibrium steady states. *Journal of Statistical Mechanics: Theory and Experiment*, 2007(07):P07012–P07012, jul 2007.

[94] Francisco Barahona. On the computational complexity of Ising spin glass models. *Journal of Physics A: Mathematical and General*, 15(10):3241–3253, oct 1982.

[95] A.B. Bortz, M.H. Kalos, and J.L. Lebowitz. A new algorithm for Monte Carlo simulation of Ising spin systems. *Journal of Computational Physics*, 17(1):10 – 18, 1975.

[96] W M Young and E W Elcock. Monte Carlo studies of vacancy migration in binary ordered alloys: I. *Proceedings of the Physical Society*, 89(3):735–746, nov 1966.

[97] Daniel T Gillespie. A general method for numerically simulating the stochastic time evolution of coupled chemical reactions. *Journal of Computational Physics*, 22(4):403 – 434, 1976.

[98] Martin Plenio and Peter Knight. The quantum-jump approach to dissipative dynamics in quantum optics. *Reviews of Modern Physics*, 70:101–144, Jan 1998.